博士学位論文

Dynamic Orientation Control of Gold Nanorods on Polymer Brush Substrates

(ポリマーブラシ基板上における金ナノロッドの動的配向制御)

関澤 祐侑

北海道大学大学院生命科学院

ソフトマター専攻

2024 年 3 月

Contents

Chapter 1

General introduction

1-1. Top-down and bottom-up approach in nanotechnology

Nanotechnology enables precise manipulation of materials at the nanoscale. One of the reasons for the focus on nanotechnology in materials science is the demand for miniaturization of devices.[1,2] For this reason, various nanostructures have been developed. Nanostructure fabrication methods can be broadly classified into top-down and bottom-up approaches (**Figure 1-1**). For example, the top-down approach is mainly used in semiconductor engineering. A nanoscale pattern is created by exposing photosensitive resin using a photomask, followed by etching to create a fine fabrication.[3] By repeating this process, microcircuits are fabricated. This method, characterized by microfabrication techniques, enables the creation of intricate structures with minimal symmetry and ordered arrays.[4,5] The top-down strategy, however, is costly encounters obstacles in achieving structures below 10 nm, preventing optimal device miniaturization. In contrast, the bottom-up approach, in which nanostructures are fabricated by assembling molecules, has been attracting attention in recent years.[6,7] In this method, molecules are strategically designed for particular interactions, and structures are formed through induced assembly mechanisms. This approach has the potential to generate smaller, more efficient devices at a lower expense, due to its ability to simultaneously develop multiple devices.[8,9] Although the bottom-up approach has the potential, creating structures in the tens to hundreds of nanometers range is challenging due to the increased complexity. Considering the background, the establishment of a method to fabricate complex nanostructures using a bottom-up approach is required to further advance nanotechnology.

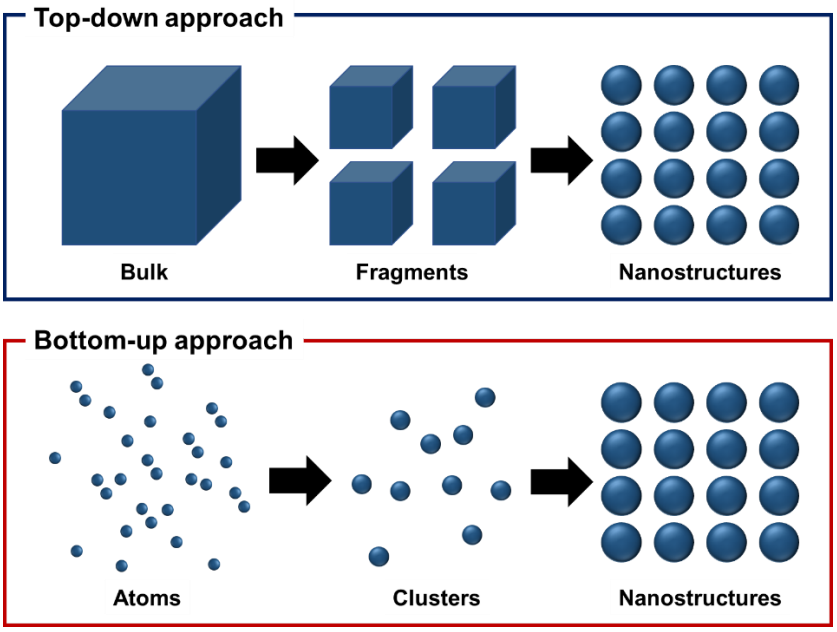

Figure 1-1. Fabrication of nanostructures by top-down (top) and bottom-up (bottom) approaches

1-2. Gold nanoparticles in nanotechnology

Transitioning from the bottom-up manipulation of single atoms or molecules to larger dimensional materials with increased complexity, metallic nanoparticles have attracted significant interest. These nanoparticles, composed of assembled metal atoms, exhibit unique properties that are distinctly different from those of bulk metals and single atoms. One notable property is localized surface plasmon resonance (LSPR), as shown in **Figure 1-2**.[10] This phenomenon appears in metal nanoparticles, such as gold, silver, copper, and platinum. Free electrons localized on the surface of nanoparticles vibrate collectively, and the vibrations resonate with the electric field of light, causing absorption of light at a specific wavelength. The vibrational state of the free electrons is influenced by factors such as particle morphology, surface topography, environmental conditions, and spatial proximity between particles. Consequently, the optical properties of the metallic nanoparticles can be modulated by controlling their assembly. Among these metal nanoparticles, gold nanoparticles are particularly distinguished owing to their ease of size and shape manipulation, robust stability, and pronounced biocompatibility. To date, a number of research on gold nanoparticle assembly have been conducted. In addition to research on reversible control of gold nanoparticle assembly using external stimuli such as light,[11,12] temperature[13] and pH,[14] recent studies have shown the development of one-dimensional assemblies,[15,16] of gold nanoparticles arranged in lines, two-dimensional assemblies of gold nanoparticles,[17,18] and three-dimensional assemblies represented by vesicles (hollow structures)[19–21] (**Figure 1-3**).

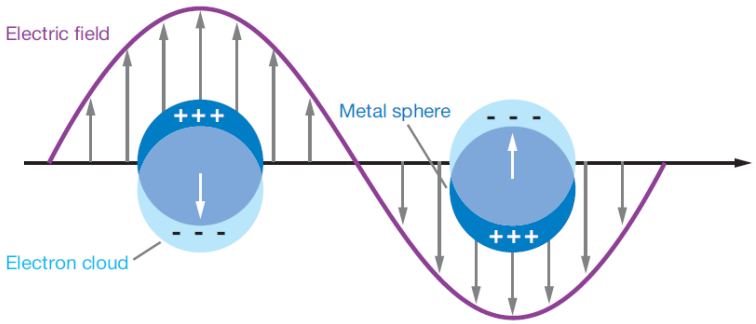

Figure 1-2. Schematic illustration of surface plasmon resonance.[10]

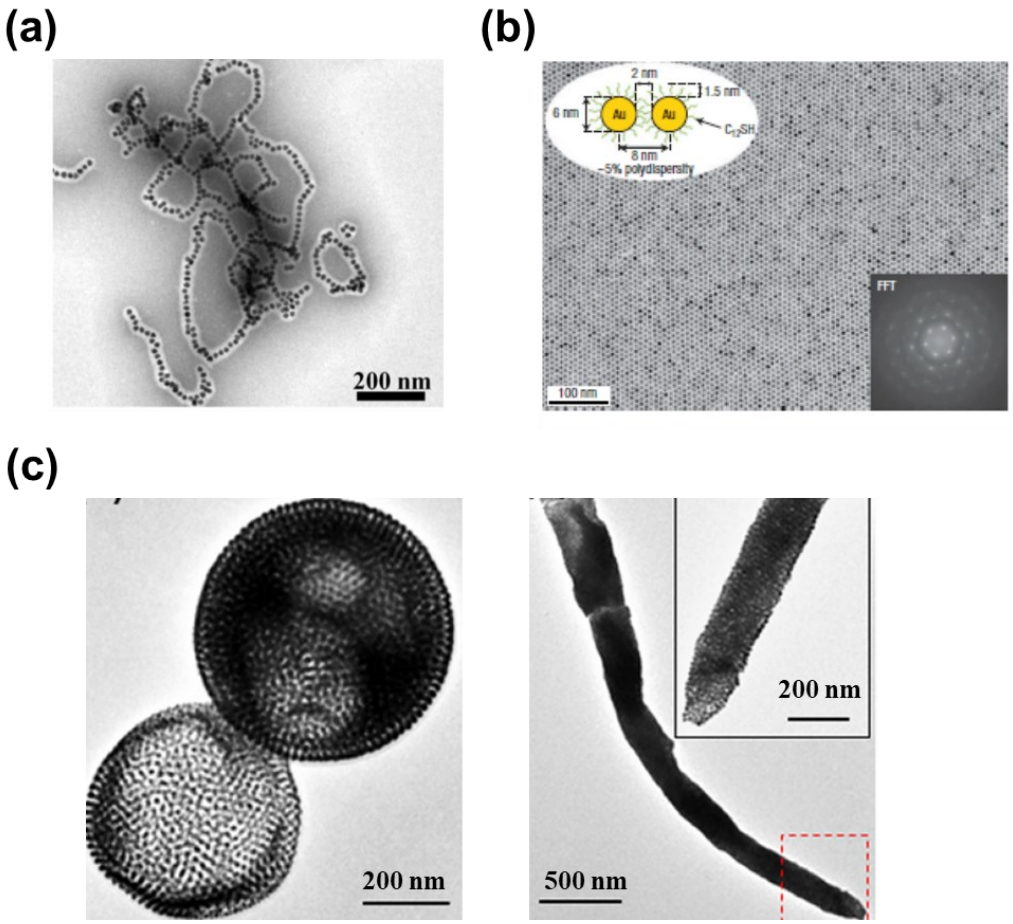

Figure 1-3. Examples of gold nanoparticle assemblies. (a) One-dimensional assembly of gold nanoparticles in a straight line.[15] (b) Two-dimensional assembly on substrates.[18] (c) Three-dimensional assemblies forming a hollow structure (modified from ref [21])

1-3. Properties of rod-shaped gold nanoparticles (gold nanorods; AuNRs) and their control

Gold nanoparticles can be fabricated in a variety of shapes. They can be broadly classified into isotropic gold nanoparticles, such as spherical gold nanoparticles, and anisotropic gold nanoparticles, such as rod-shaped gold nanoparticles and triangular gold nanoparticles. Compared to isotropic gold nanoparticles, anisotropic gold nanoparticles have unique properties.[22,23] For example, rod-shaped gold nanoparticles (gold nanorods; AuNRs) have two plasmon absorption peaks: transverse-localized surface plasmon resonance (T-LSPR) originating from the short axis and longitudinal-localized surface plasmon resonance (L-LSPR) from the long axis (**Figure 1-4**).[24] As the L-LSPR absorption peak wavelength depends on the aspect ratio of the AuNRs, the absorption wavelength range can be tuned from visible to near-infrared light by adjusting the aspect ratio during AuNR fabrication (**Figure 1-5**).[25] When AuNRs are dispersed in solution, the color of the AuNRs depends on the aspect ratio. In addition, AuNRs exhibit different optical properties depending on the angle of the AuNRs in relation to the irradiated light due to their anisotropic structure.[26] The L-LSPR intensity of AuNRs varies with the angle of the AuNRs in relation to the incident light (**Figure 1-6**). Therefore, control in AuNR orientation enable effective and controllable light absorption within a specific wavelength range.

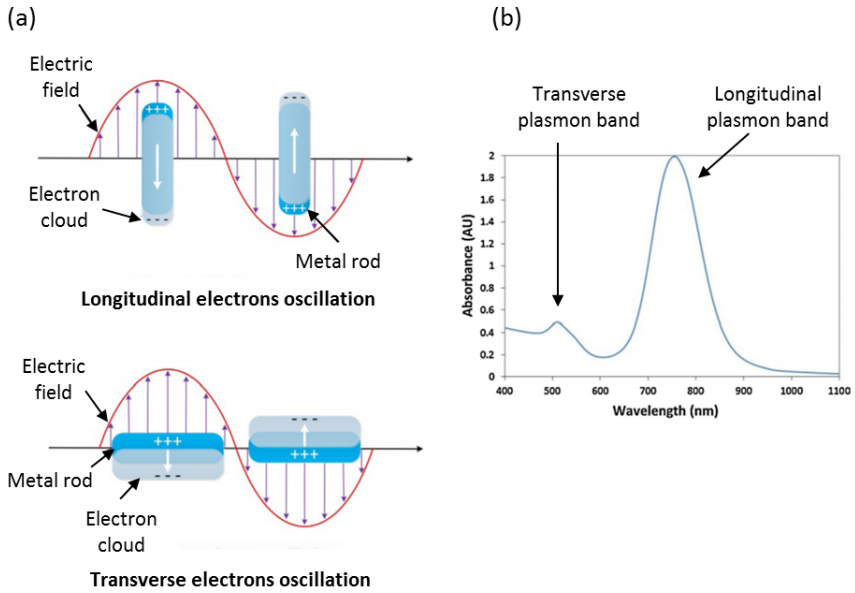

Figure 1-4. Two types of localized surface plasmon resonance (LSPR) exhibited by AuNRs.[27] (a) Electron oscillation in the long (top) or short (bottom) axis direction. (b) Extinction spectra of AuNRs.

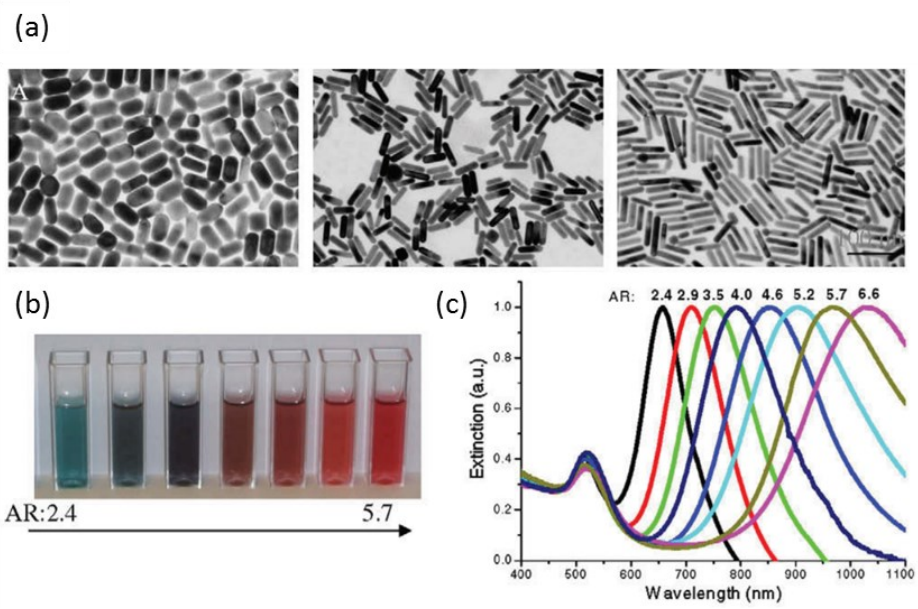

Figure 1-5. Optical properties of AuNRs according to aspect ratio.[28] (a) Scanning transmission electron microscopy (STEM) image of AuNRs. (b) Photographs of AuNR solutions with various aspect ratios. (c) Extinction spectra of AuNRs with different aspect ratios (AR).

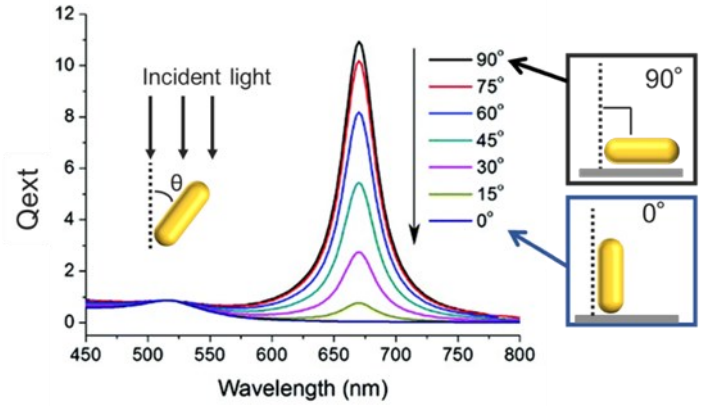

Figure 1-6. Orientation-dependent extinction intensity change of AuNRs in relation to irradiated light.[26]

1-4. Orientation control in AuNRs

In light of recent advancements, multiple techniques to control AuNR orientation have been reported. These techniques can be classified with two types of methods for controlling the orientation of AuNRs. The first approach is to control the orientation of dispersed AuNRs with external stimuli.[29–31] For example, the orientation of AuNRs was successfully controlled with magnetic Fe_3O_4 particles by a magnetic field (**Figure 1-7a**).[32,33] Liu et al. reported a method to control the orientation of AuNRs by an electric field (**Figure 1-7b**).[34] Controlling the orientation of dispersed AuNRs in solution is a relatively simple system because the focus is on the surface modification of the AuNRs or the properties of the solvent, and various other studies have been accomplished in addition to the aforementioned studies.[35–38] However, as gold nanoparticles have a much higher surface energy than atoms or molecules, there are concerns of precipitation or aggregation, which could be obstacle for the application and long-term use.

The second method for orientation control of AuNRs is template-based orientation control. By fixing AuNRs to a template, precipitation and aggregation do not occur, and it is expected to be more suitable for long-term operation of devices and various environments. The templates used for AuNRs are (i) hard templates[39–46] and (ii) soft templates such as gels[47] and elastomers.[26,48–50] One of the representative study using hard template is to align AuNRs in one direction applying AuNR onto a template with nano-sized holes (**Figure 1-7c**).[40] By using a hard template, the position, density, and angle of AuNRs can be precisely fixed. However, the hard template is not suitable for dynamic orientation control of AuNRs because AuNR orientation cannot be moved after fixing the AuNRs. For soft template-mediated orientation control, studies have been reported in which AuNRs are embedded in polymers and the orientation of the AuNRs is

changed by stretching the polymer (**Figure 1-7d**).[48,50] Although dynamic change in the AuNR orientation is possible by using the soft templates, the method using polymer stretching is not suitable for application to nano-optical materials because it requires a large area of operation.

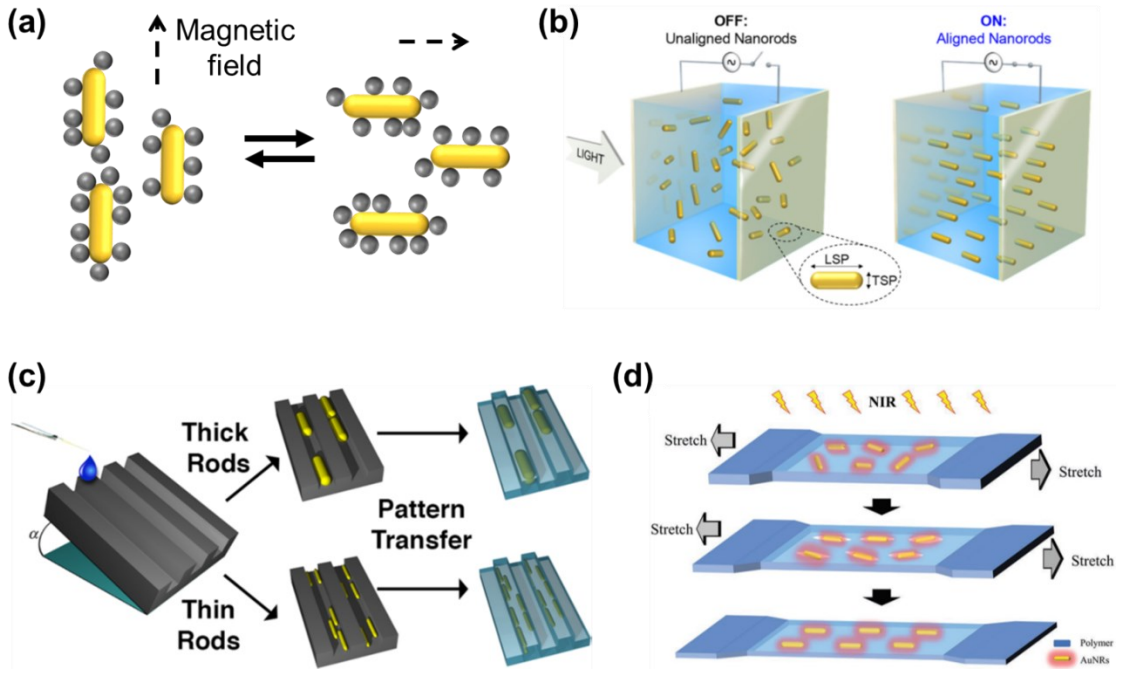

Figure 1-7. (a-b) Orientation control methods for dispersed AuNRs: (a) Alignment control by magnetic field using magnetic particles.[32,33] (b) Orientation switching between aligned/dispersed orientation by electric field.[35]
(c-d) Orientation control methods for immobilized AuNRs on solid substrates: (c) Alignment control using patterned templates.[40] (d) orientation change using stretching of soft matter.[48]

1-5. Orientation control in AuNRs with polymer brushes

Among various types of templates, polymer brushes offer greater advantages in terms of nanoscale devices as their nanostructure can be flexibly controlled on solid substrates without extensive size changes.[51–56] Polymer brushes consist of densely grafted polymer chains extending from a solid substrate or interface. These chains are immobilized at one end and extend away from the surface due to steric and/or electrostatic repulsion between polymer chains. These extended polymers are shrunk by addition of poor solvent (**Figure 1-8a**). Addition of electrolyte (e.g. NaCl) also shrink polyelectrolyte brushes (**Figure 1-8b**).[57] Not only shrink/extend dynamics, but distortion of brushes is also induced by addition of nanoparticles, and the shape of brushes depends on variety of factors such as particle size,[58,59] brush-particle interaction strength (**Figure 1-8c**).[60]

In recent years, controlling the assembly of gold nanoparticles on the surface of polymer brushes[53,55,61–65] and controlling the position of gold nanoparticles using the structural change of polymer brushes[52,66–73] have been investigated. However, control in the orientation of anisotropic gold nanoparticles such as AuNRs have not been accomplished. When the orientation control of AuNRs can be achieved using a polymer brush as a template, it will open up new approaches to regulation of plasmonic properties on solid substrates without requiring a large operating area and energy consumption.

In previous study in our group, DNA polymer brushes (DNA brushes) were prepared by immobilizing DNA on substrates, and AuNRs were successfully aligned in the double-stranded DNA (dsDNA) brushes.[74] Adjustment of the strength of electrostatic interactions between cationic AuNR and dsDNA via tuning of cationic amount around its surface allowed the AuNRs to be attached along with DNA polymer, resulting in perpendicular orientation to the substrates. On the other hand, highly cationic AuNRs

showed a tilted orientation, possibly due to the conformational changes in the polymer brushes from excessive interactions strength between the AuNRs and polymers. This research suggests that the electrostatic interaction strength between AuNRs and polymers critically affects the AuNR orientation (**Figure 1-9**).

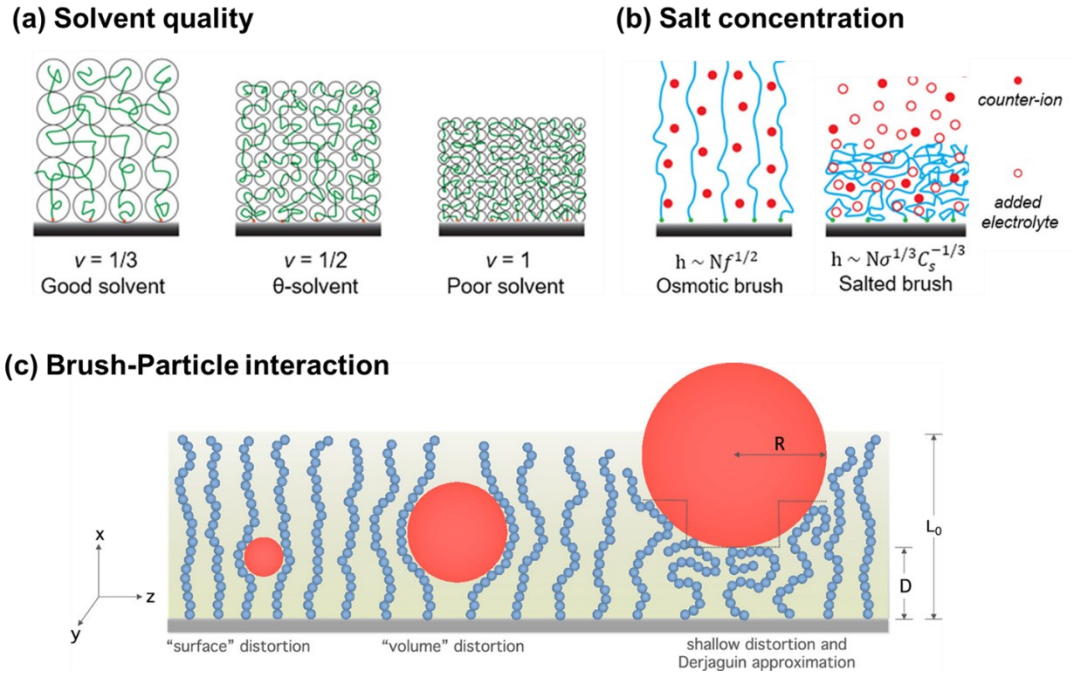

Figure 1-8. Flexible structural change of polymer brushes with (a) solvent quality (b) salt concentration,[57] and (c) brush-particle interaction.[59]

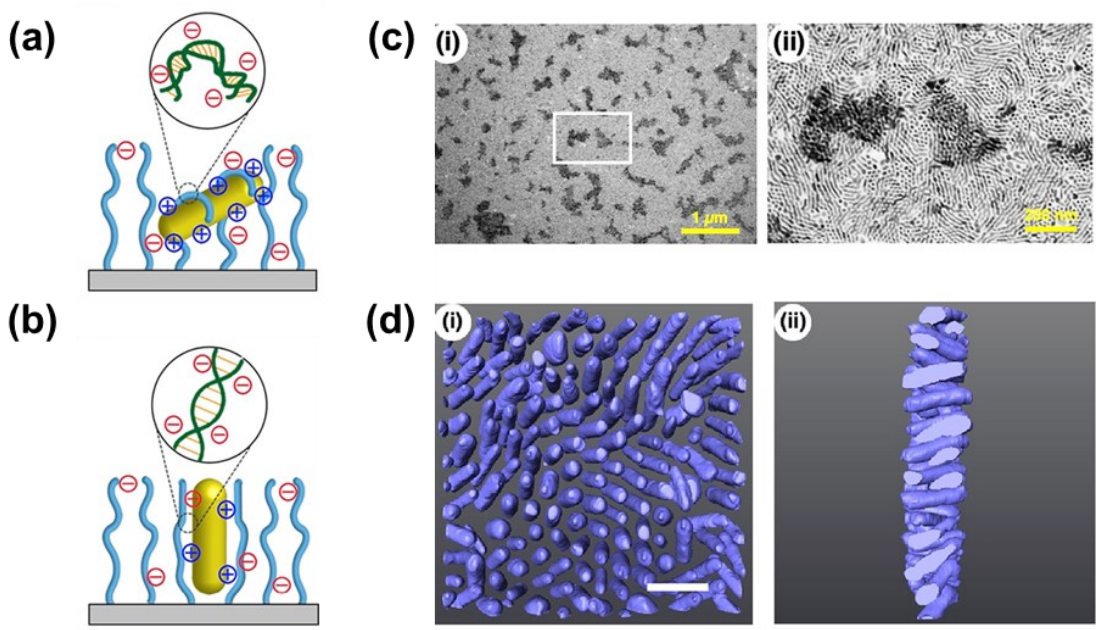

Figure 1-9. Previous study of AuNR alignment with DNA brushes in our lab.[75] Schematic illustration of the attached AuNR in DNA brushes with AuNR surface modification by (a) high-cationic charge density and (b) mild-cationic charge density. (c) STEM (bright-field) image of vertical AuNR arrays in the 148 bp DNA brushes. (i) Large-area image with a 1 μm scale bar. (ii) Magnified inside the white frame marked in (i). The scale bar represents 200 nm. (d) Electron tomography reconstructed images of vertical AuNR arrays in the 148 bp DNA brushes. (i) Front view and (ii) cross-sectional view. The scale bar represents 50 nm.

1-6. Objective

Once polymer brush-mediated dynamic orientation control is established, the platform will contribute to the flexible manipulation of nanomaterials through a bottom-up approach. Thus, building on the AuNR alignment strategy with DNA brushes in the previous research, I focused on dynamic orientation control of AuNRs with the support of polymer brushes as templates (**Figure 1-10**).

In Chapter 2, I focused on DNA-AuNR interaction strength to change AuNR orientation. I prepared cationic AuNRs coated with alkane thiol ligands, including 10% with the primary amino group at the terminus, and investigated their changes in orientation on the DNA brushes composed of either double- or single-stranded DNAs as rigid and flexible anionic polymers, respectively, via changes in their surface potential through variations in solution pH.

In Chapter 3, I demonstrate dynamic changes in AuNR orientation via changes in the thickness of polymer brushes. Here, single-stranded DNA (ssDNA) was used as DNA possesses a monodispersed chain length and the structure changes in DNA brushes have been extensively investigated in previous reports.[76–79] Salt concentration changes were used to control the brush thickness. Then, orientation of the AuNRs embedded in the DNA brushes against brush thickness was investigated for varied DNA lengths, salt types, and AuNR lengths, providing a general insight into the stimuli-responsive control of AuNR orientation on the substrates via changes in the thickness of polymer brushes.

In Chapter 4, to expand the applicability of the dynamic orientation control system, I fabricated poly(styrene sulfonate) brushes with tuning of their density and thickness, and show reversible orientation changes in AuNRs in the PSS brushes with their shrinkage and extension. I synthetized PSS brushes by “grafting-from” method, in which

polymerization is conducted on substrates. With suitable density of PSS brushes, the AuNRs attached to the PSS brushes were aligned. Further, Dynamic orientation change in AuNRs was achieved through shrinkage/extension of the PSS brushes.

In Chapter 5, I summarize the thesis and afford the significance and prospects.

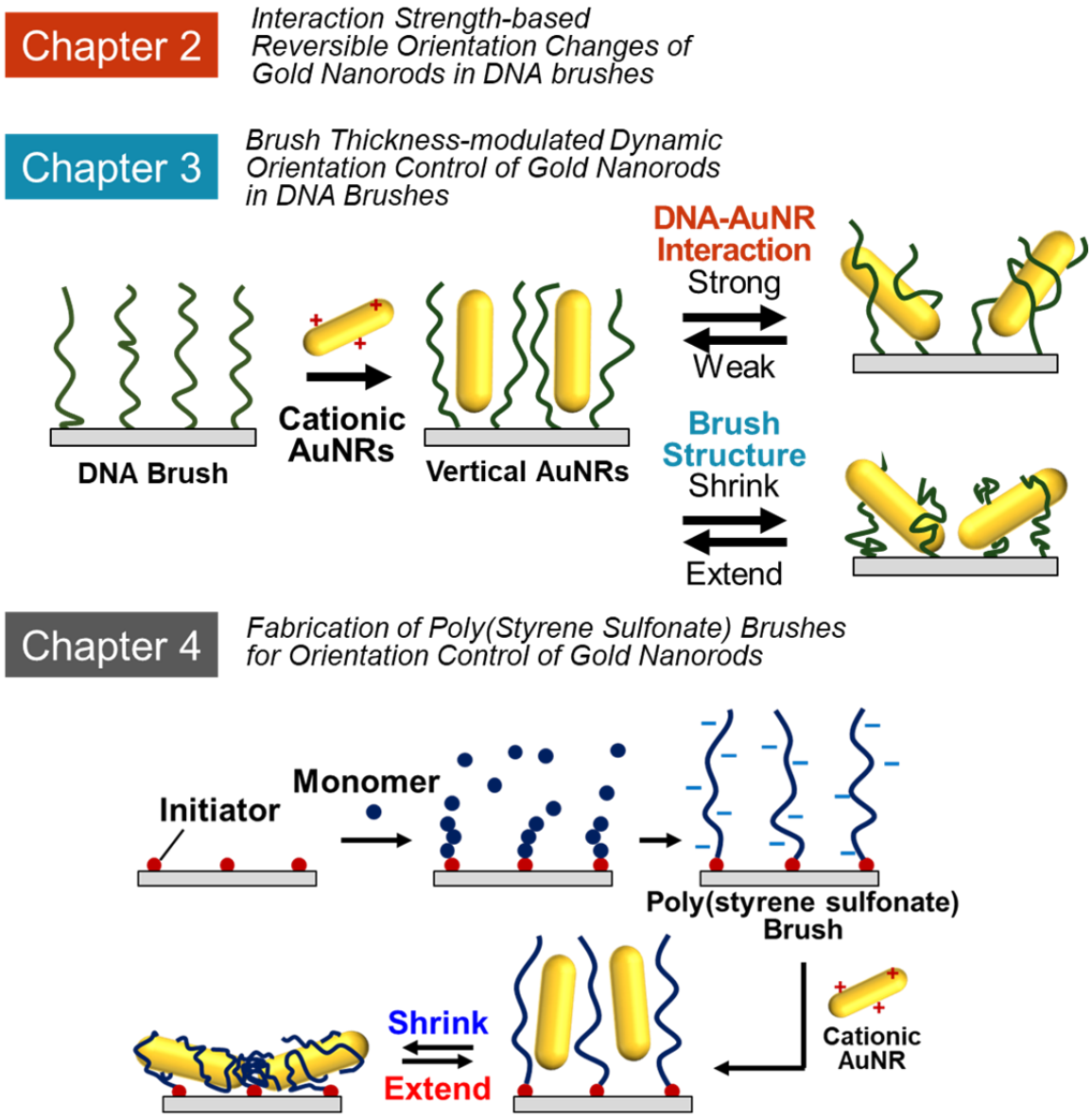

Figure 1-10. Schematic illustration of my doctoral thesis

Chapter 2

Interaction Strength-based Reversible Orientation Changes of Gold Nanorods in DNA brushes

2-1. Introduction

Nanoparticles exhibit a number of unique optical, magnetic, and electronic properties. One notable example of these properties is localized surface plasmon resonance (LSPR), which is induced by strong light-metal interactions, on metal nanoparticles. As LSPR is sensitive to geometrical or spatial conditions, the arrangement of metal nanoparticles is an important issue.[80–87] Recently, the active arrangement (reversible tuning) of plasmonic structures has attracted a good deal of attention as a challenging new field.[88–91] This arrangement is classified broadly into two approaches; gold nanoparticles (AuNPs) are controlled as (i) dispersions in a solution or (ii) on/in substrates. At typical example of the former approach is stimuli-responsive assembly/disassembly using temperature-[92–94], pH-[95–97], and photo-responsive[98,99] AuNPs. For gold nanorods (AuNRs), which exhibit two specific plasmonic absorptions for transverse and longitudinal localized surface plasmon resonance (T- and L-LSPR), factors related to their control become more complicated.[100] As there are two types of ordering of the assembled structures, known as side-by-side and end-to-end assembly causing blue-shift and red-shift of L-LSPR, respectively, the assembly configuration must be properly controlled.[101–103] The orientation of AuNRs to the incident light is also a significant factor in L-LSPR excitation. Thus, the active control of AuNR orientation when dispersed in solution was performed with the aid of a liquid crystal[104], magnetic nanoparticles[105], and the application of an electric field[106]. On the other hand, arrays fabricated on substrates provide an excellent platform for practical applications due to the various advantages in terms of their ease of handling, long-term stability, and so on. Thus, the latter approach, such as the embedding into or attachment onto soft materials such as elastomers and gels as a supporting matrix, is promising in that it allows their distances

to be tuned through stretching or compressing the matrices by mechanical forces[107–109] or the changing of the matrix volume through variations in the swelling conditions. [110–112] These changes in matrix shape were also applied to actively change the AuNR orientations.[113] From the viewpoint of applications, arrays on the solid substrates are more preferable.[86,87] Therefore, polymer brushes, which is consist of a soft matrix attached on a solid substrate, are the best candidate. To date, a number of actively tunable plasmonic arrays based on changes in distance using spherical nanoparticles have been reported.[111,114–116] However, there are no reports of the active control of AuNR orientation using polymer brushes on the solid substrates, despite its obvious importance.

In previous study in our lab, a method for the vertical alignment of AuNRs using polymer brushes as a template has developed as mentioned above (**Figure 1-9**).[75,117] As the polymer brushes are soft matrices, it is expected that the AuNR orientation can be actively tuned through some kinds of stimulation. In those reports, AuNRs formed vertically aligned arrays when mildly cationized AuNRs were attached on negatively charged polymer (DNA) brushes via moderate electrostatic interactions. On the other hand, highly cationic AuNRs showed a tilted orientation, probably due to the conformational changes in the polymer brushes from too strong interactions between the AuNRs and polymers. This finding suggests that modulation of the electrostatic interactions between AuNRs and polymers can induce reversible changes in the AuNR orientation between the vertical and non-vertical on solid substrates. Thus, in this study, I prepared cationic AuNRs coated with alkane thiol ligands, including 10% with the primary amino group at the terminus, and investigated their changes in orientation on the polymer brushes composed of double- and single-stranded DNAs as rigid and flexible

anionic polymers, respectively, via changes in their surface potential through variations in solution pH (**Figure 2-1**).

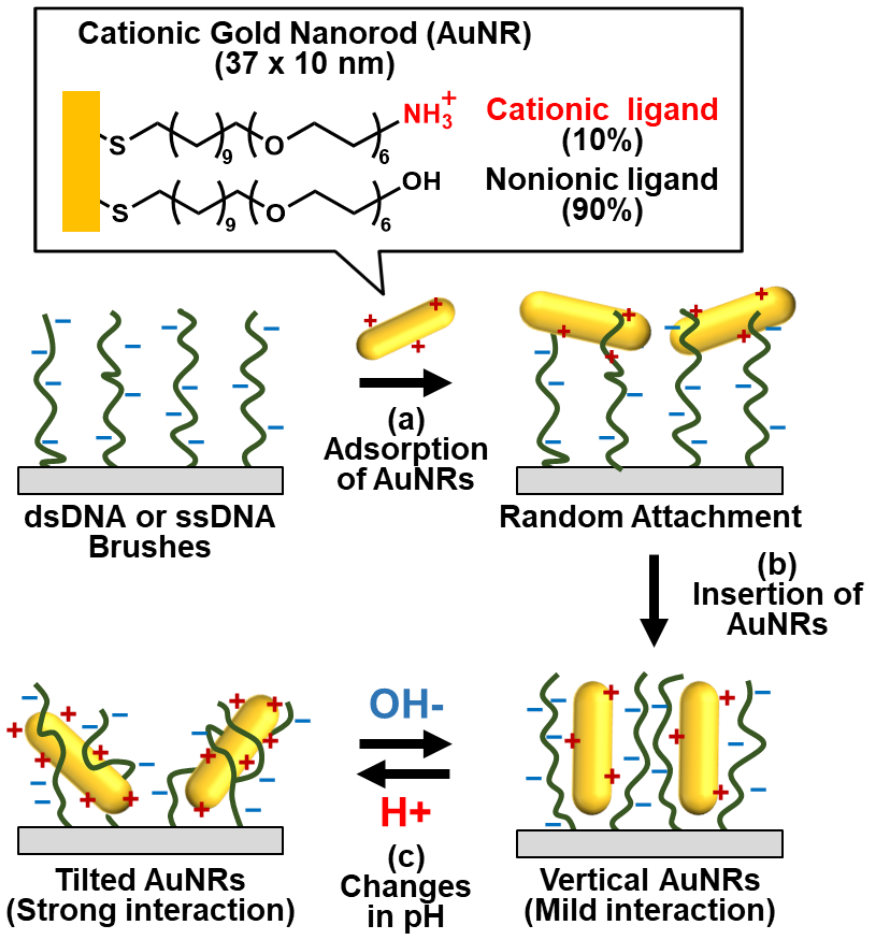

Figure 2-1. Preparation of vertical gold nanorod arrays and their pH-responsive changes in orientation.

2-2. Experimental section

2-2-1. Materials and Instruments

20-(11-Mercaptoundecanyloxy)-3,6,9,12,15,18-hexaoxaeicosane-1-amine, hydrochloride ($NH_2EG_6C_{11}$), 11-Mercaptoundecanol hexaethyleneglycol ether ($OHEG_6C_{11}$), and 1-Ethyl-3-(3-dimethylaminopropyl) carbodiimide, hydrochloride (EDC) were purchased from Dojindo Laboratories (Japan). 2-[4-(2-Hydrixyethyl)-1-piperazinyl] ethanesulfonic acid (HEPES), $HAuCl_4 \cdot 3H_2O$ and $NaBH_4$ were purchased from Sigma-Aldrich, Inc. (USA). 2-(Carbomethoxy)ethyltrichlorosilane (CMETS) was purchased from Fluorochem, Ltd. (U.K.). Amine-PEG_2-Biotin was purchased from Thermo Fisher Scientific, Inc. (USA). All other salts and reagents were purchased from Wako Pure Chemical Industries, Ltd. (Japan) unless otherwise specified. Ultrapure water (18.2 MΩ/cm, Milli-Q, Millipore) was used to prepare all solutions. Cuvettes with an optical path length of 1 mm were purchased from TOSOH Co., Ltd. (Japan). Oligonucleotides are purchased from Thermo Fisher Scientific, Inc. (USA) or Integrated DNA Technologies, Inc (USA). The sequences of the oligonucleotide and the chemical structure of the linker between DNA and modification site are shown in **Table 2-1**.

Table 2-1. Oligonucleotides sequences used in chapter 2.

Description	Sequence（5'→3'）
Biotin-Primer	biotin-GAGCCCGTCGCCATCGACTTACG
Alexa647-Primer	Alexa647-GAGCCCGTCGAGAATACTGGC
Biotin-T148	Biotin-T_{148}

λ-DNA was purchased from Nippon Gene Co., Ltd. (Japan). QIA quick PCR Purification Kit was purchased from Qiagen, Inc. (Germany). PCR was performed with Life Pro thermal cycler (Bioer Technology Co., Ltd). Extinction spectra were recorded with a V-730 or V-770 UV-vis spectrometer (JASCO Corp., Japan). Fluorescence intensity measurements were performed with a Pharos FX Molecular Imager (Bio-Rad Laboratories Inc., USA). Scanning transmission electron microscopic (STEM) images were obtained using a STEM HD-2000 system (Hitachi High-Tech Manufacturing & Service Co., Ltd., Japan) with a 200 kV acceleration voltage. The zeta-potentials of cationic AuNRs and DNAs were measured with a Zetasizer Nano ZS (Malvern Panalytical Ltd. UK). The circular dichroism (CD) spectra of dsDNA brushes were measured with a J-820 system (JASCO Corp., Japan) with 10-times integration. The buffers used in this study were as followings; 10 mM acetate buffer (pH4.0, 4.5, 5.0, and 5.5), 10 mM 2-(N-morpholino)ethanesulfonic acid (MES) buffer (pH 6.0 and 6.5), and 10 mM Tris(hydroxymethyl)aminomethane (Tris-HCl) buffer (pH 7.0 and 7.6).

2-2-2. Preparation of AuNRs (36 × 10 nm)

AuNRs (36 × 10 nm) were synthesized using the seed-mediated method with slight modification.[118] Gold seed particles were firstly prepared by a standard reduction process. Under gentle shaking, a 0.01 M ice-cold $NaBH_4$ solution (600 μL) was added to a mixture of a 0.01 M $HAuCl_4 \cdot 3H_2O$ solution (250 μL) and a 0.1 M CTAB solution (7.5 mL). The seed solution was then kept in an incubator (30°C) for 2 h. For the growth reaction, growth solutions were prepared from a 0.1 M CTAB solution (38 mL) by adding a 0.01 M $HAuCl_4 \cdot 3H_2O$ solution (1.6 mL), a 0.01 M $AgNO_3$ solution (240 μL), and an 0.1 M ascorbic acid solution (256 μL), in this order. The gold seed solutions (320 μL) were injected to the growth solutions, while the growth solution was stirred gently. Then, the growth solutions were left undisturbed in an incubator (30°C) for at least 3 h. The AuNR solution was stored under 30°C. For TEM measurement, the remaining CTAB and other reagents were diluted 1000-fold by two-times centrifugation (18,000 g, 20 min, 30°C) before dropping onto a TEM grid.

2-2-3. Surface modification of AuNRs with two types of thiol-ligands

Cationic ligands ($NH_2EG_6C_{11}$) and nonionic ligands ($OHEG_6C_{11}$) were dissolved in methanol. The two types of ligand solutions were mixed, adjusting the total ligand concentration (10 mM). The percentages of cationic ligands were 10%. Before adding ligand solution to the AuNR solution, the AuNR solution (1 mL) were centrifuged (18,000 g, 20 min, 30°C), and MilliQ-water (940 μL) was added after the supernatant (940 μL) was removed. This centrifugal purification procedure was repeated twice so that the CTAB concentration was approximately 0.36 mM, a concentration suitable for ligand modification. After purification, the mixed ligand solution (50 μL) was added to the purified AuNR solution (950 μL) in a 1.7 mL plastic tube. The AuNR solution with the

ligands was vortexed and kept undisturbed at 42°C for at least 12 h. Next, the AuNR solution (1,000 μL) was centrifuged (18,000 g, 20 min, 25°C), the supernatant (950 μL) was removed, and MilliQ-water (950 μL) was added, and the solution was then vortexed. This purification procedure was performed twice. Finally, to obtain a concentrated AuNR solution, the AuNR solution was centrifuged (18,000 g, 20 min, 25°C), and the supernatant (700 μL) was removed.

2-2-4. Evaluation of pH responsiveness of AuNRs

The surface-modified AuNR dispersion (200 μL), buffer (Acetate buffer, MES buffer, and Tris-HCl buffer were used depending on the pH range) and MilliQ water (700 μL) were mixed. The surface charge of the prepared AuNRs was evaluated by zeta potential measurement, and the dispersion state was evaluated by extinction spectrum measurement.

2-2-5. Fabrication of the streptavidin-modified substrate

The streptavidin-modified substrate was prepared using an established method as described in our previous paper.[74,75,119] Briefly, carboxylic acid on the inner wall of a cuvette was reacted with amine-PEG_2-biotin in water including EDC. After washing unreacted reagents with 10 mM Tris-HCl (pH 7.6), streptavidin was immobilized on the substrate through avidin-biotin interactions.

2-2-6. Immobilization of DNA polymers onto the streptavidin surface

The streptavidin-modified substrate was immersed in a 10 mM Tris-HCl solution with biotin-modified ssDNA (2 μM) and NaCl (1 M) for 2 h to fabricate DNA brushes. After the reaction, the solution was taken out from the cuvette, and unreacted DNA was washed out by adding and removing 10 mM Tris-HCl at least three times.

2-2-7. Calculation of the density of the DNA polymer brushes

The amounts of 148-bp dsDNA on the substrates were calculated from the fluorescence intensities of Alexa 647 modified with the 3' side of ssDNA and the peak absorption intensity at 260 nm. For 148-base ssDNA modified substrates, the peak absorption intensity of DNA at 260 nm was utilized to quantify DNA brush densities. Density evaluation of DNA brushes was performed according to the following calculation formula.

Considering that DNA is immobilized on both sides inside the cuvettes, the relationship between the DNA concentration in the cuvettes and the immobilization density of the DNA polymer brush is as follows:

$$\sigma = \frac{C \times V \times N_A}{S}$$

where σ is DNA immobilization density, C is the DNA concentration in cuvettes, V is the volume of the solution, N_A is the Avogadro constant, and S is surface area of the substrate on which DNA is immobilized.

To calculate the interchain distance of DNA, I assume that the DNA molecules are arranged in a hexagonal close-packed pattern. From the estimation, the interchain distance (D_{DNA}) can be calculated by the following formula:

$$D_{\mathrm{DNA}} = \sqrt{\frac{\sqrt{3}}{\sigma \times 2}}$$

From the above calculations, the density of DNA brushes and the distance between DNAs were obtained.

2-2-8. Attachment of ligand-modified AuNRs onto DNA polymer brushes

The thiol ligand-capped AuNR (cationic AuNR) solution was poured into the inner wall of DNA brush cuvettes. After 10 min incubation, the solution was removed using a pipette

and the cuvette was rinsed with a 10 mM Tris-HCl (pH 7.6) solution at least 3 times to completely wash out non-adsorbed AuNRs from the cuvette.

2-2-9. Investigation of the pH-dependent AuNR orientation change

To change pH condition, the solution on the AuNR-adsorbed DNA brush substrate was replaced with another solution with a different pH after washing with the latter solution more than 3 times by pipetting to change the environment completely. In the extinction spectrum analysis, the incident light was non-polarized and its direction was perpendicular to the cuvette containing the adsorbed AuNRs unless otherwise specified.

2-3. Results and Discussion

2-3-1. pH-responsive reversible orientation change of AuNR arrays on double-stranded DNA brushes

First, I prepared vertically aligned AuNR arrays using double-stranded DNA (dsDNA) brushes as a template according to our previous paper.[75] Briefly, after streptavidin immobilization at the quartz surfaces, biotinylated dsDNA, which has a 148-bp random sequence, was immobilized through avidin-biotin interactions, providing dsDNA brush substrates. The DNA density was calculated as ca. 21000 ± 2900 chains/μm^2 (7.5 ± 0.5 nm as an average DNA interchain distance) (**Figure 2-2**). Then, cationic AuNRs (37 × 10 nm) were attached on the DNA brushes via electrostatic interactions in Milli-Q water (**Figure 2-1a**, **Figure 2-3**). When the solution was changed to the buffer (10 mM Tris-HCl, pH7.6), the L-LSPR peak around 800 nm gradually decreased over several hours without any significant changes in the extinction of T-LSPR around 520 nm (**Figure 2-4a**). This decrease in the L-LSPR-specific peak indicates a change in the alignment of AuNRs from random to vertical as it originates from the angle dependence against incident light as mentioned above (**Figure 2-1b**). The extinction spectra under polarized light strongly support the vertical alignment of AuNRs in the buffer solution (**Figure 2-4b**).[117] A p-polarized light-specific L-LSPR peak can be observed around 640 nm (highlighted in yellow). This blue-shift from the original L-LSPR peak at around 800 nm indicates plasmon coupling in a side-by-side configuration, which also supports vertical array formation. Based on our previous simulation, I estimate the center-to-center distance of the 10-nm AuNRs to be ca. 30 nm (a gap distance of ca. 20 nm).[117] Further, as the extinction value at 400 nm is a simple indicator of the amount of AuNRs due to their absorption and scattering, I evaluated the AuNR density on this array to be ca. 1500

particles/μm^2 on 21,000 chains/μm^2 dsDNA brushes by a comparison of the absorption value in **Figure 2-1a** with that in our previous report.[75] In addition, the vertically aligned arrays after incubation in buffer (pH 7.6) did not show any spectral change on replacement of the solution back to Milli-Q water (**Figure 2-4c**). These results indicated the successful preparation of vertically aligned arrays with enough free spaces around each AuNR to afford an energetically stable configuration (**Figure 2-1b**). Next, I examined the changes by the replacement of buffer solutions. When pH fell to pH 4.0, the L-LSPR peak at around 800 nm increased tremendously together with a slight decrease in the T-LSPR peak at around 520 nm (**Figure 2-4d**). As explained above, this increase in L-LSPR intensity indicates that the vertical alignment of the AuNRs was changed to a tilted alignment due to the change in pH.[117] For quantitative discussion, the extinction value was normalized as the ratio of extinction at L-LSPR/extinction at T-LSPR ($E_{\text{L-LSPR}}/E_{\text{T-LSPR}}$). On changing the pH from 7.6 to 4.0, $E_{\text{L-LSPR}}/E_{\text{T-LSPR}}$ changed from 0.27 to 2.2. As this change is thought to include plasmon coupling effects, it is difficult to estimate the tilt angles. However, this is quite a large change compared to those in the previous papers on dispersed AuNR orientation tuning by magnetic or electric fields, even though the AuNRs were immobilized on polymer brushes in our system.[105,106] Importantly, this pH-responsive change in intensity (orientation) is very quick (about a second) and reversible for at least several cycles (**Figure 2-1c**, **Figure 2-4e, and Figure 2-5**).

A more detailed investigation on the pH-responsiveness was next performed (**Figure 2-6**). When the pH was decreased from 7.6 to 4.0, the L-LSPR intensity increased, especially between pH 4.5 and 4.0 (**Figure 2-6a**). Also, when the pH was increased from 4.0 to 7.6, the L-LSPR intensity decreased, especially between 4.5 and 5.5, and returned to the original intensity at pH 6.0 (**Figure 2-6b**). The L-LSPR intensities with regard to

change in pH are plotted in **Figure 2-6c**, which shows that the L-LSPR changed markedly between pH 4.0 and 5.5. It is a noteworthy fact that there is a clear hysteresis. As the pH decreases, amino groups at the AuNR surface are protonated and form ionic bonds with the DNA. As the system gains a large energetic merits from this ionic bond formation, it becomes energetically more stable. When this energy gain is larger than the energy loss from DNA bending or disarrangement, the DNA configuration is thought to change, causing a change in AuNR orientation. This kind of energetic relationship is supported by theoretical reports.[120] On the other hand, as the pH increases, amino groups at the AuNR surface are deprotonated and their ionic bonding is disrupted, causing changes in both the DNA and AuNR configuration via energy loss and gain. Thus, it is expected that these energy gain-loss relationships, which represent energetically different pathways, can explain the observed hysteresis. In other words, this hysteresis supports the notion that the AuNR orientation can be tuned by changes in the interactions between the anionic polymers and moderately cationic coated AuNRs on the dsDNA brushes.

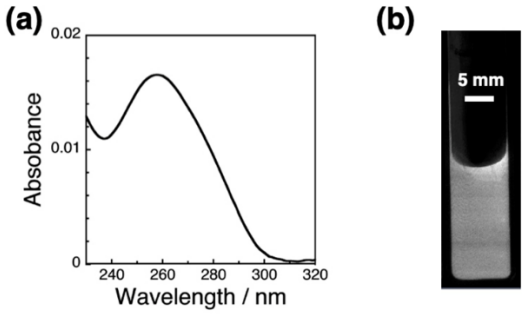

Figure 2-2. Absorption spectrum (a) and fluorescent image (b) of the dsDNA brushes. The DNA density was calculated as ca. 21000 ± 2900 chains/μm^2 (7.5 ± 0.5 nm as an average DNA interchain distance) from the absorbance at 260 nm and ca. 25,000 ± 1900 chains/μm^2 (6.8 ± 0.3 nm as an average DNA interchain distance) from the fluorescence intensity of Alexa Fluor 647 at the terminus, respectively, according to our previous report.[75]

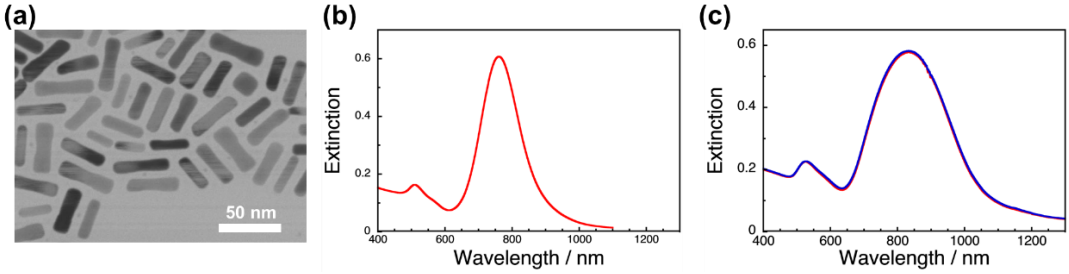

Figure 2-3. STEM image (a) and extinction spectrum (b) of prepared AuNRs. (c) Extinction spectrum of adsorbed AuNRs on dsDNA brushes in Milli-Q water. AuNR size was determined as 9.9 ± 2.0 nm in diameter and 37 ± 4.7 nm in length (300 particles counted). Extinction spectra did not show any changes after incubation for 12h (blue) in Milli-Q water, suggesting a kinetically stable AuNR configuration in a random orientation. Broadening of this L-LSPR peak was expected to derive from plasmon coupling effects on a random distribution.

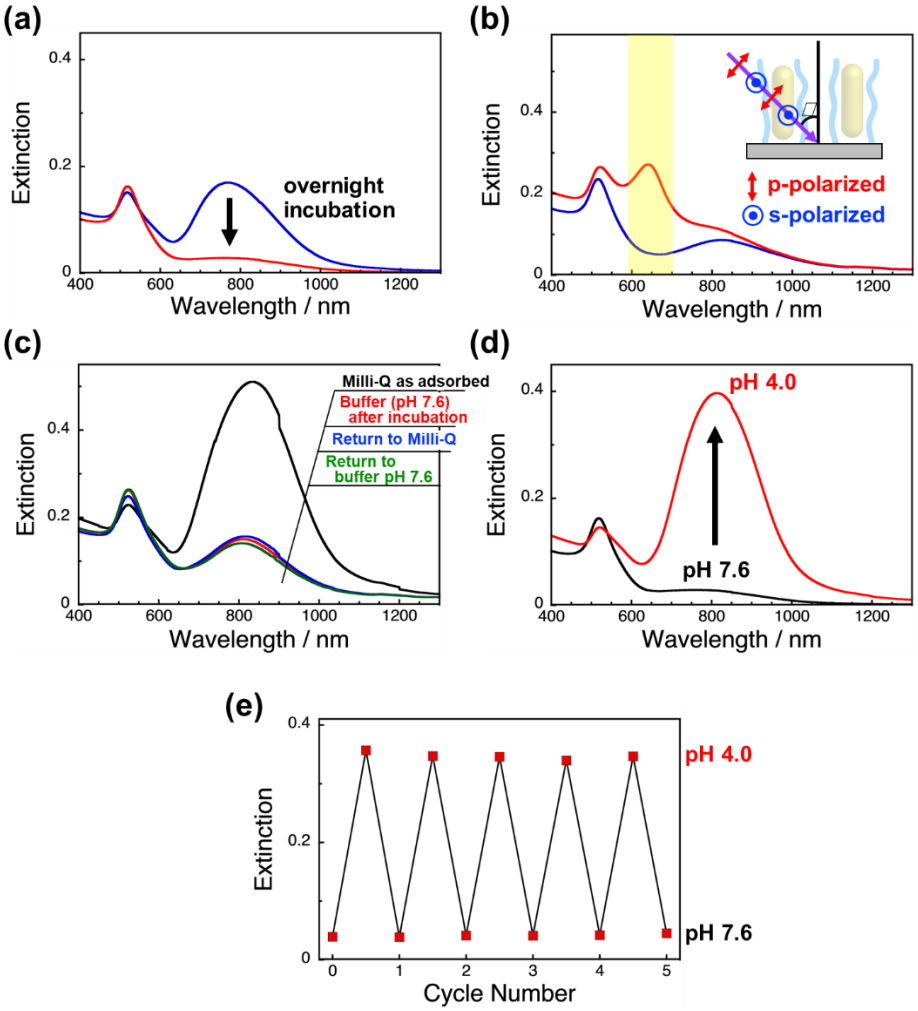

Figure 2-4. Extinction spectra of AuNRs attached on dsDNA brushes. (a) Time-dependent spectral change after replacement of the solution with the buffer; soon after replacement (blue) and after overnight incubation (red). (b) Extinction spectra after overnight incubation measured under p-polarized (red) and s-polarized light (blue) at θ = 45°, where θ is the angle of the incident light to the substrate. (c) Extinction spectra of AuNRs attached on the dsDNA brushes as adsorbed in Milli-Q water (black), after overnight incubation in 10 mM Tris-HCl buffer, pH 7.6, (red), return to Milli-Q water after incubation in the buffer (blue), and return to buffer again (green). (d) Extinction spectra for a change in pH from 7.6 (black) to 4.0 (red). (e) Extinction values for the L-LSPR peak for repeated changes of pH between 7.6 and 4.0.

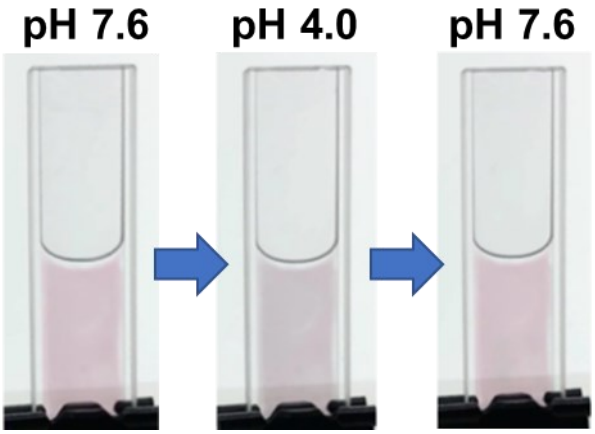

Figure 2-5. Snapshot of pH-responsive color changes for the AuNRs attached on the dsDNA brushes. The color change is not drastic because the large spectral changes are observed in Near-IR region.

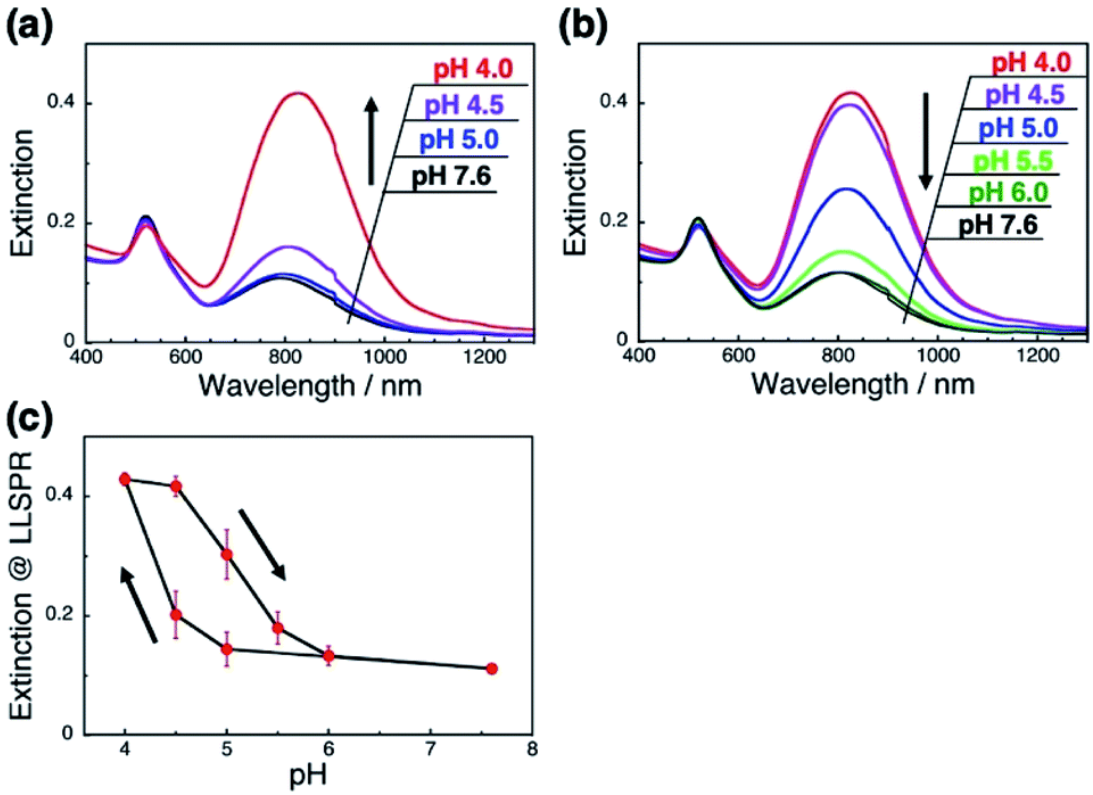

Figure 2-6. pH-Responsive spectral changes for the AuNRs on dsDNA brushes. (a) A decrease in pH from 7.6 to 4.0. (b) An increase in pH from 4.0 to 7.6. Spectra are shown in black (pH 7.6), green (pH 6.0), light green (pH 5.5), blue (pH 5.0), purple (pH 4.5), and red (pH 4.0). (c) Extinction values for the L-LSPR peak according to pH. Error bars represent standard deviation of 3 repeated cycles.

2-3-2. Mechanism of pH-responsive orientation change of AuNR arrays on dsDNA brushes

To clarify the mechanism underlying this pH-responsive change in AuNR orientation on dsDNA brushes, I investigated the zeta-potential of the cationic AuNRs and dsDNA in these buffers, as the electrostatic interactions between the DNA and AuNRs are important for their vertical orientation.[117] The zeta-potentials of the cationic AuNRs gradually increased from +1 to +15 mV as the pH decreased from 10 to 4.0 (**Figure 2-7a**). This gradual increase is thought to be a nearest neighbor effect of the amino groups.[121,122] On the other hand, as expected, the dsDNA did not show any significant changes in zeta-potential between pH 7.6 and 4.0 (-34 ~ -39 mV) (**Figure 2-7b**). As the change in orientation mostly occurred between pH 4.0 and 5.0, these results suggested that there is another dominant factor, other than the electrostatic interactions between DNA and AuNRs, contributing to change in orientation. Thus, I checked the effects of pH on the LSPR of the AuNRs and the absorption of the DNA by spectroscopy. Cationic AuNRs did not show any changes in extinction spectra (**Figure 2-7c**). On the other hand, the dsDNA on the substrates showed a spectral change in this pH range (**Figure 2-8a, b**). When the pH fell to 4.0, the absorption peak was red shifted from 258 nm to 265 nm and A_{260}/A_{280} also showed a change from ca. 1.8, which is a normal value for dsDNA, to 1.2. It is noticeable that this change was marked between pH 4.0 and 5.0. Further, this spectral change was also reversible (**Figure 2-8c, d**). To obtain more information about the structure of the dsDNA on the substrates, I examined the effects of pH on the circular dichroism (CD) spectra (**Figure 2-8e**). The CD spectra of the dsDNA brushes showed a negative band at around 250 nm and a positive band at around 280 nm under neutral pH conditions. The data indicated that the dsDNA brushes prefer a B-type double-stranded structure on the substrates under neutral buffer solutions (pH 7.6 to 5.0).[123] In sharp

contrast, a drastic change in dsDNA structure was induced by decreasing the pH down to 4.0 from 5.0 as indicated by the CD spectral change. These spectral studies of absorption and CD show that the orientation of the AuNR arrays on the dsDNA brushes was reversible through changes in the solution pH accompanied with DNA conformational changes, suggesting that pH-dependent conformational changes in dsDNA, rather than electrostatic interactions, are a dominant factor contributing to pH-responsive changes in AuNR orientation on dsDNA brushes. It is expected that DNA is too rigid to bend or be rearranged under neutral pH conditions due to their double helical structures; however, when the DNA helix structure is deformed by a decrease in pH (< pH 5), it becomes more flexible and allows changes in AuNR orientation via change in the interactions between the DNA and AuNRs.

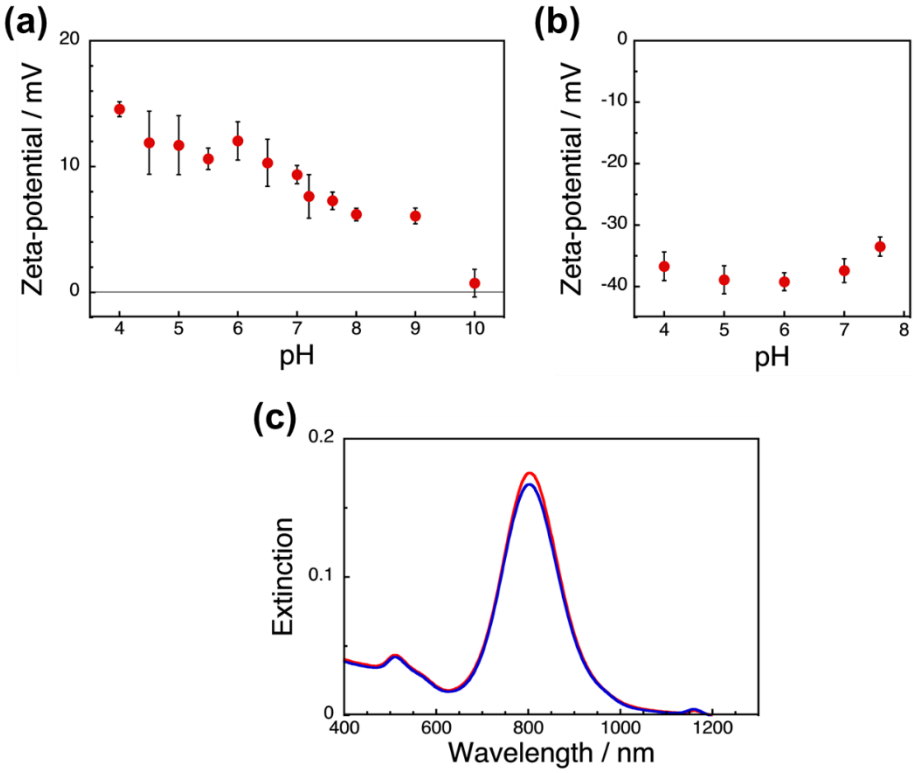

Figure 2-7. (a) Zeta-potential of 10% cationic ligand-modified AuNRs and (b) 148bp-dsDNA in a buffer solution. (c) Extinction spectra of 10% cationic AuNRs at pH 7.6 (blue) and 4.0 (red).

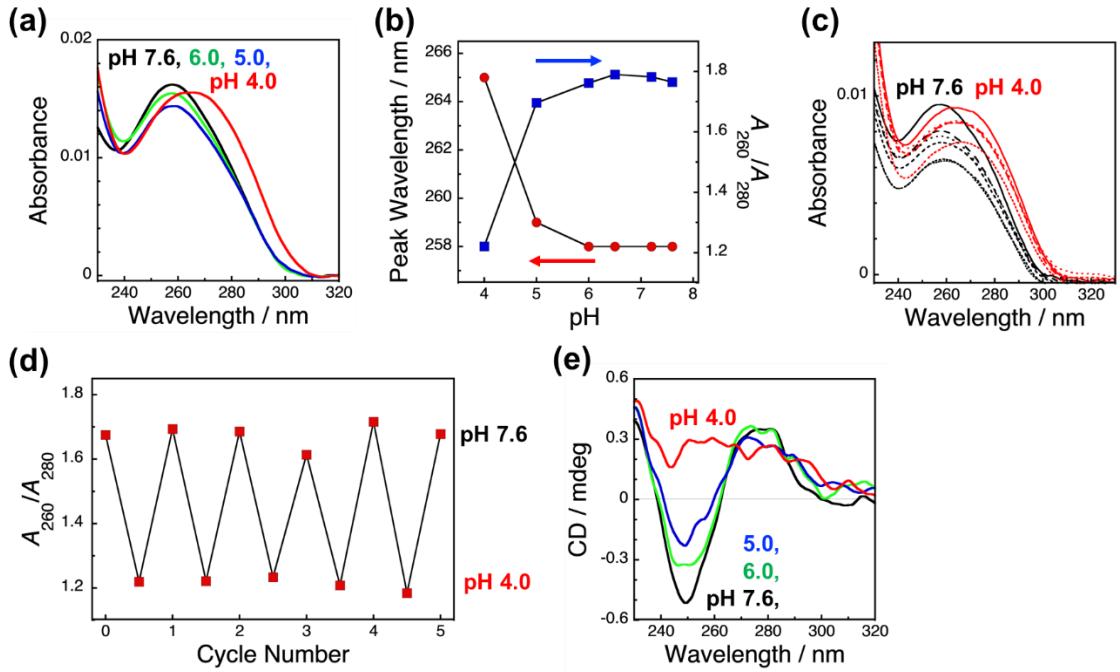

Figure 2-8. (a) Absorption spectra of dsDNA brushes in the buffer at various pH values and (b) the peak wavelength (blue) and absorbance ratio of A_{260} / A_{280} (red) at each pH value. Absorption spectra of dsDNA brushes (c) and absorption ratio as A_{260}/A_{280} (d) on repeated changes in buffer pH from 7.6 to 4.0. (e) Circular dichroism (CD) spectra of dsDNA brushes in the buffer at various pH values. Absorption and CD spectrum at each pH value are shown in black (pH 7.6), light green (pH 6.0), blue (pH 5.0), and red (pH 4.0).

2-3-3. pH-responsive reversible orientation change of AuNR arrays on single-stranded DNA brushes

As it is expected that the rigidity of the polymer is an important factor in the changes in the orientation of AuNRs on polymer brushes, I next applied a flexible polymer to this system. Fortunately, I have already reported that the vertical AuNR alignment can also be performed on the single-stranded DNA (ssDNA) brushes,[75] which are more flexible and share the same lack of well-ordered structures as general synthetic polymers.[124,125] Thus, I investigated the tuning of AuNR orientation by changes in the interactions between polymers and AuNRs on the ssDNA brushes. To avoid any effects of pH on the polymer itself, I used 148-base poly(dT) as the ssDNA. I successfully prepared the ssDNA brushes (**Figure 2-9a**) and vertical AuNR arrays (**Figure 2-10**) by the same procedures as described above. As expected, ssDNA[poly(dT)] did not show any significant changes (shift) in absorption spectra or zeta-potential when the pH was changed between 7.6 and 4.0 (**Figure 2-9b, c**). When the pH was decreased from 7.6 to 4.0, the L-LSPR intensity gradually increased, suggesting a gradual change in AuNR orientation (**Figure 2-11a**). Also, when the pH was increased from 4.0 to 7.6, the L-LSPR intensity decreased and returned to the original value (**Figure 2-11b**). The L-LSPR intensities with regard to the changes in pH were plotted in **Figure 2-11c**, which shows that L-LSPR markedly changed between pH 4.0 and 6.5. This spectral change is gentler and in a wider pH range than that observed for dsDNA. This is well correlated with the changes in zeta-potential according to pH (**Figure 2-7a**). A clear hysteresis was also observed as with the dsDNA brushes. These results perfectly met my expectation, and indicate that the reversible change in the orientation of the AuNR arrays on polymer brushes was induced by the modulation of the electrostatic interactions between the AuNRs and polymers via changes in the solution pH. As ssDNA possesses a similar

persistence length to that of synthetic polymers, these findings indicate that a broad range of synthetic stimuli-responsive polymers could be applicable to this approach, leading to a wide range of applications.

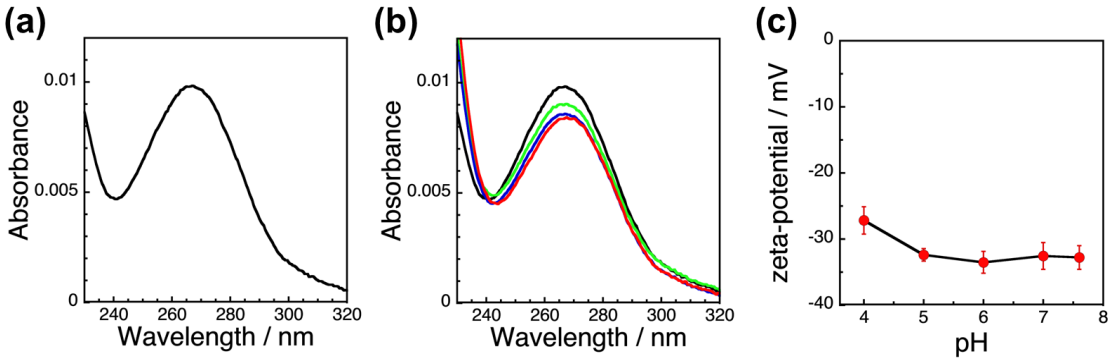

Figure 2-9. (a) Absorption spectrum of the prepared ssDNA [poly(dT)] brushes. The DNA density was calculated as ca. 19000 ± 880 chains/μm^2 (7.9 ± 0.2 nm as an average DNA interchain distance) from the absorbance at 260 nm. (b) pH-Independence of ssDNA [poly(dT)] brushes on absorption spectra. Spectra are shown as black (pH 7.6), light green (pH 6.0), blue (pH 5.0), and red (pH 4.0). (c) Zeta-potential of ssDNA [poly(dT)] in solution at various pH values.

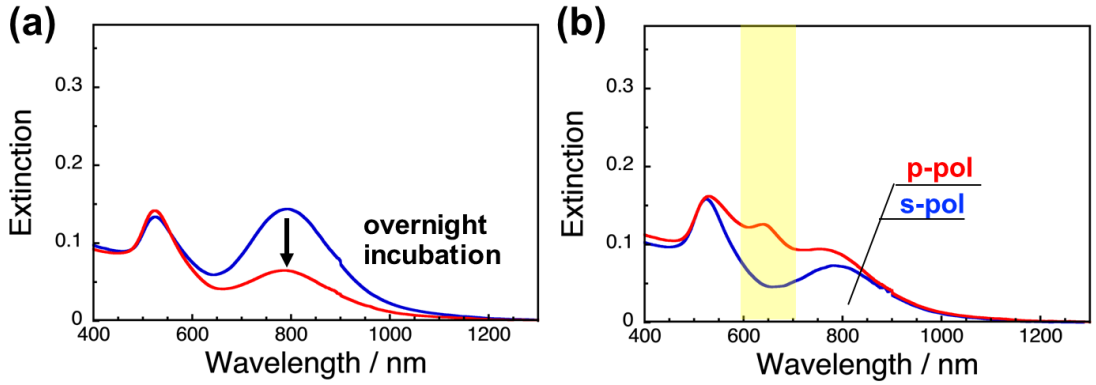

Figure 2-10. Extinction spectra of AuNRs adsorbed on the ssDNA [poly(dT)] brushes. (a) Time-dependent spectral changes after replacement of solution to buffer; soon after replacement (blue) and after overnight incubation (red). (b) Extinction spectra after overnight incubation measured under p-polarized (red) and s-polarized light (blue) at θ = 45°.

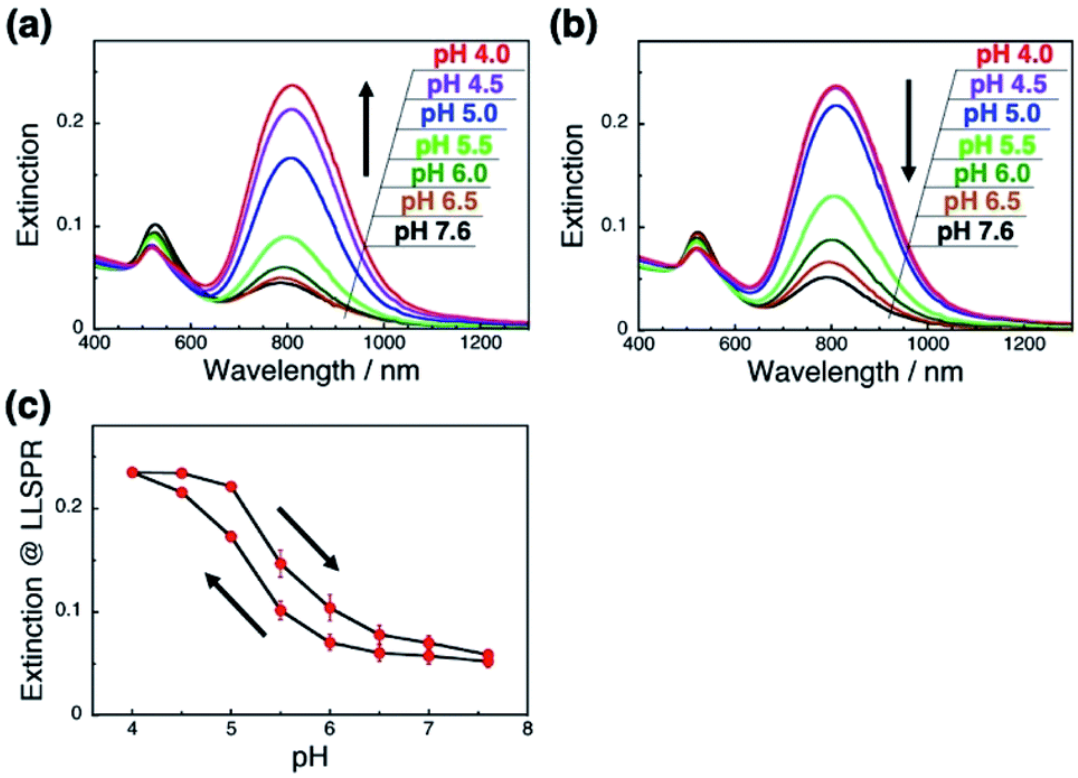

Figure 2-11. pH-Responsive spectral changes for AuNRs on ssDNA[poly(dT)] brushes. (a) An increase in pH 7.6 to 4. (b) A decrease in pH from 4.0 to 7.6. Spectra are shown in black (pH 7.6), brown (pH 6.5), green (pH 6.0), light green (pH 5.5), blue (pH 5.0), purple (pH 4.5), and red (pH 4.0). (c) Extinction values for the L-LSPR peak with regard to pH changes. Error bars represent standard deviation of 3 repeated cycles.

2-4. Conclusion

I prepared AuNR arrays attached on anionic polymer (dsDNA and ssDNA) brushes via electrostatic interactions and investigated their pH-responsive changes in orientation. As the AuNRs were modified with 10% amine-terminated ligands, the zeta-potential of the AuNRs gradually increased with decrease in the solution pH. The AuNR orientation on the DNA brushes was reversibly changed by the modulation of the electrostatic interactions between the AuNRs and polymers via changes in the solution pH. The L-LSPR peak change is gentler and in a wider pH range (pH 4.0–7.6) on ssDNA brushes, while the L-LSPR peak changed drastically and in a narrow pH range (pH 4.0–5.0) on the dsDNA brushes. I consider that dsDNA is too rigid to bend or be rearranged at a neutral pH due to its double helical structure. However, when the DNA helix structure is deformed by a decrease in pH (<pH 5), it will behave like a soft polymer and then AuNR orientation can be tuned via changes in the interactions between the DNA and AuNRs. As these extensive AuNR arrays are prepared via easy bottom-up processes, AuNR surface properties are easily tuned by simple modification, and DNAs could be replaced with various synthetic polymers, I believe that this study will lead to the development of next-generation materials and devices with actively tunable structures.

Chapter 3

Brush Thickness-modulated Dynamic Orientation Control of Gold Nanorods in DNA Brushes

3-1. Introduction

In Chapter 2, I demonstrated dynamic orientation changes via changes in interaction strength between the AuNR and DNA. These study suggests that modulation of AuNR surface properties provides opportunities for further tuning of AuNR motion in DNA brushes. In contrast, as AuNR orientation depends on the conformation of polymer brushes as templates, control of AuNR orientation with the structural changes of the polymer brush can be a versatile system for actively tunable plasmonic substrates via various stimulation by applying to a broad range of polymers.

To realize this concept, in Chapter 3, I demonstrate dynamic changes to AuNR orientation via changes in the thickness of polymer brushes (**Figure 3-1**). Here, single-stranded DNA was used as DNA possesses a monodispersed chain length and the structure changes in DNA brushes have been extensively investigated in previous reports.[76–79] Salt concentration changes were used to control the brush thickness. Then, the orientation of the AuNRs embedded in the DNA brushes against brush thickness was investigated for varied DNA lengths, salt types, and AuNR lengths, providing a general insight into the stimuli-responsive control of AuNR orientation on the substrates via changes in the thickness of polymer brushes.

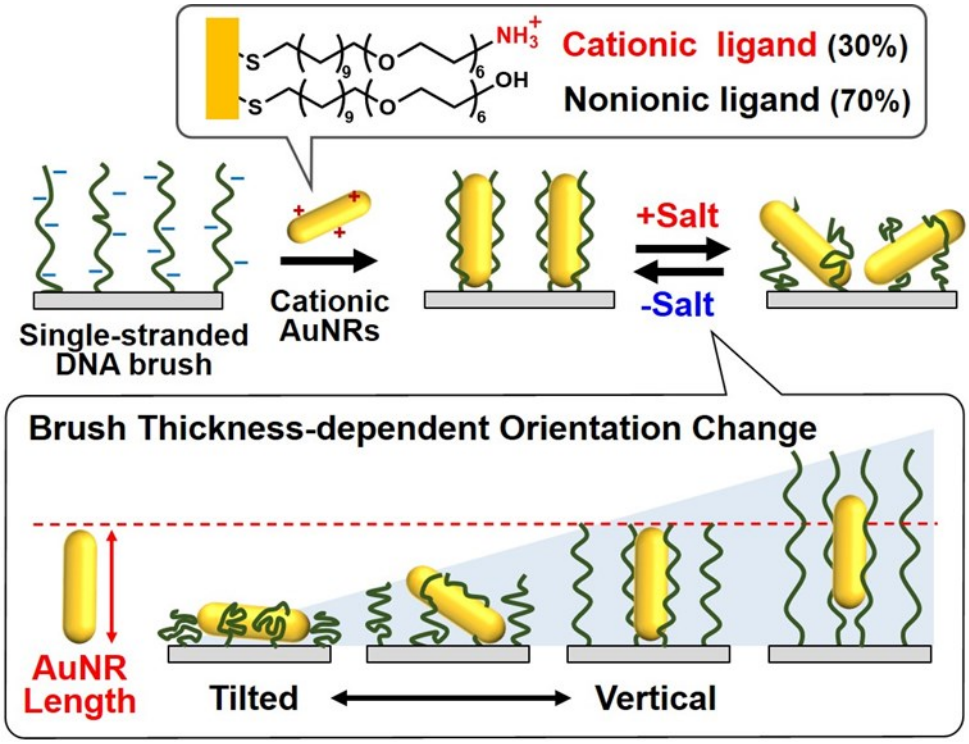

Figure 3-1. Dynamic orientation change of AuNRs inserted into DNA brushes based on shrinkage/extension of the DNA brushes.

3-2. Experimental section

3-2-1. Materials and Instruments

5'-Biotinylated and 3'-Alexa647-modified single-stranded DNA of 50- and 100-base poly(dT) was purchased from Thermo Fisher Scientific Inc. 5'-Biotinylated single-stranded DNA of 148-, 175- and 200-base poly(dT) was purchased from Integrated DNA Technologies, Inc. 20-(11-Mercaptoundecanyloxy)-3,6,9,12,15,18-hexaoxaeicosane-1-amine ($NH_2EG_6C_{11}$) was purchased from ProChimia Surfaces, Sp.zo.o. Fluorescence intensity measurements were performed with a WSE-5300 Printgraph CMOSI (ATTO Corp.). Scanning electron microscope (SEM) images were obtained using a SU-8230 system (Hitachi High-Tech Co., Ltd., Japan). All other salts, reagents and instruments used in this chapter are listed in Chapter 2.

3-2-2. Fabrication of the streptavidin-modified substrate

The streptavidin-modified substrate was prepared using an method described in Chapter 2 (**2-2-5.**).

3-2-3. Immobilization of DNA polymers of various lengths onto the streptavidin surface

The streptavidin-modified substrate was immersed in a 10 mM Tris-HCl solution with biotin-modified ssDNA and NaCl for 2 h to fabricate DNA brushes. Due to the differences in reaction efficiency depending on DNA Polymer length, the concentrations of the ssDNA and NaCl was tuned for 50-base (ssDNA: 200 nM, NaCl: 200 mM), 100-base (ssDNA: 200 nM, NaCl: 50 mM), 148-base (ssDNA: 2 μM, NaCl: 1 M), 175-base (ssDNA: 2 μM, NaCl: 1M), and 200-base ssDNA (ssDNA: 2.5 μM, NaCl: 1 M) to prepare DNA brushes of nearly the same density. After the reaction, the solution was taken out

from the cuvette, and unreacted DNA was washed out by adding and removing 10 mM Tris-HCl at least three times.

3-2-4. Preparation of AuNRs of different lengths

AuNRs with a 24-nm longer axis were acquired commercially (Nanopartz, Inc. Product number A12-10-650-CTAB-DIH-1-100). AuNR with a 36-nm longer axis were fabricated with same procedure indicated in Chapter 2 (**2-2-2.**). AuNRs (45 × 10 nm) were synthesized using the seed-mediated method with slight modification.[126] Gold seed particles were firstly prepared by a standard reduction process. Under gentle shaking, an ice-cold $NaBH_4$ solution (0.01 M, 8.05 mL) was added to a mixture of a $HAuCl_4 \cdot 3H_2O$ solution (0.01 M, 5.15 mL) and a CTAB solution (0.1 M, 200.85 mL). The seed solution was then kept in an incubator at 27°C for 2 h. For the growth reaction, growth solutions were prepared from a CTAB solution (0.1 M, 225 mL) by adding a $HAuCl_4 \cdot 3H_2O$ solution (0.01 M, 12.5 mL), a $AgNO_3$ solution (0.01 M, 2.5 mL), a HCl solution (1.0 M, 5 mL), and an ascorbic acid solution (0.1 M, 2.0 mL), in this order. The gold seed solutions (25 mL) were injected to the growth solutions, while the growth solution was stirred gently. Then, the growth solutions were left undisturbed in an incubator at 30°C for at least 3 h. The AuNR solution was stored under 30°C. For TEM measurement, the remaining CTAB and other reagents were diluted 1000-fold by two-times centrifugation (18,000 g, 20 min, 30°C) before dropping onto a TEM grid.

3-2-5. Surface modification of AuNRs with two types of thiol-ligands

Surface modification of the three distinct AuNR variants was carried out as described in Chapter 2, **Section 2-2-3**. Cationic ($NH_2EG_6C_{11}$) and nonionic ($OHEG_6C_{11}$) ligands were separately dissolved in water. These ligand solutions were then mixed to achieve a

combined concentration of 10 mM, with the cationic ligands representing 30% of the total. Prior to the surface modification, CTAB was removed. The reaction parameters, purification process, and concentration adjustments for the modified AuNRs adhered to the procedures outlined in Chapter 2, **Section 2-2-3**.

3-2-6. Attachment of ligand-modified AuNRs onto DNA polymer brushes

AuNR attachment onto DNA brushes was conducted as described in Chapter 2 (**2-2-8.**).

3-2-7. Investigation of the NaCl concentration-dependent AuNR orientation change

To change NaCl concentration, the solution on the AuNR-adsorbed DNA brush substrate was replaced with another solution with a different NaCl concentration after washing with the latter solution more than 3 times by pipetting to change the environment completely. When the AuNRs were detached from DNA brush (high NaCl concentration), the replacement was performed until the AuNRs were removed completely from the DNA brush. In the extinction spectrum analysis, the incident light was non-polarized and its direction was perpendicular to the cuvette containing the adsorbed AuNRs unless otherwise specified.

3-2-8. Sigmoidal Curve Fitting for Generalization of AuNR Orientation

L-/TLSPR intensity data from AuNRs in DNA brushes were fit with Boltzmann sigmoidal curve to visualize the relationship between the AuNR orientation and brush thickness, and determine the maximum and minimum values. To do so, experimental data is fitted to the Boltzmann sigmoid equation, given by:

$$y = \frac{A_1 - A_2}{1 + e^{(x - x_0)/dx}} + A_2$$

Where y is L-/T-LSPR intensity, x is brush thickness, x_0 is the mid-range of brush thickness for dynamic orientation change, d is the slope factor, and A_1 and A_2 are the maximum and minimum L-/T-LSPR intensities, respectively.

3-3. Results and Discussion

3-3-1. AuNR orientation in DNA brushes with various thickness

First, I investigated orientation of the attached AuNRs on DNA brushes of different thicknesses. Single-stranded DNA (ssDNA) brushes were fabricated following our previously established method with slight modifications.[74,75,119] Briefly, biotinylated ssDNA was immobilized on streptavidin-immobilized substrates through avidin-biotin interactions. To achieve varied thicknesses, six ssDNA lengths (50, 100, 125, 148, 175, and 200 bases) were selected for each ssDNA brush. The DNA densities were adjusted to a constant value (20 000 chains μm^{-2}, ≈8 nm as the interchain distance, **Figure 3-2, Figure 3-3**) on the basis of their absorption or fluorescent intensity. Subsequently, cationic AuNRs, which surface was modified with a mixture of cationic and nonionic ligands at a 30:70 ratio, were attached to the ssDNA brushes via electrostatic interactions (Length: 36 nm, Width: 10 nm, **Figure 3-4**).

Figure 3-5 shows the extinction spectra of AuNRs attached to DNA brushes with various DNA lengths in 10 mM Tris-HCl (pH 7.6) buffer by conventional measurement in which the light was irradiated perpendicular to the substrate. The AuNRs in the 50-, 100-, and 125-base DNA brushes exhibited high L-LSPR intensity, with the shorter DNA brushes showing a particularly heightened L-LSPR peak intensity. As AuNRs show stronger L-LSPR intensity at a higher angle (≈90°) of incident light to the AuNRs, these results suggest that AuNRs were adsorbed at a greater incline in the thinner DNA brushes. In contrast, the extinction spectrum of the AuNRs attached to 148-base DNA brushes showed an approximately five times weaker L-LSPR peak intensity (≈800 nm) than T-LSPR peak intensity. This result is the same as our previous research, indicating that the attached AuNRs were parallel to the immobilized DNA (oriented vertically to the

substrates).[74,75,119] The vertical alignment of AuNRs awas further supported by a p-polarized light-specific L-LSPR peak ≈640 nm induced by the plasmon coupling from side-by-side assemblies of AuNRs (**Figure 3-6**).[127–129] As for longer DNA length (175- and 200-base DNA) brushes, the LLSPR intensity did not show any significant difference compared to the results for the 148-base DNA brushes, indicating that the AuNRs were also aligned vertically to the substrates in brushes with over 148-base DNA.

To further discuss the effect of brush thickness, I focused on the thickness of the polymer brushes under each set of conditions. For the determination of polymer brush thickness at a relatively low density, an experimental examination is quite demanding due to the ambiguity regarding the brush interface.[130] Therefore, the Daoud-Cotton model (DCM) was introduced, which was extensively investigated previously.[79] The modified DCM for a flat surface is given by

$$h \approx kNd(l_k\sigma\lambda_D)^{1/3} \quad (1)$$

where k is a constant (close to unity), N is the number of ssDNA bases, d is the average internucleotide distance, l_k is the Kuhn length, σ is the ssDNA surface density, and λ_D is the Debye length. The values of l_k and d were taken from reference 46, and λ_D was calculated from the following equation, applied to Debye-Hückel theory with two ionic species:[131]

$$\lambda_D = \sqrt{\frac{\varepsilon_r\varepsilon_o RT}{2e^2z^2N_AC}} \quad (2)$$

where ϵ_r is the zero-frequency dielectric constant of the continuous medium, ϵ_0 is the permittivity of free space, R is the gas constant, T is the temperature, e is the elementary charge, z is the number of charges on an ion, N_A is the Avogadro constant, and C is the salt concentration.

To quantitatively discuss the difference in AuNR orientation by brush thickness, I utilized the intensity of the L-LSPR peak at a longer wavelength divided by that of the T-LSPR peak at a shorter one (L-/T-LSPR) as an indicator of the orientation of AuNRs.[26,75] The L-/T-LSPR intensity exhibited a value of 3.7 for 12 nm brush thickness, 1.7 for 25 nm brush thickness, and 0.9 for 34 nm brush thickness (**Figure 3-7)**. On the other hand, the L-/T-LSPR intensity is significantly lower, ca. 0.2, when brush thickness exceeds 40 nm. These results indicate that the orientation of AuNRs shows thickness-dependent and -independent regions with the threshold value of DNA brushes at ≈35 nm, which is comparable with the length of the AuNR.

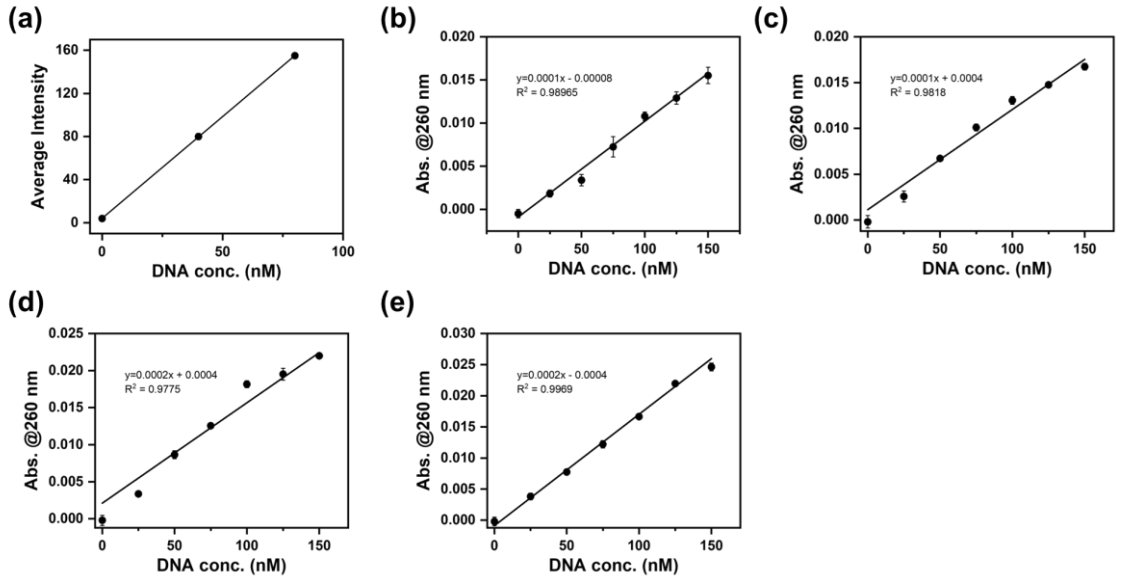

Figure 3-2. Plot for (a) the fluorescent intensity of Alexa-647-immobilized DNA, and the peak absorption intensity at 260 nm of (b) 125-base, (c) 148-base, (d) 175-base, and (e) 200-base DNA against DNA concentration, showing linear relationships. Error bars represent standard deviation (n=3)

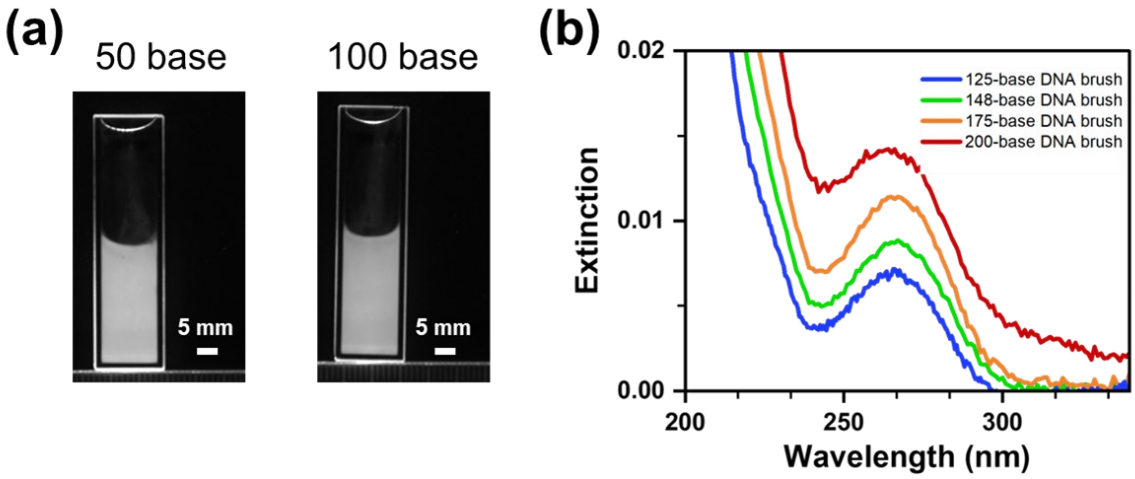

Figure 3-3. (a) Fluorescent images of the ssDNA brushes (left: 50-base, right: 100-base). The fluorescence intensities are from Alexa Fluor 647 at the terminus. (b) Absorption spectra of the 125-, 148-, 175-, and 200-base ssDNA brushes.

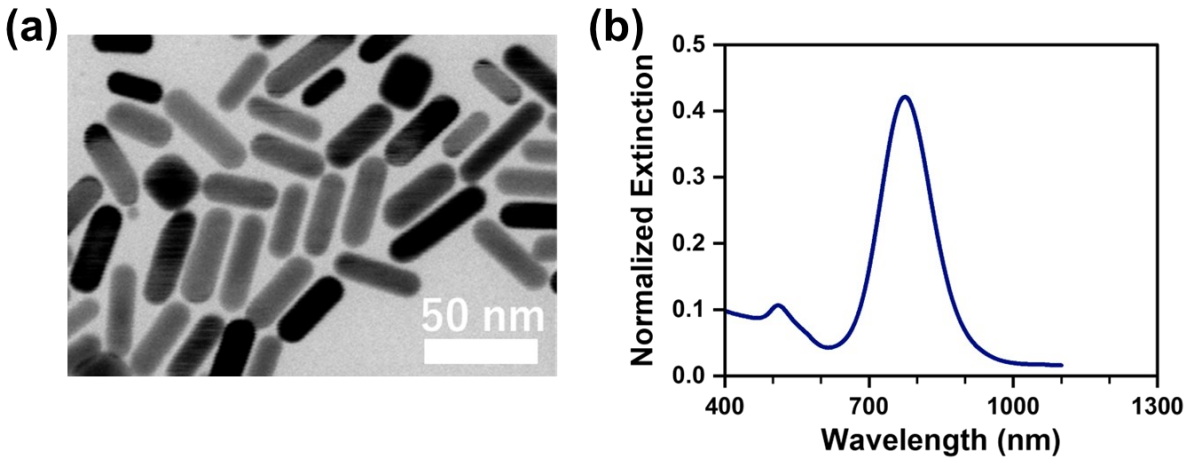

Figure 3-4. STEM image of (a) 36 × 10 nm AuNRs and (b) extinction spectrum of dispersed AuNRs. AuNR size was determined as 10 ± 1.5 nm in diameter and 36 ± 7.5 nm in length (236 particles counted).

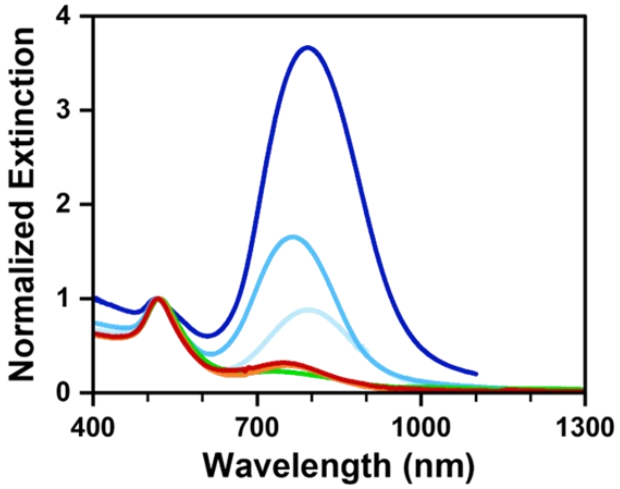

Figure 3-5. Extinction spectra of attached AuNRs (36 × 10 nm) in 50-base (blue), 100-base (sky-blue), 125- base (light blue), 148-base (green), 175-base (orange), and 200-base (red) ssDNA brushes in 10 mM Tris-HCl buffer (pH 7.6). Extinction intensities are normalized at T-LSPR. Non-polarized light was irradiated perpendicular to the substrates in these measurements.

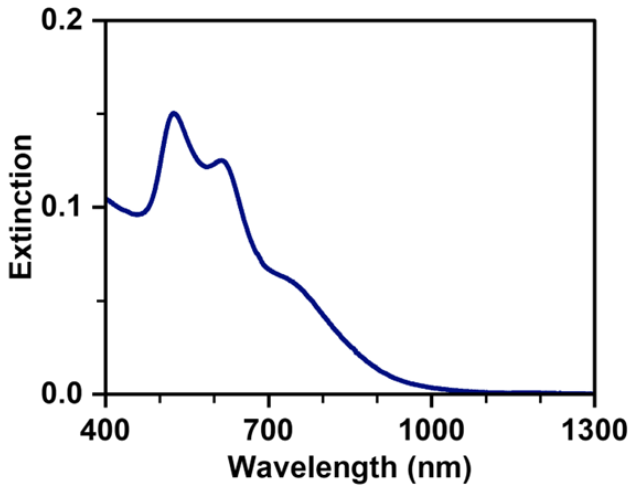

Figure 3-6. Extinction spectrum of AuNRs vertically attached to 148-base DNA brushes under p-polalized light at an angle of 45 degrees to the substrate.

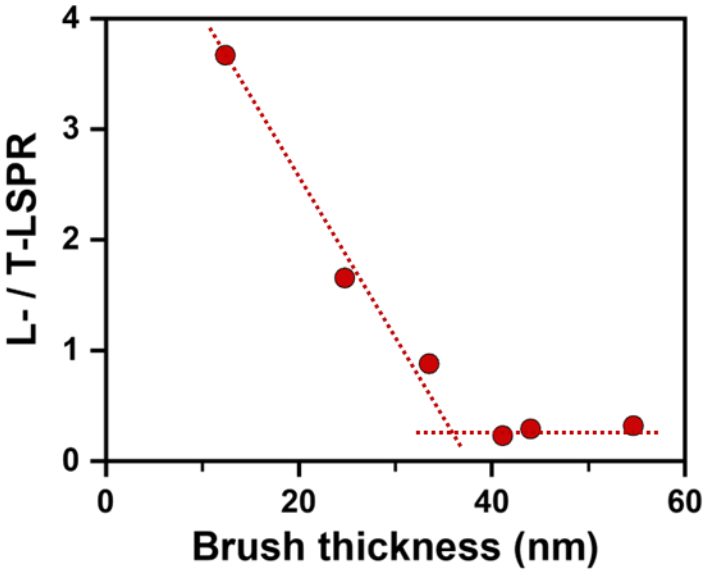

Figure 3-7. L-/T-LSPR values in relation to brush thickness calculated from modified DCM. The dashed lines are guides for the eye.

3-3-2. Dynamic orientational change of AuNRs in the DNA brushes with varied NaCl concentration

Next, I demonstrated dynamic orientation change of vertically attached AuNRs induced by the shrinkage of DNA brushes via increase in salt concentration (x mM NaCl + 10 mM Tris-HCl (pH 7.6)). Following the vertical attachment of AuNRs (36 × 10 nm), NaCl concentration was changed by solvent replacement. The L-LSPR peak intensity exhibited a corresponding increase without significant changes in T-LSPR as the NaCl concentration increased from 0 to 40 mM (**Figure 3-8a**). This result indicates that the orientation of the attached AuNRs gradually tilted with the increase in NaCl concentration. The calculated thickness of the 148-base DNA brushes was 41.5 nm at 0 mM NaCl, and 30.8 nm at 40 mM NaCl. As AuNR orientation differs depending on brush thickness, this dynamic orientation change occurs due to the thickness changes. With regard to NaCl concentrations of 50 mM or higher, the 30% cationic AuNRs adsorbed in the DNA brushes were detached due to the weakened electrostatic attraction between the AuNRs and DNA.

Additionally, the dynamic motion of AuNRs endows this material with the ability to switch plasmon coupling as the side-by-side coupling of the AuNRs undergoes sensitive change due to their configuration (**Figure 3-8b**). The vertical alignment of the AuNRs effectively leads to the side-by-side coupling phenomenon. When vertical AuNRs in the DNA brushes were irradiated with p-polarized light at a 45-degree angle, an extinction peak was observed ≈640 nm (highlighted in red), originating from the blueshifted L-LSPR peak by the side-by-side coupling. Meanwhile, configuration change of the AuNRs from a vertical to a tilted state on increases in NaCl concentration induced a decrease in the extinction of blueshifted L-LSPR and an increase in the extinction of the original L-LSPR with longer wavelengths (highlighted in blue), indicating decoupling of their

plasmon via AuNR configuration changes. This active plasmonic system, based on the vertical (uniform) / tilted (random orientation) switching of AuNRs, holds promising potential for applications, such as colorimetric display.[132]

Further, I investigated the reversibility of this dynamic orientation change. With the decrease in NaCl concentration, the L-LSPR peak intensity decreased and returned to its initial intensity at 0 mM NaCl. This result indicates that the tilted AuNRs returned to a vertical alignment when the NaCl concentration decreased. Upon repeated solvent exchange between 0 and 40 mM NaCl, the L-/T-LSPR intensity of the attached AuNRs changed reversibly for at least ten cycles (**Figure 3-8c**). It is noteworthy that no hysteresis was observed when plotting the L-LSPR intensities in relation to the changes in NaCl concentration (**Figure 3-9**). This result supports the notion that the mechanism underlying the orientational change differs from our previously established system of pH-triggered orientational tuning, which relies on the electrostatic interaction strength between DNA and cationic AuNRs.[119] Whereas the interaction strength is indeed an important factor for the AuNR orientation, as I have reported in chapter 2,[74] decreases in the interaction strength by increases in pH (from the initial strength to the strength at AuNR detachment) did not induce the AuNR orientation change until AuNR detachment (**Figure 3-10**). Furthermore, dynamic orientation change did not occur in double-stranded DNA (dsDNA) brushes, which are more rigid than ssDNA brushes (persistence length: approximately 50 nm for dsDNA,[133] 2-3 nm for ssDNA[134,135]) (**Figure 3-11**). These observations support the notion that the shrinkage of polymer brushes is a dominant factor in the dynamic orientation change of the AuNRs in this system.

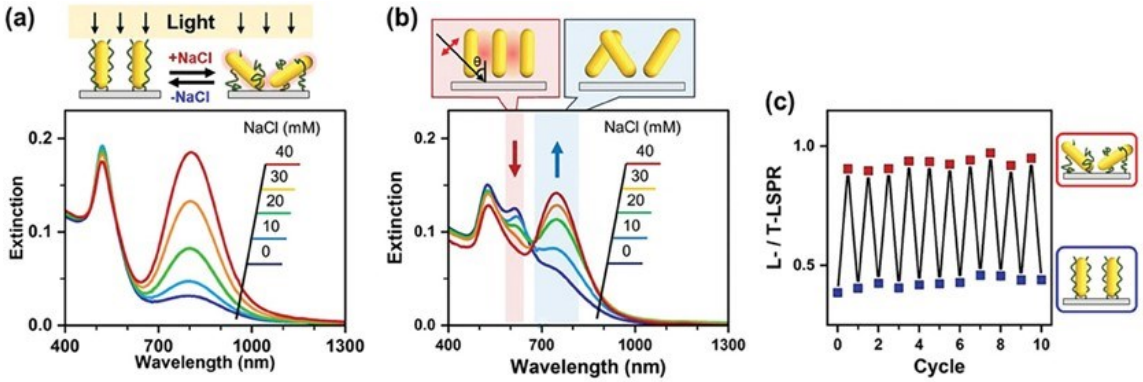

Figure 3-8. Salt-triggered spectral changes of AuNRs (36 × 10 nm) in 148-base ssDNA brushes. (a) Extinction spectra in a range of 0 to 40 mM NaCl. Non-polarized light was irradiated perpendicular to the substrates in these measurements. (b) Extinction spectra under p-polarized light at an angle of 45 degrees relative to the substrate with NaCl concentration. (c) L-LSPR/T-LSPR values on repeated changes in NaCl concentration between 0 and 40 mM.

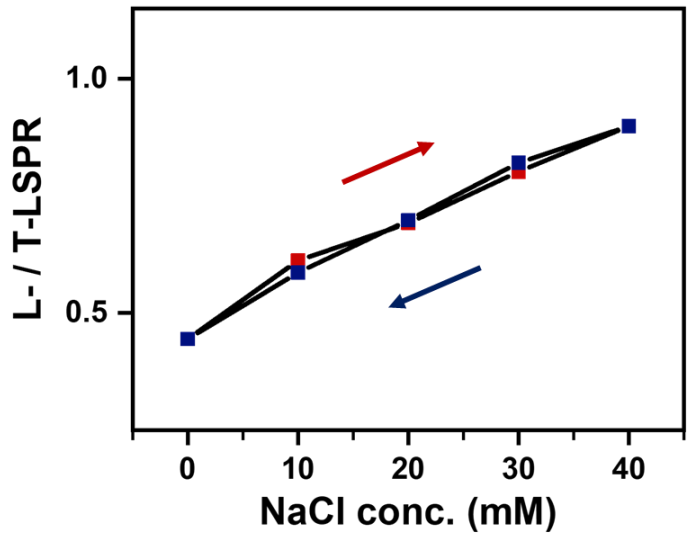

Figure 3-9. L-LSPR/T-LSPR values of AuNRs in DNA brushes according to NaCl concentration.

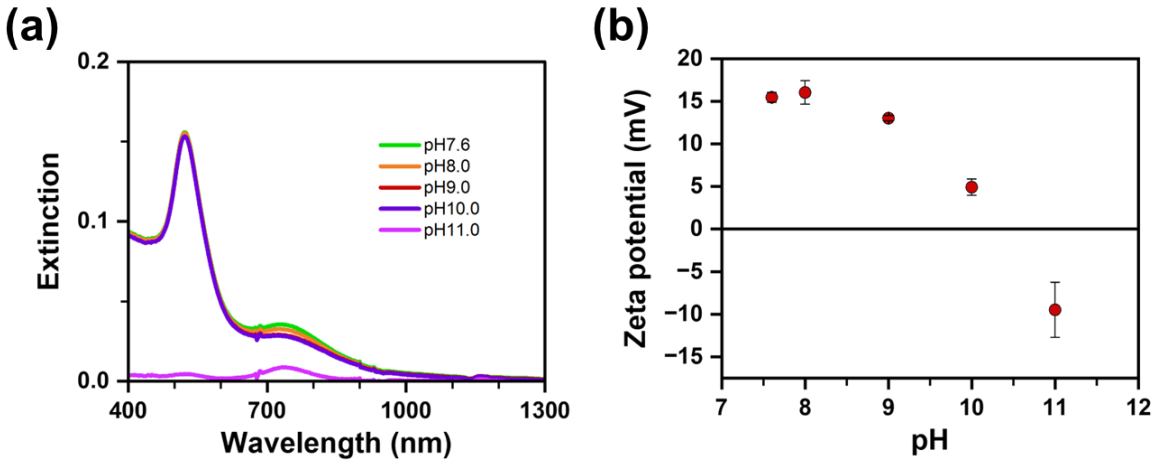

Figure 3-10. (a) Extinction spectra of 30% cationized AuNRs (36 × 10 nm) in 148-base ssDNA brushes with increases in pH. The extinction spectra did not change significantly, with the L-/T-LSPR value remaining at around 0.2. The AuNRs in the ssDNA brushes were detached at pH 11.0 due to weakened electrostatic interactions. (b) Zeta potential of dispersed 30% cationized AuNRs against pH. The zeta potential of the AuNRs decreased with increases in pH.

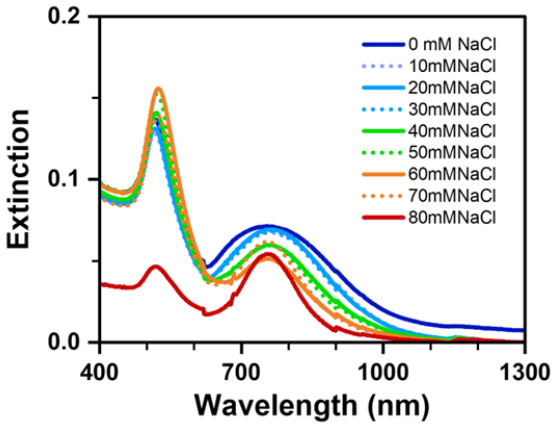

Figure 3-11. Extinction spectra of 30% cationized AuNRs (36 × 10 nm) in double-stranded DNA brushes against salt concentration. Although salt concentration increased, the orientation of the attached AuNRs did not change until the AuNRs were detached at a high salt concentration.

3-3-3. Generalization of AuNR orientational change by shrinkage/extension of polymer brushes

In order to establish a general framework for this system, I further investigated the dynamic orientation change of 36 nm AuNRs across a broad range of thicknesses using ssDNA of 50-, 100-, 125-, 175-, and 200-bases in length. The corresponding spectral changes are shown in **Figure 3-12**. AuNRs attached to ssDNA brushes of 50- or 200-bases in length, which are significantly shorter and longer than the AuNR length, respectively, did not show any spectrum changes in response to varying NaCl concentrations (**Figure 3-12a, e**). When NaCl concentration was increased in 100-base and 175-base ssDNA brushes with AuNRs, the AuNRs exhibited a slight increase in L-LSPR peak intensity corresponding to the NaCl concentration (**Figure 3-12b, d**). As for 125-base ssDNA brushes, whose thickness is slightly shorter than the AuNR length, the L-LSPR peak intensity of the slightly tilted AuNRs showed corresponding increase to the NaCl concentration (**Figure 3-12c**). To estimate the tilt angle in this intricate plasmonic system, the L-/T-LSPR intensity of AuNRs directly attached on bare glass substrates at the same AuNRs density was determined at a 90° angle; that is, parallel to the substrates, as a reference. The SEM image revealed that all of the adsorbed AuNRs were not piled on the substrate, suggesting that they were adsorbed parallel to the substrate, and the extinction spectrum showed an L-/T-LSPR intensity of 3.92 (**Figure 3-13**). To elucidate the relationship between AuNR orientation and brush thickness, all L-/T-LSPR intensities were normalized with respect to the value obtained at a 90° angle (3.92) and plotted against brush thickness (**Figure 3-14**). When the brush thickness was below half that of the AuNR length (less than 18 nm), the tilt angle of the AuNRs showed a maximum value on the DNA brushes. The normalized L-/T-LSPR intensity approached 0.9, suggesting that the maximum angle to the substrate was close to 90°. For brush thicknesses within

the range between 18 and 36 nm, which are comparable to the AuNR length, the orientation of the attached AuNRs was dependent on the brush thickness, enabling dynamic orientation change of the AuNRs. When the brush thickness exceeded the attached AuNR length, the AuNRs in DNA brushes were almost vertical to the substrate. This relationship between AuNR length and brush thickness indicates that the origin of the motive force for their tilting was energy gain from electrostatic bonding between cationic AuNR and DNA. In other words, AuNRs tilt to reduce energetic loss from exposure of the cationic surface to the solution.

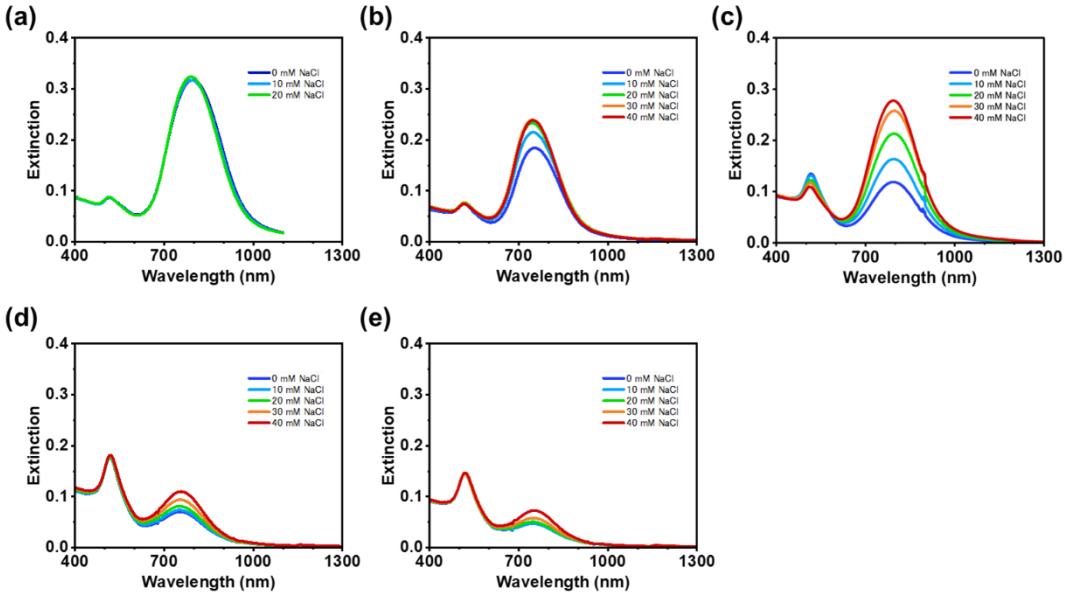

Figure 3-12. Extinction spectra of attached AuNRs (36×10 nm) in DNA brushes composed of (a) 50-base, (b) 100-base, (c) 125-base, (d) 175-base, and (e) 200-base ssDNA at various NaCl concentrations.

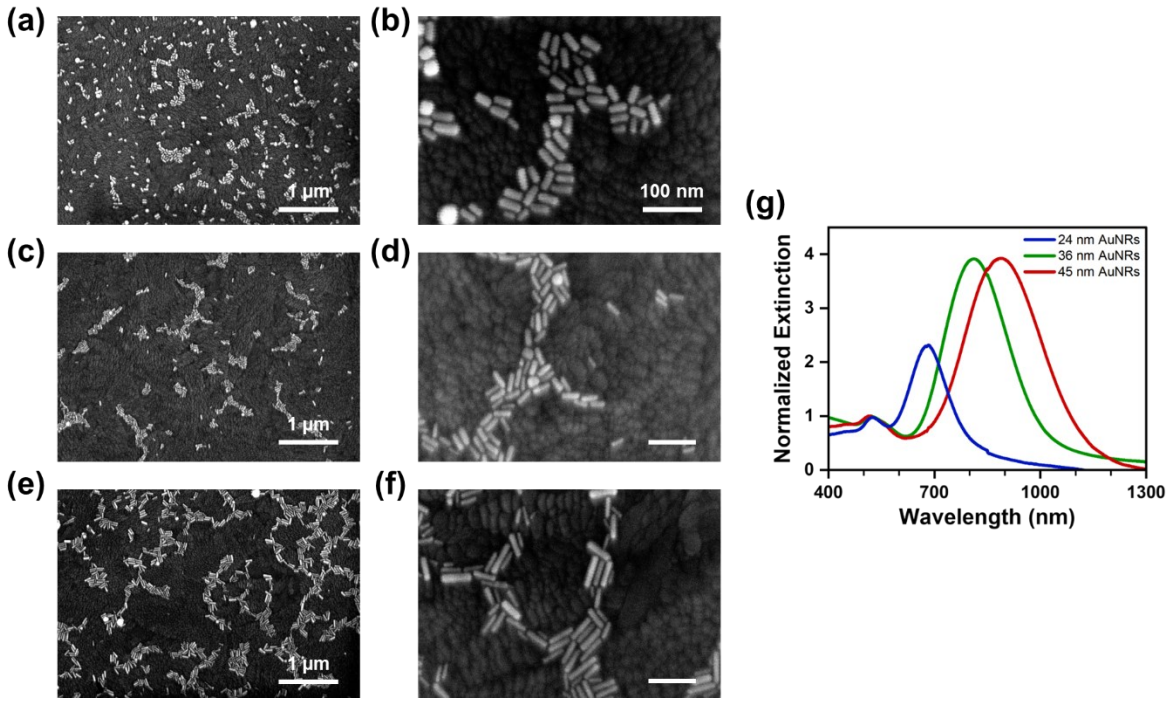

Figure 3-13. SEM images of 30% cationized AuNRs adsorbed on bare ITO substrates. (a-b) 24 × 10 nm AuNRs at (a) low-magnification and (b) high-magnification. (c-d) 36 × 10 nm AuNRs at (c) low-magnification and (d) high-magnification. (e-f) 45 × 10 nm AuNRs at (e) low-magnification and (f) high-magnification. Scale bars are 1 μm (low-magnification) and 100 nm (high-magnification). (g) Extinction spectra of the AuNRs on bare substrates. Extinction intensities are normalized at T-LSPR. The L-/T-LSPR is 2.16 for 24-nm AuNRs, 3.92 for 36-nm AuNRs, and 3.93 for 45-nm AuNRs.

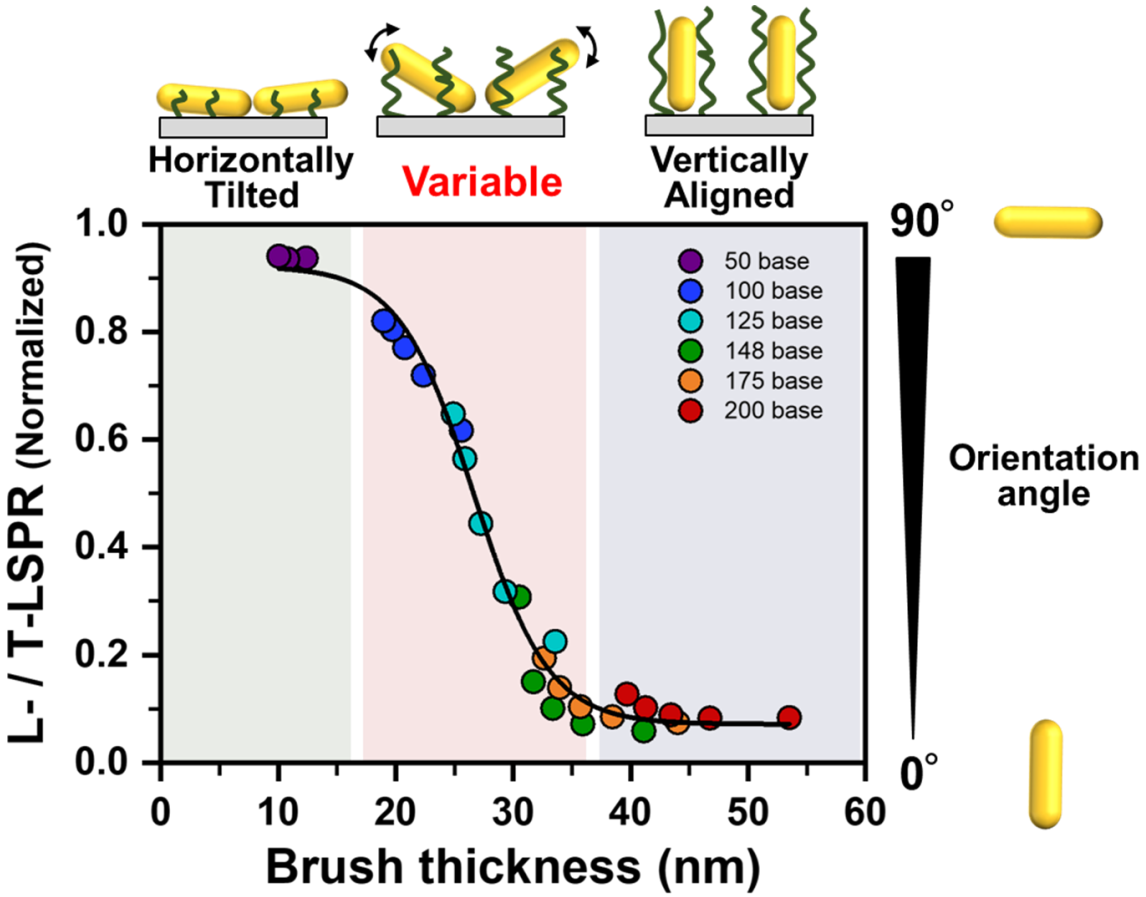

Figure 3-14. L-/T-LSPR values of AuNRs (36 × 10 nm) against calculated brush thickness. Concentration of NaCl was varied (from 0 to 40 mM) to shrink and extend each DNA brush. Black solid line is curve-fitted from the obtained data.

Furthermore, I investigated the effect of other types of salt (KCl, $CaCl_2$, and $MgCl_2$), whose shrinkage effect on ssDNA brushes has been extensively explored.[79] The L-LSPR peak intensity of AuNRs in 148-base ssDNA brushes exhibited a corresponding increase as the KCl concentration was raised from 0 mM to 40 mM (**Figure 3-15a**). In contrast, a slight increase in the number of divalent ions (1~5 mM $MgCl_2$ and 1~6 mM $CaCl_2$) caused a drastic tilt in the attached AuNRs, resulting in the L-/T-LSPR intensity ranging from 0.4 to 3.4 (the normalized intensity: 0.1~0.9, **Figure 3-15b, c**). When the acquired data were

plotted, all the data exhibited an excellent fit to the same sigmoidal curve shown in **Figure 3-14** (**Figure 3-15d**). Although the spectrum changes with the divalent ions were not perfectly reversible, likely due to insufficient ionic exchange in strongly attracted divalent ions,[136] these results show that the dynamic orientation changes can be achieved across a wide range of angles.

Finally, I generalized this system by varying AuNR length, using 24-nm and 45-nm AuNRs (**Figure 3-16**). I selected 100- and 175-base ssDNA brushes for dynamic orientation change in 24 and 45 nm AuNRs, respectively. As expected, dynamic orientational change of the 24 nm AuNRs was successfully obtained in 100-base ssDNA brushes (**Figure 3-16a, b**). When the NaCl concentration increased stepwise from 0 mM to 30 mM, the L-/T-LSPR intensity correspondingly increased. Likewise, a similar dynamic orientation change was observed with 45 nm AuNRs attached to 175-base ssDNA brushes (**Figure 3-16c, d**). These results revealed that the orientation of attached AuNRs of different lengths can be tuned dynamically by tailoring the brush thickness.

Figure 3-16e summarizes the orientation (normalized L-/T-LSPR; references are shown in **Figure 3-17**) of these three types of AuNRs relative to brush thickness. All the data were collected using the same methods as for the experiment using 36-nm AuNRs (**Figure 3-17 - Figure 3-19**). The orientation of both the 24 and 45 nm AuNRs follows the same trend as that of the 36 nm AuNRs. All fitted-curves reach their maximum when the "brush thickness/AuNR length" falls below half the length of the AuNRs. These maximum intensities reached ≈0.95, indicating that the AuNRs were nearly parallel to the substrate. In the range of "brush thickness/AuNR length" from 0.5 to 1.0, the orientation of the attached AuNRs depended on brush thickness, enabling dynamic orientation tuning of AuNRs across a wide range of angles. When the "brush thickness/AuNR length" was

close to unity or greater, the AuNRs in the DNA brushes were almost vertical to the substrate. The minimum intensity of the 24 nm AuNRs was higher than that of the longer AuNRs due to the spectrum overlap of T-LSPR on L-LSPR. These results indicate that this is a generalized system for the controlling the AuNR orientation using polymer brush thickness changes, as AuNR orientation responds to the ratio of "brush thickness/AuNR length". This work not only clarified the relationship between AuNR orientation in polymer brushes and brush thickness but also offers a framework for novel plasmonic devices using active AuNR orientation control on the solid substrates.

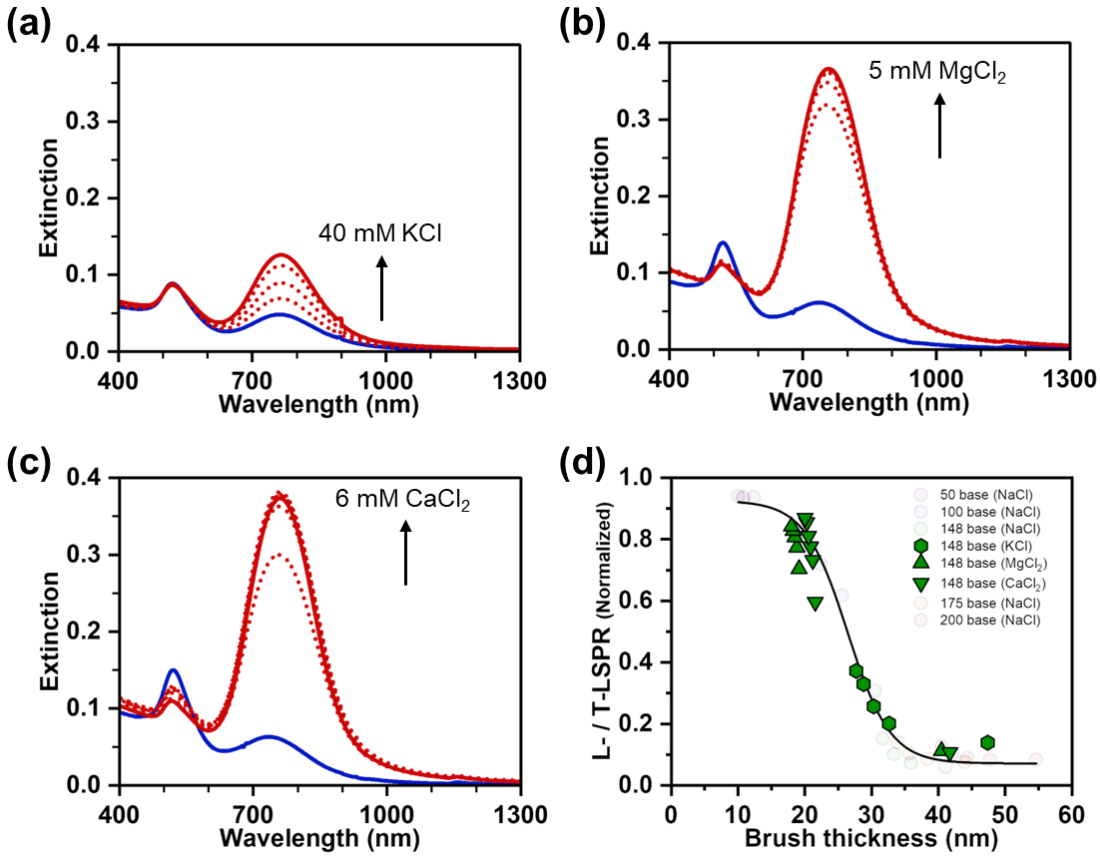

Figure 3-15. Spectral changes of AuNRs (36 × 10 nm) attached to 148-base ssDNA brushes at various (a) KCl concentrations (0 mM to 40 mM), (b) $MgCl_2$ concentrations (0 mM to 5 mM), and (c) $CaCl_2$ concentrations (0 mM to 6 mM). (d) Plot for the L-/T-LSPR intensity of the attached AuNRs in 148-base ssDNA for different salt types. The solid line is obtained from **Figure 3-14**.

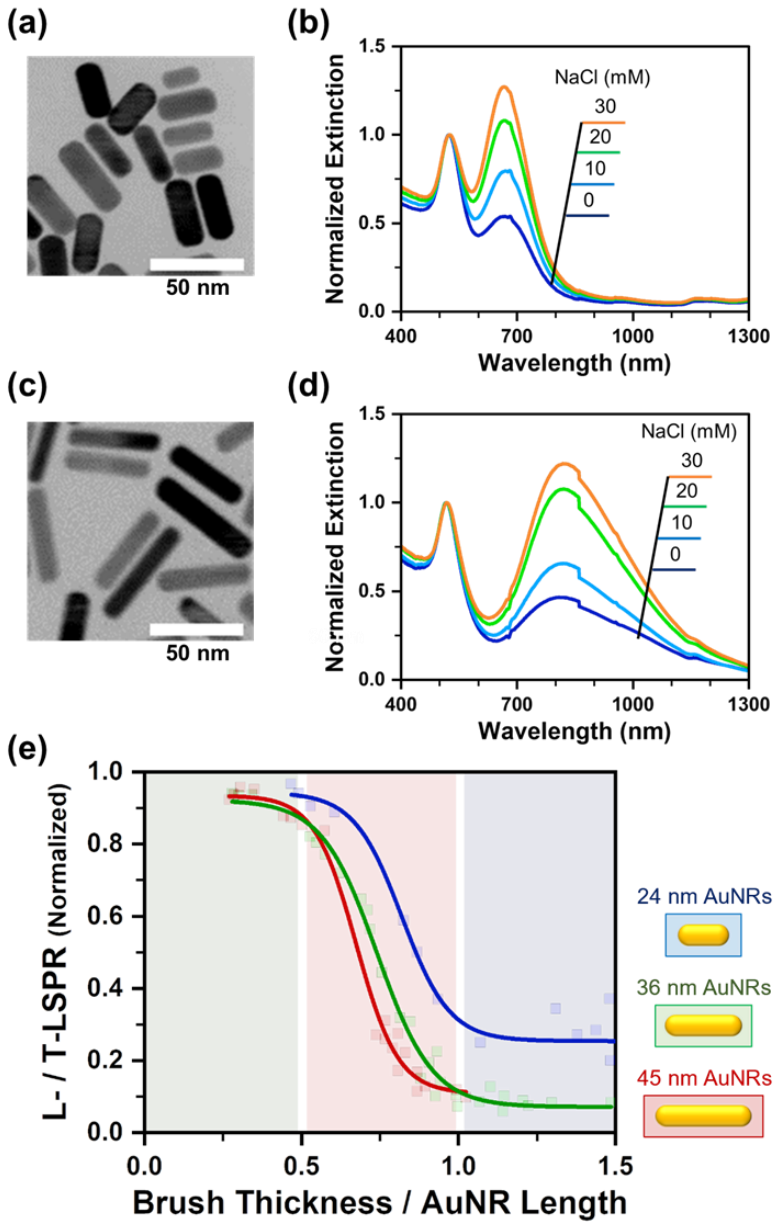

Figure 3-16. (a) TEM image of AuNRs (24 × 10 nm), and (b) salt-triggered extinction spectral change of AuNRs (24 × 10 nm) attached on 100-base ssDNA brushes. (c) TEM image of AuNRs (45 × 10 nm) and (d) salt-triggered extinction spectral change of AuNRs (45 × 10 nm) attached on 175-base ssDNA brushes. Extinction intensities are normalized at T-LSPR. (e) L-/T-LSPR values of three types of AuNRs against calculated brush thickness divided by AuNR length. Each solid line (blue: 24 × 10 nm AuNRs, green: 36 × 10 nm AuNRs, red: 45 × 10 nm AuNRs) is curve-fitted from the obtained data.

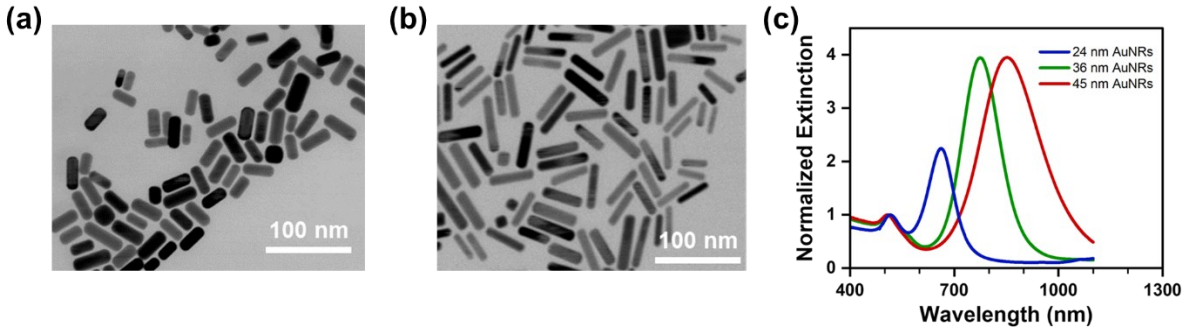

Figure 3-17. (a) STEM image of 24 × 10 nm AuNRs. The AuNRs were acquired commercially. (b) STEM image of 45 × 10 nm AuNRs. AuNRs size was determined as 10 ± 1.8 nm in diameter and 45 ± 10.1 nm in length (300 particles counted). (c) Extinction spectra of dispersed AuNRs with different AuNR lengths (24 × 10 nm, 36 × 10 nm, and 45 × 10 nm). Extinction intensities are normalized at T-LSPR.

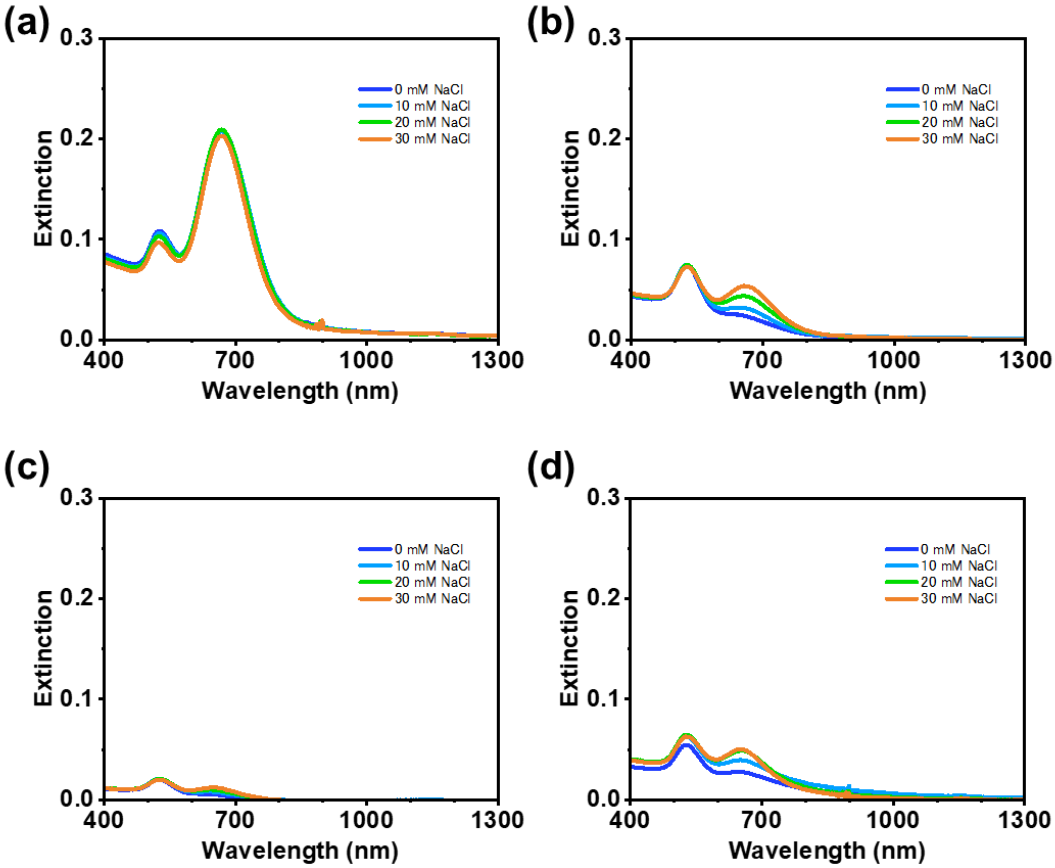

Figure 3-18. Extinction spectra of attached AuNRs (24 × 10 nm) in DNA brushes composed of (a) 50-base, (b) 148-base, (c) 175-base, and (d) 200-base ssDNA at various NaCl concentrations.

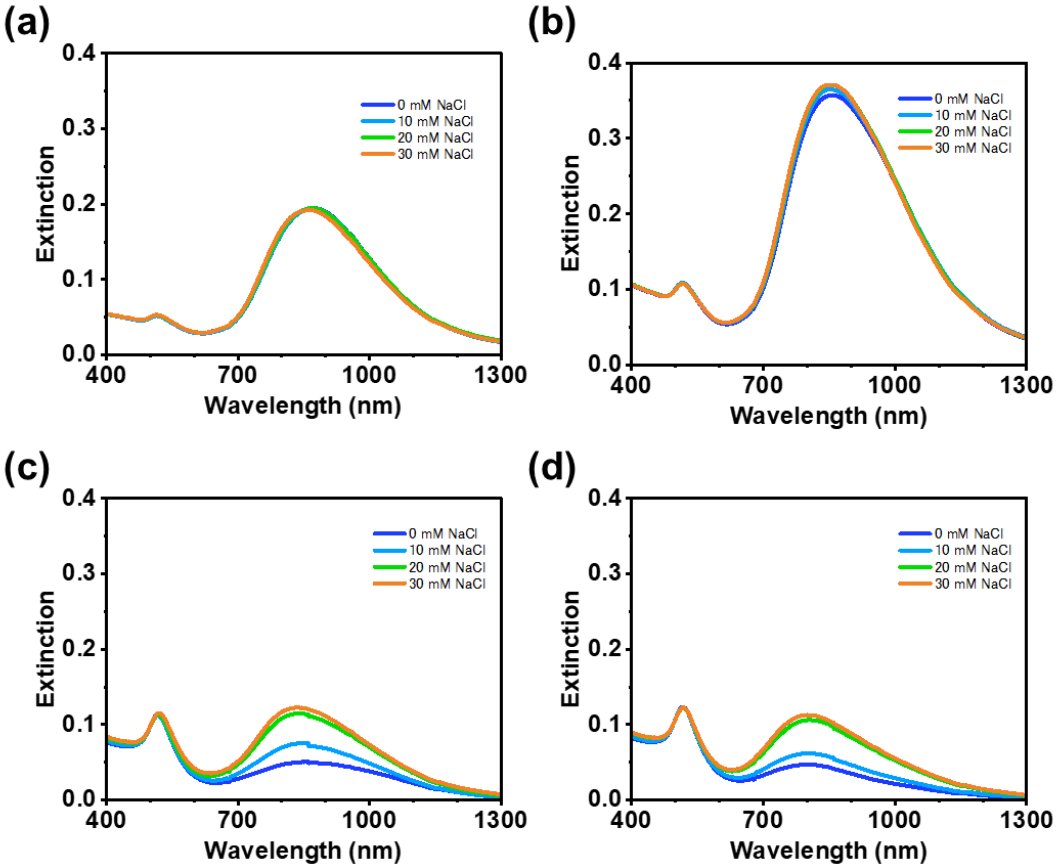

Figure 3-19. Extinction spectra of attached AuNRs (45 × 10 nm) in DNA brushes composed of (a) 50-base, (b) 100-base, (c) 148-base, and (d) 200-base ssDNA at various NaCl concentrations.

3-4. Conclusion

I have achieved the reversible orientation control of AuNRs in anionic polymer brushes through the structural changes of the polymer induced by salt concentration. The orientation of cationic AuNRs attached to DNA brushes dynamically changes depending on NaCl concentration because of NaCl-induced thickness changes. The dynamic control between the vertical (uniform) and tilted (random) orientation of the AuNRs enables not only absorption intensity changes in L-LSPR but also the switching of plasmon coupling. Furthermore, I generalized the orientation of AuNRs on the anionic polymer brushes with brush thickness as a variable by calculating the DNA brush thickness using the Daoud–Cotton model for a flat surface. The AuNRs on the brushes vertically align toward the substrates when the thickness is longer than the AuNR length. In cases where the thickness is shorter than the AuNR length, the attached AuNRs tilt depending on the thickness with a wide range of angles, and the tilt orientation reaches close to parallel when the thickness decreases to almost half of the AuNR length. Here, salt-triggered thickness changes in anionic polymer brushes were applied as a simple model. The generalized insights obtained from this research lead expansion of this platform to a variety of polymer brushes with different stimulus-induced shrinkage and swelling properties. This platform offers great potential for hybrid materials composed of polymer brushes and anisotropic nanoparticles by design.

Chapter 4

Fabrication of Poly(Styrene Sulfonate) Brushes for Orientation Control of Gold Nanorods

4-1. Introduction

Synthetic polymer brushes have received considerable attention in numerous fields due to their versatility in diverse applications.[137–139] While synthetic polymer brushes have been applied for functional surface materials, their potential can be further enhanced through strategic combinations with other materials, such as lipid layers,[140–143] supramolecules,[144,145] nanopore,[146–148] and organic/inorganic particles.[149,150]

One particularly promising candidate for such combinations is a gold nanoparticle (AuNP), owing to their distinctive features, including localized surface plasmon resonance (LSPR) and chemical stability. The optical performance of the LSPR depends on the particle size, shape, and distance between particles, allowing versatile application by controlling their assembly such as sensing[151–153] and dynamic color display.[132,154]

In the realm of AuNP assembly, hybrids of brushes and AuNPs stand out compared to dispersed AuNPs and other plasmonic substrates. Unlike dispersed AuNPs, those integrated into polymer brushes receive protection against aggregation, thereby preserving their functionality. In contrast, plasmonic substrates that immobilize AuNPs on surfaces struggle with the dynamic motion of individual nanoparticles due to strong interactions. Brush/AuNP hybrids provide an active tuning of plasmonic properties at the nanoscale. Incorporation of AuNPs in polymer brushes results in mildly fixing nanoparticles on substrates through electrostatic interaction[61,155] or hydrogen bonding.[53,55] This mild immobilization enables dynamic motion of single nanoparticle on substrates.

Extensive efforts have been dedicated to gaining fundamental insights into nanoparticle motion within polymer brushes and applying nanoparticle/brush hybrids in

applications such as colorimetric sensing,[156,157] surface-enhanced Raman scattering (SERS) detection,[52,155] and nanoparticle size separations.[56]

While most of these hybrids involve spherical gold nanoparticles, the unique LSPR properties of anisotropic gold nanoparticles, particularly rod-shaped gold nanoparticles (gold nanorods: AuNRs), introduce an added dimension. AuNRs exhibit distinctive optical properties, exemplified by two specific plasmonic absorptions: transverse and longitudinal LSPR (T- and L-LSPR). The absorbance resulting from L-LSPR can be modulated by changing the angle of the AuNRs in relation to incident light. These L-LSPR properties enable effective and controllable light absorption within a specific wavelength range.

In Chapters 2 and 3, I demonstrated the alignment of gold nanorods (AuNRs) within DNA brushes through electrostatic interaction. Additionally, I also displayed dynamic orientation control by modifying DNA-AuNR interaction and changing DNA brush thickness. Given the ubiquity of structural changes in polymer brushes, the potential for orientation control coupled with thickness modulation explained in Chapter 3, extends beyond DNA brushes. This method shows significant potential for use with a variety of polymer brushes, expanding the range of controls for achieving precise orientation control of AuNRs. Application of the theory established in Chapter 3 to synthetic polymer brushes suggests potential of versatile application of brush/nanorod hybrids while remaining obstacles must be overcome stemmed from differences of properties between biopolymers and synthetic polymers.

In this chapter, alignment and orientation change of AuNRs is demonstrated with poly(styrene sulfonate) (PSS) brushes as PSS is a representative polymer of anionic polymer (**Figure 4-1**). At specific polymer brush densities, cationic AuNRs were

adsorbed into PSS brushes along with PSS (vertical to substrates). Additionally, the shrinkage of PSS brushes induced by an increase in salt concentration or the introduction of a poor solvent for PSS resulted in dynamic and reversible changes in the orientation of the attached AuNRs. Considering the varying morphology of PSS brushes under different salt types or solvents, I aimed to explore the morphological distinctions within the AuNR array.

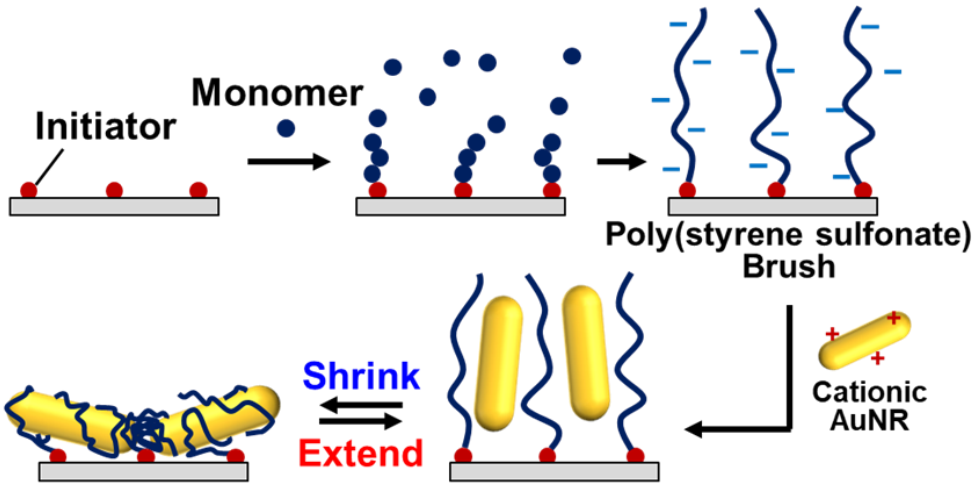

Figure 4-1. Alignment of gold nanorods and their dynamic orientation control in poly(styrene sulfonate) brushes via brush shrinkage and extension.

4-2. Experimental section

4-2-1. Materials and Instruments

3-(Trichlorosilyl)propyl 2-bromo-2-methylpropanoate and (aminomethyl)phosphonic acid were purchased from Tokyo Chemical Industry Co., Ltd (TCI). *p*-Styrenesulfonic acid sodium salt, 2,2'-bipyridyl, copper(I) bromide, 99.9% were purchased from Wako Pure Chemical Industries, Ltd. (Japan). 2-Bromoisobutyryl bromide was purchased from Sigma-Aldrich, Inc. (USA). Quartz substrates (26 mm × 76 mm) with 1.0 mm thickness were purchased from Kenis, Ltd. (Japan). Indium tin oxide (ITO) substrates were purchased from GEOMATEC Co., Ltd. XPS (APEX ESCA, ULVAC-PHI, Inc.) was operated with a monochromatized Al *K*α X-ray source at 1.49 keV at 150 W under 3×10^{-7} Pa. The emission angle of photoelectrons was set to 45° and the beam diameter was 1.2 mm. The neutralizer was set at 0.2 eV and 10.0 μA. Wide-scan spectra (0–1200 eV) were acquired at an energy step of 1.0 and high-resolution spectra (narrow scan) of Na_{1s}, O_{1s}, C_{1s}, and S_{2p} were at 0.2 eV. Scanning electron microscope (SEM) images were obtained using a SU-8230 (Hitachi High-Tech Co., Ltd., Japan). xy-dimensional height images were obtained using an amplitude modulation-atomic force microscopy (AM-AFM) (BioScope Resolve, Bulker). FM-AFM was performed using an SPM-8100FM microscope (Shimadzu Co., Japan). All other salts, reagents and instruments used in this chapter are listed in Chapter 3.

4-2-2. Preparation of AuNRs

AuNR with a 36-nm longer axis were fabricated with same procedure indicated in Chapter 2 (**2-2-2.**).

4-2-3. Surface modification of AuNRs with two types of thiol-ligands

Surface modification of the AuNRs was carried out as described in Chapter 3, **Section 3-2-5**.

4-2-4. Preparation of poly(styrene sulfonate) (PSS) brushes on quartz substrates

For fabricating polyelectrolyte brushes on quartz surfaces, the substrates (20 mm × 15 mm) were firstly cleaned with piranha solution (a 3:1 mixture of concentrated H_2SO_4 with H_2O_2) for 1 h to remove possible residual organics and render surfaces rich of hydroxyl groups. The cleaned substrates were rinsed in MilliQ, and incubated in vacuum at 60°C for 2 h. After perfectly remove H_2O on the quartz surface, the treated substrates were placed in a N_2-filled glovebox, and immersed in superdehydrated toluene with 2 mM 3-(trichlorosilyl)propyl 2-bromo-2-methylpropanoate at 30°C overnight. After anchoring initiators on the surface, the samples were washed with excess acetone with a few seconds sonication, methanol, water, and acetone successively. For the polymerization process, initiator-immobilized substrates were sealed in 200 mL separable flask, and cyclically evacuated and N_2-backfilled to purge all oxygen. Meanwhile, the reaction solvents were prepared. Five grams of Na-SS, 75 mg of Bpy, and 35 mg of CuBr were added into 50 mL of water/methanol mixture (1:1, v/v). The reaction solution was degassed by three freeze-pump-thaw cycles. Three μL ethyl 2-bromoisobutyrate (sacrificial initiator) in 10 mL methanol was also degassed with different glass vessel by three freeze-pump-thaw cycles. Reaction solution (50 mL) and 100 μL of sacrificial initiator solution were injected into the glass vessel in which the initiator-functionalized substrates were placed. The polymerization was carried out at 25°C for various lengths of time without stirring, after which the substrates were removed from the polymerization solution. Afterwards, the substrates were immersed in 100 mM ethylenediaminetetraacetic acid (EDTA) for 30 min,

followed by immersing in water for 30 min to remove residual CuBr and unreacted monomers. The polymer brush substrates were finally dried under a nitrogen flow. To obtain polymer generated by the free initiator, the reaction residue was passed through a silica column to remove CuBr with adequate water/ethanol solution. The transparent solution was evaporated, and remaining white product was dissolved in water. The polymer solution were purified using dialysis (3.5 kDa MWCO) against deionized water for more than one week and were subsequently evaporated.

4-2-5. Preparation of poly(styrene sulfonate) (PSS) brushes on indium tin oxide (ITO) substrates

PSS brushes were fabricated on ITO substrates for SEM measurement. The substrates (20 mm × 15 mm) were first cleaned with an ozone cleaner for 30 min to remove any possible residual organics and render surfaces rich in hydroxyl groups. After 20 min of sonication in MilliQ water, the cleaned substrates were sonicated in ethanol for an additional 20 min. Finally, the substrates were cleaned again with an ozone cleaner for 30 min. The substrates were reacted by immersing them in ethanol containing 2 mM (aminomethyl)phosphonic acid at 30°C overnight. After anchoring the amine moiety on the surface, the samples were washed successively with excess acetone (with a few seconds of sonication), methanol, water, and acetone. The amine-immobilized ITO substrates were then placed in a N_2-filled glovebox and immersed in superdehydrated toluene (20 mL) containing 780 μL of 2-bromoisobutyryl bromide and 900 μL of triethylamine for 1 h at room temperature. After anchoring initiators on the surface, the samples were washed successively with excess acetone, methanol, water, and acetone, each for a few seconds with sonication. Polymerization and subsequent experimental methods were conducted using the same method indicated in **4-2-4.** .

4-2-6. Attachment of ligand-modified AuNRs onto polymer brushes

The thiol ligand-capped AuNRs were attached to PSS brushes through electrostatic interaction (**Figure 4-2**). The thiol ligand-capped AuNR (cationic AuNR) solution was dropped onto the polymer brush substrate. After 5 min incubation, the solution was removed and the substrate was rinsed using a pipette with a 10 mM Tris-HCl (pH = 7.6) solution at least 3 times to completely wash out nonadsorbed AuNRs from the polymer brush. Quartz cell with 1 mm lightpath was assembled with one polymer brush substrate, one clean quartz substrate, and fluororubber sheet as a spacer. On one side of the inside of the cell, polymer brushes with attached AuNRs are present.

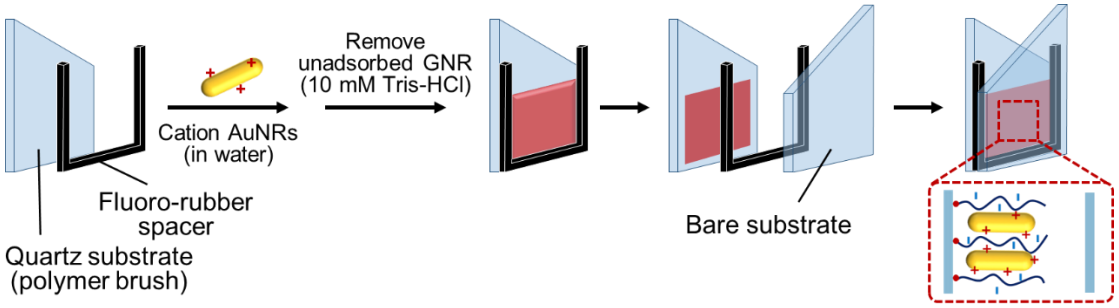

Figure 4-2. Schematic illustration of AuNR attachment to PSS brushes.

4-2-7. Determination of polymer brush density

To quantify the amount of polymer on the substrates, I utilized the absorption intensity at 225 nm, corresponding to the poly(styrene sulfonate) (PSS) peak, as a measure for the polymer brush density. The density of the polymer brushes was evaluated using absorption spectroscopy, with the same calculation with Chapter 2 (**2-2-7.**).

4-2-8. AuNR orientation change with different solution and its investigation

To change the environment surrounding the attached AuNRs in PSS brushes, the solution on the AuNR-adsorbed brush substrate was replaced with another solution. The initial

solution was rinsed at least three times by pipetting to ensure a complete environmental change. Especially, in cases where the AuNRs detached from the PSS brush, the solution was replaced until no AuNRs were detached from the PSS brush. In the extinction spectrum analysis, the incident light was non-polarized and its direction was perpendicular to the cuvette containing the adsorbed AuNRs unless otherwise specified.

4-3. Results and Discussion

4-3-1. Characterization of PSS brushes

Firstly, the PSS brushes were fabricated through "grafting-from" method and the PSS brush density, a key parameter for the alignment of AuNRs, was estimated by its absorption intensity. The absorbance peak intensities (225 nm) of the PSS brushes polymerized for 3 h and 15 h, were 0.2 and 0.03, respectively (**Figure 4-3a, b**). The molecular weight of dispersed PSS, which was synthesized simultaneously with the PSS brush, was determined by size exclusion chromatography (SEC) to be approximately 110,000 (**Figure 4-3c**). To determine the brush density, the absorbance intensities of the PSS brushes were compared with that of the dispersed PSS (**Figure 4-3d, e**). The PSS brushes exhibited an absorbance of 0.03 (15 h polymerization time), equivalent to that of a dispersed PSS solution at a concentration of 32 nM. Calculations yielded a brush density of approximately 19,000 chains/μm² and an estimated interchain distance of approximately 7.8 nm. This density is comparable to that of DNA brushes, which are suitable for AuNR alignment. However, as for PSS brush with 3 h polymerization time, the calculated brush density was approximately 130,000 chains/μm² and interchain distance of approximately 3.0 nm. These results imply that the density of polymer brush decreased with increasing polymerization time. One of the possible cause is degrafting of polymer brush by aqueous liquids due to hydrolysis of silane compounds.[158,159] Although these results make concerns of long-time stability, introduction of hydrophobic part in silane coupling reagent moiety may solve this problem.

The wide-scanned X-ray photoelectron spectroscopy (XPS) spectra of the PSS brush (polymerization time: 3 h) reveal the presence of peaks derived from Na_{1s}, O_{1s}, C_{1s}, and S_{2p} (**Figure 4-4a**). Atomic ratios of each element were calculated from peak areas of the

high-resolution spectra (**Figure 4-4b**). The observed atomic ratio of each atom Na_{1s} O_{1s}, C_{1s}, and S_{2p} is 10.7, 3.0, 0.6, and 1 (normalizing S_{2p} as 1), respectively. Tho observed values are close to the theoretical atomic ratio of PSS (Na_{1s} O_{1s}, C_{1s}, and S_{2p} is 8, 3, 1, and 1), confirming the successful synthesis of the PSS brush.

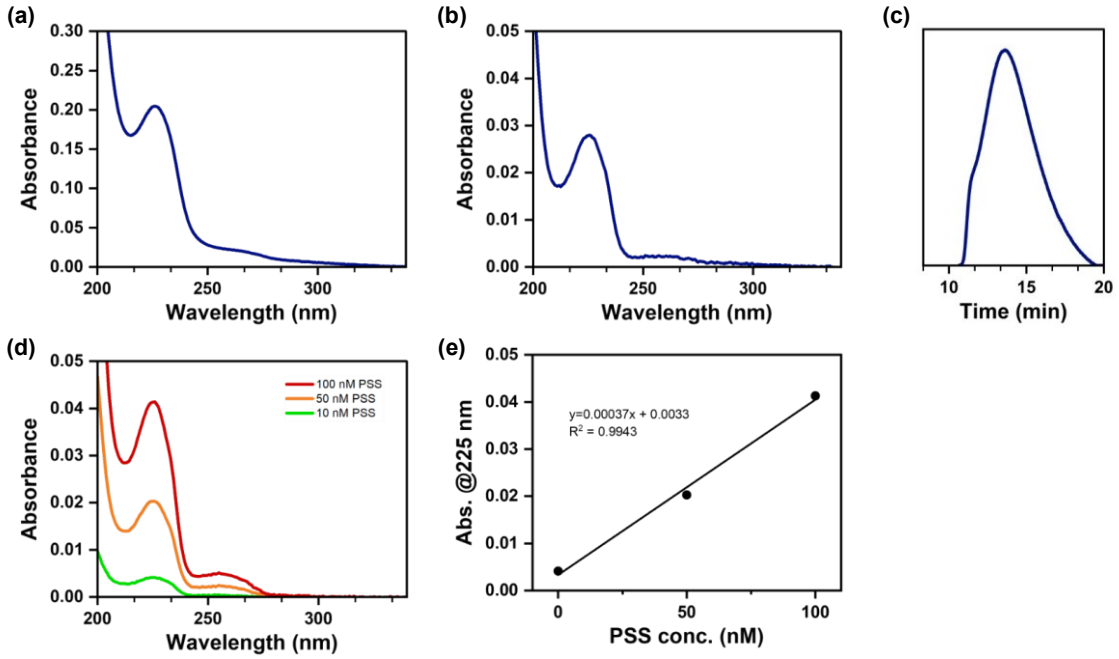

Figure 4-3. (a-b) Absorption spectra of PSS brushes polymerized for (a) 3 h, and (b) 15 h. (c) SEC measurement of the polymerized PSS (d) Absorption spectra of dispersed PSS in water with different concentration. (e) Plot for the peak absorption intensity at 225 nm of PSS against PSS concentration, showing linear relationships.

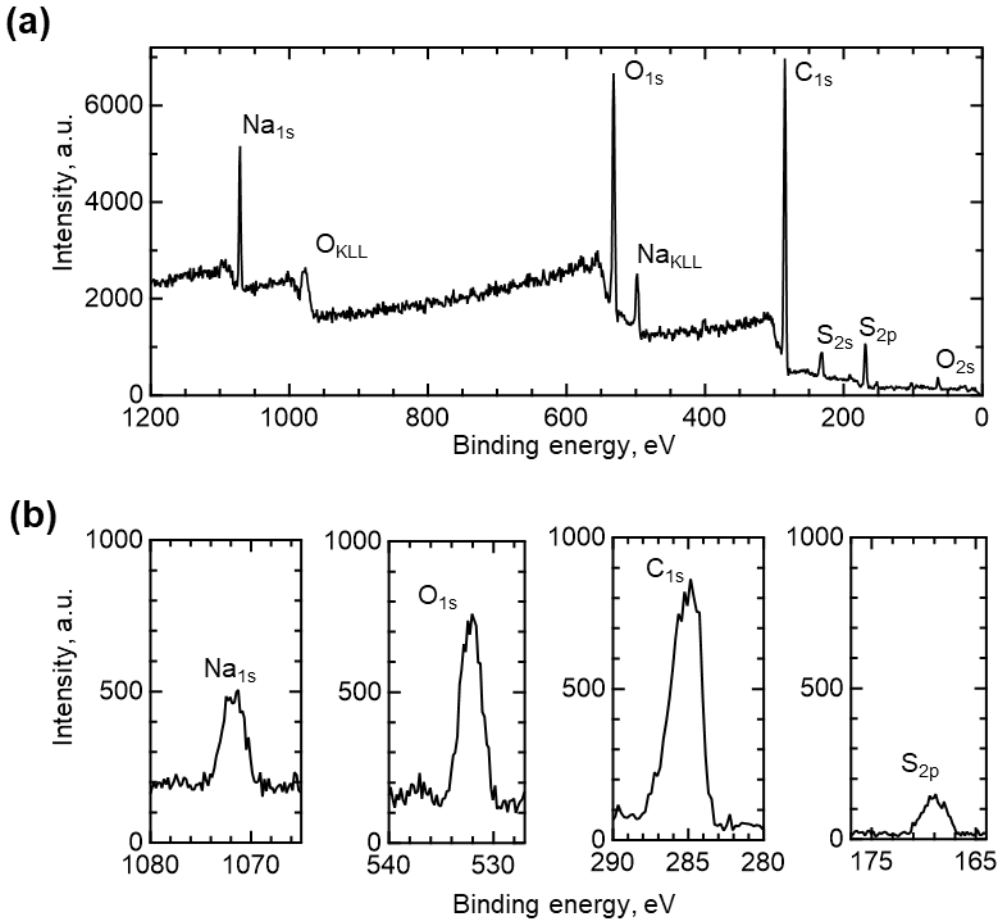

Figure 4-4. XPS spectra of (a) wide scan and (b) high-resolution scan of Na_{1s}, O_{1s}, C_{1s} , and S_{2p} region for a PSS brush surface on a glass substrate.

4-3-2. Characterization in thickness of PSS brushes

The subsequent analysis focused on estimating the thickness of the PSS brushes. Measuring the thickness of polyelectrolyte brushes, particularly at lower densities, is challenging with traditional methods such as ellipsometry and X-ray reflectivity, due to the ambiguity of the brush interface. Despite the importance of thickness measurement, this challenge can be overcome by using frequency modulation atomic force microscopy (FM-AFM). This system enables the detection of minuscule interaction forces exerted on the cantilever probe under optimized experimental conditions. It allows for the resolution and imaging of weak repulsive forces within water-enriched domains at the brush/non-brush interface. FM-AFM imaging on a PSS-grafted quartz substrate revealed the presence of a repulsive layer as shown in shades of blue and white to represent frequency shift gradations (**Figure 4-5a**). The profile of frequency shift (Δf) profile averaged over the entire lateral extent (250 nm), as shown in **Figure 4-5b**, indicates that the distances from the substrates (y axis) at the initiation point of changing frequency ($\Delta f \approx 0$) were clearly different between the PSS brushes polymerized for 3 h and 15 h. These results indicate that the thickness of the polymer brushes differs under the two different conditions. The thickness of the PSS polymerized for 3 h and 15 h was 182 nm and 37 nm, respectively (**Figure 4-5c**). This result is consistent with other reports.[136,160]

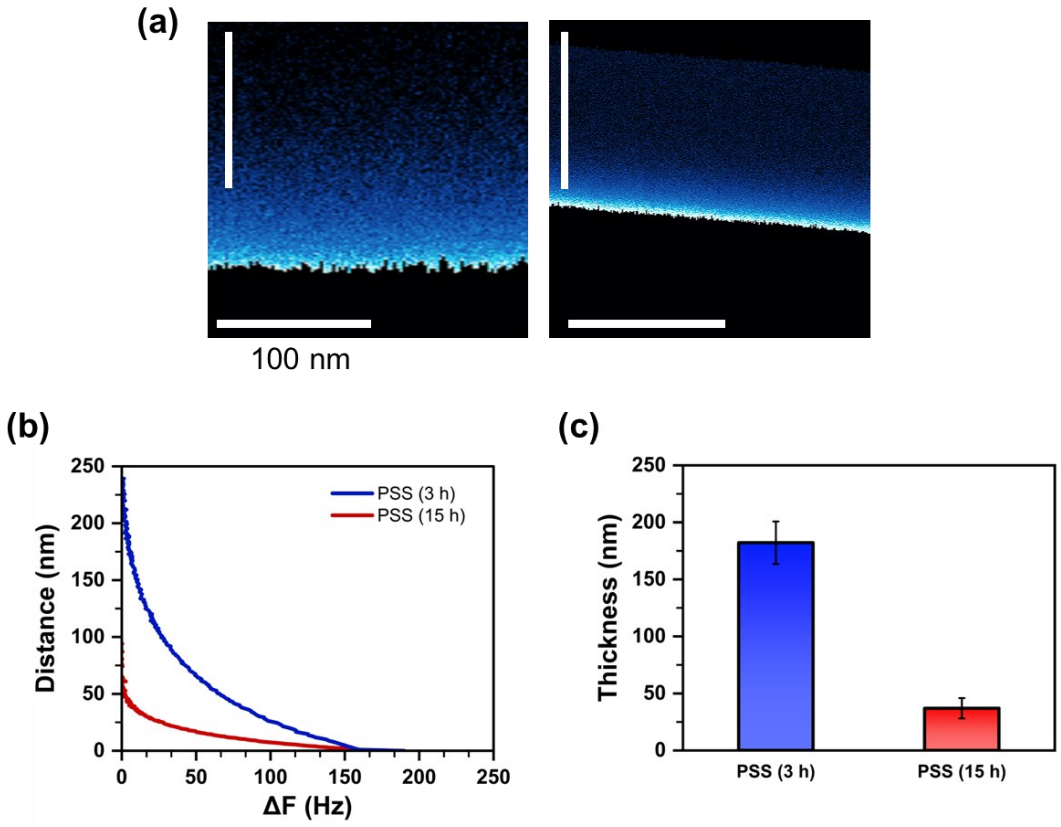

Figure 4-5. (a) FM-AFM images of PSS brushes in 10 mM Tris-HCl (pH 7.6) polymerized for (left) 3 hours, and (right) 15 hours. (b) Distance from substrate against frequency difference of AFM. As $\Delta F = 0$ indicates the initiation of frequency change, y axis around $\Delta F = 0$ implies the thickness of PSS brushes. (c) Thickness of PSS brushes polymerized for 3 and 15 hours. The thickness of PSS brushes is defined at $\Delta F = 5$ of FM-AFM measurement to suppress the noise effect.

4-3-3. Vertical alignment of AuNRs with PSS brushes

Next, vertical alignment of AuNRs was demonstrated with the PSS brushes. Cationic AuNRs were attached to PSS brushes (interchain distance: 3.0 nm) through electrostatic interaction. The extinction spectrum revealed that the L-LSPR intensity is higher than the T-LSPR intensity, resulting in an L-/T-LSPR intensity ratio of 1.95 (**Figure 4-6a**). The results suggest that the AuNRs tilt on the quartz substrate, likely on the surface of high density PSS brushes, as they exhibit a stronger L-LSPR intensity at higher incident light angles (~ 90°) compared to the AuNRs. In contrast, the extinction spectrum of the AuNRs attached to the PSS brushes, with an interchain distance of 7.8 nm, resulted in the L- / T-LSPR value of 0.17 (**Figure 4-6b**). To investigate the position of AuNRs and their effect on brush thickness, FM-AFM of PSS brushes with vertical AuNRs was measured. The FM-AFM image shows the existence of a frequency change area near the substrate (**Figure 4-6c**). Comparison of the thickness between PSS brushes with and without AuNRs revealed that the thickness of both PSS brushes was almost the same (**Figure 4-6d**). This result indicates that the attached AuNRs do not affect the brush thickness, suggesting insertion of the AuNRs into the PSS brushes. The AFM height map did not show a distinct height peak on the PSS brushes, despite a slight increase in surface roughness (**Figure 4-6e**). This result suggests that while there is a slight increase in surface roughness implying the presence of a second layer of AuNRs on the PSS brushes, most of the AuNRs are embedded within the PSS brushes.

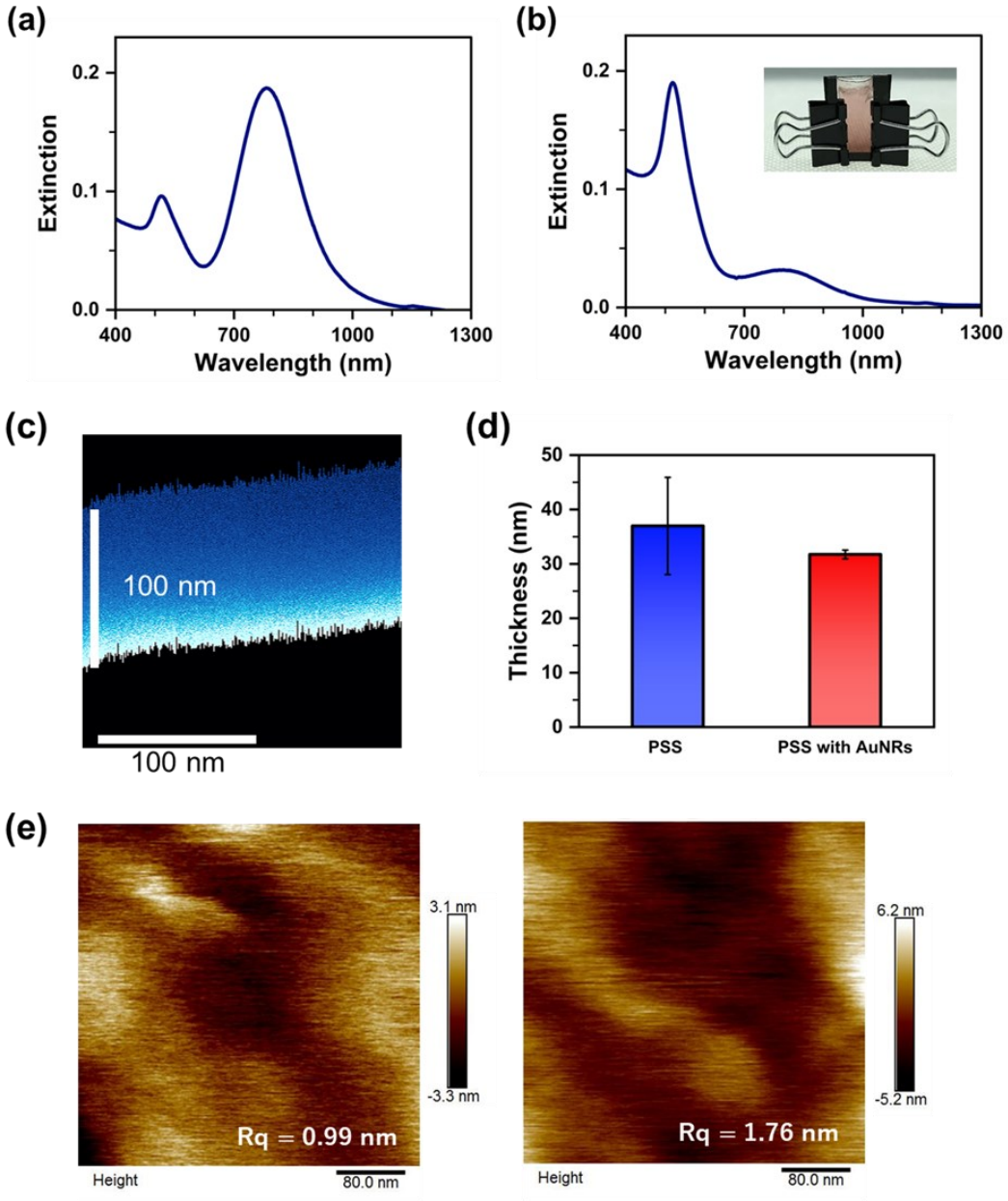

Figure 4-6. Extinction spectra of AuNRs in PSS brushes ((a) 3.0 nm interchain distance, and 182 nm thickness. (b) 7.8 nm interchain distance, 37 nm thickness). The inset denotes the photograph of the attached AuNRs in polymer brush substrates. (c) FM-AFM image of PSS brushes with AuNRs. (d) Thickness of PSS brushes with and without AuNRs. The thickness of PSS brushes is defined at $\Delta F = 5$, obtained from FM-AFM measurement. (e) AFM height images of PSS brushes (left) without AuNRs and (right) with AuNRs in 10 mM Tris-HCl (pH 7.6). Scan size, 400 nm × 400 nm (scale bars, 80 nm).

4-3-4. Effect of cationic amount on the surface of AuNRs for their orientation in PSS brushes

The effect of cationic content on AuNR surface on its orientation in PSS brushes was investigated. Previous study has shown that a moderate amount (10% to 30%) of cationic ligands on the surface of AuNRs is suitable for their alignment. Strong electrostatic interactions, on the other hand, result in a strong attachment to DNA with a random orientation.[74] In this experiment, I fabricated AuNRs with varying cationic ratios and attached them onto a PSS brush substrate with an interchain distance of approximately 8 nm (**Figure 4-7a**). The zeta-potential of the dispersed AuNRs showed a positive correlation with the mixing ratio of the cationic ligands (**Figure 4-7b**). When AuNRs with varying amounts of cationic ligands were attached, the extinction spectra showed a more tilted orientation for weaker (5% and 10%) and stronger (40% and 60%) cationic intensities, as compared to those with 20% (**Figure 4-7c, d**). Based on these findings, I have concluded that AuNRs with a cationic ratio of 20% provide optimal for AuNR alignment and thus the AuNRs were employed for subsequent experiments.

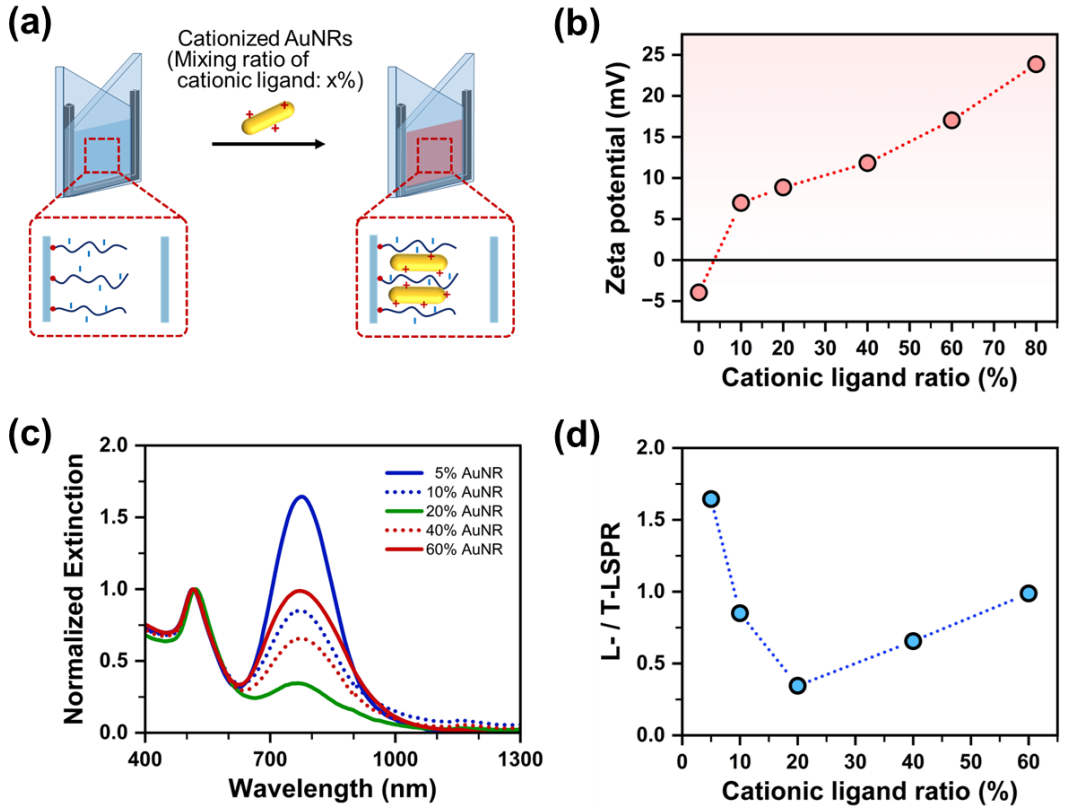

Figure 4-7. (a) Schematic illustration of AuNR attachment to PSS brushes with varying cationic ratios of AuNRs. Experimental details are provided in 4-2-6. and Figure 4-2. (b) Zeta potential of AuNRs with different ratios of cationic ligands. The measurements were conducted using 10 mM Tris-HCl (pH 7.6). (c) Extinction spectra of AuNRs with varying amounts of surface cationic ligands on PSS brush substrate and (d) L- / T-LSPR values plotted against the mixing ratio of cationic ligands.

4-3-5. Dynamic orientation change of AuNRs in PSS brushes with varied salt concentration.

Next, I demonstrated dynamic orientation change of vertically attached AuNRs induced by the shrinkage of DNA brushes by varying salt concentration (x mM NaCl + 10 mM Tris-HCl (pH 7.6)). As generally known, thickness of charged polymer brushes decreases as salt concentration increases. Based on the knowledge, dynamic orientation change of AuNRs with thickness changes were demonstrated. Following the vertical attachment of AuNRs to the polymer brushes, salt concentration was changed by solvent replacement. The L-LSPR peak intensity exhibited a corresponding increase without significant changes in T-LSPR as the NaCl concentration increased from 0 mM to 40 mM (**Figure 4-8a**). This result indicates that the orientation of the attached AuNRs tilted gradually with the increase in salt concentration. Considering that thickness of polymer brushes depends on salt concentration, these dynamic orientation changes occur due to the thickness changes. The orientation changes showed no hysteresis when plotting the L-LSPR intensities in relation to the changes in NaCl concentration (**Figure 4-8b, c)**. The phenomenon is the same as dynamic orientation change in ssDNA brushes (**Figure 3-9**), suggesting that the mechanism differs from that of electrostatic interaction strength-based orientational changes. As regards 50 mM or higher NaCl concentration, the 20% cationic AuNRs adsorbed in the PSS brushes were detached due to the weaken electrostatic attraction between AuNRs and PSS. Upon repeated solvent exchange between 0 mM and 40 mM NaCl, the L-/T-LSPR intensity of the attached AuNRs changed reversibly for at least 3 cycles (**Figure 4-8d**).

To improve understanding of the orientation dynamics of AuNRs within PSS brushes, I analyzed the correlation between the L-/T-LSPR intensities and brush thickness using the sigmoidal model derived from Chapter 3. FM-AFM revealed that the thickness

of the PSS brushes significantly decreased upon addition of 40 mM NaCl or 5 mM $MgCl_2$ (**Figure 4-9a**). Extinction spectra of AuNRs showed more significant increase in L-LSPR when $MgCl_2$ were added than NaCl (**Figure 4-9b**). All of these experimental data points were fitted on the line of a sigmoid curve (**Figure 4-9c**). This result reveals that the AuNRs orientation within PSS changes in accordance with the generalized theory established in Chapter 3. This correlation suggests that significant and reversible changes in brush thickness can effectively regulate the plasmonic properties of AuNRs.

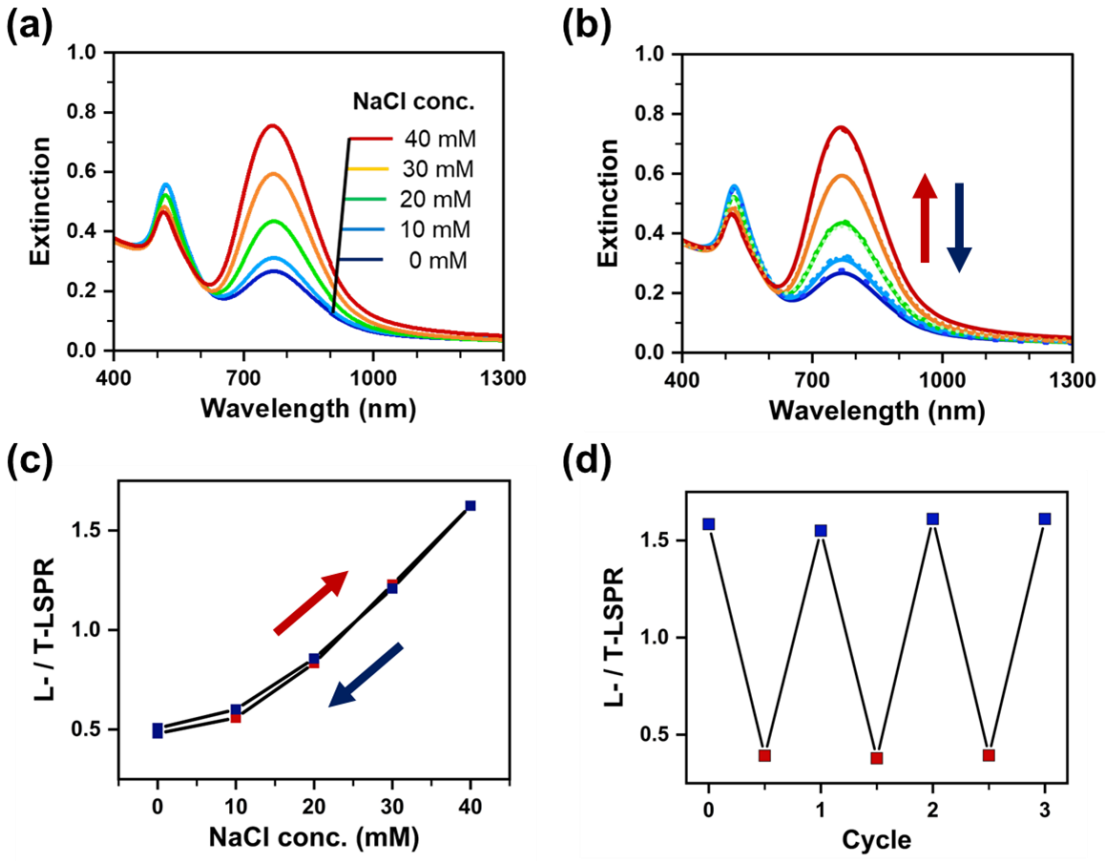

Figure 4-8. (a) Extinction spectra of AuNRs in a PSS brush at various NaCl concentrations. (b) Extinction spectra of AuNRs in a PSS brush from 0 mM to 40 mM NaCl (solid lines), and from 40 mM to 0 mM NaCl (dotted lines). (c) L-LSPR/T-LSPR intensities obtained from (a) against NaCl concentration. (d) L-LSPR/T-LSPR values on repeated changes in NaCl concentration between 0 and 40 mM.

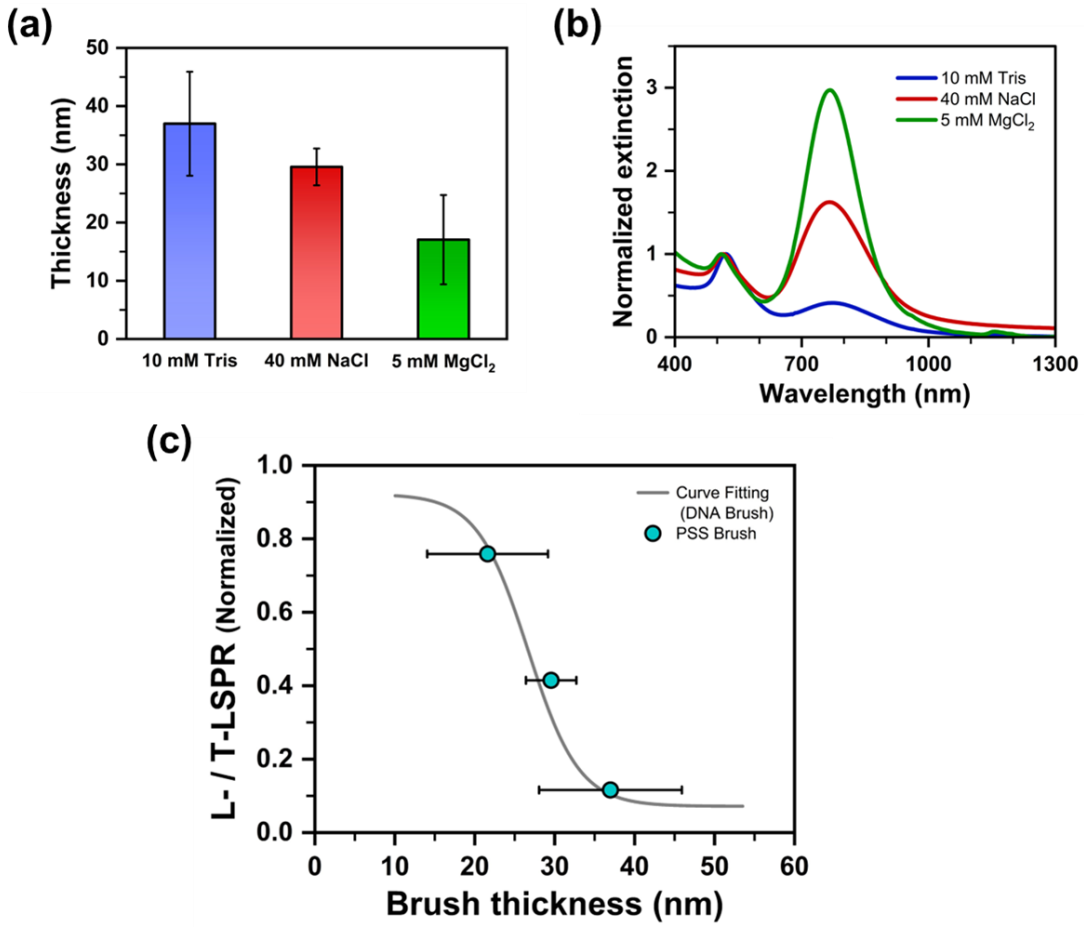

Figure 4-9. (a) Thickness of PSS brushes in 10 mM Tris-HCl (pH 7.6) with different salt concentration and type. The thickness of PSS brushes is defined at $\Delta F = 5$, obtained from FM-AFM measurement. (b) Extinction spectra of AuNRs in PSS brushes under various conditions. (c) Plot for obtained data from (a) and (b) in the fitting curve obtained from Figure 3-14.

4-3-6. Dynamic and drastic orientation change of AuNRs in PSS brushes by using solubility of polymer

To achieve significant and reversible manipulation of polymer brush thickness, the focus was shifted from salt concentration to the solubility parameters of PSS. The configuration of polymer brushes changes depending on the solvent types. In high salt concentrations, the brushes form a coiled configuration, while in a poor solvent, they form a more compact structure. This results in greater thickness variations in response to changes in polymer solubility rather than alterations in salt concentration. **Figure 4-10a** shows that the L-LSPR intensity of AuNRs in PSS brushes significantly increased upon immersion in poor solvents for PSS, such as methanol, ethanol, 2-propanol, and 1-butanol. The results indicate that the AuNRs in PSS brushes inclined due to shrinkage of the brushes in poor solvents, leading to the heightened L-LSPR intensity. This hypothesis is further investigated by the negative correlation between the L-/T-LSPR intensities and the solubility parameter of PSS,[161] as illustrated in **Figure 4-10b**. This relationship supports the notion of a thickness-induced orientation transition. Furthermore, **Figure 4-10c** and **d** demonstrate that the L-/T-LSPR intensity changes reversibly for at least 5 cycles, highlighting the tunable and robust nature of this thickness-dependent plasmonic tuning mechanism. These results indicate that dynamic orientation change in DNA brushes established in Chapter 3, is also applicable for anionic synthetic polymer brushes.

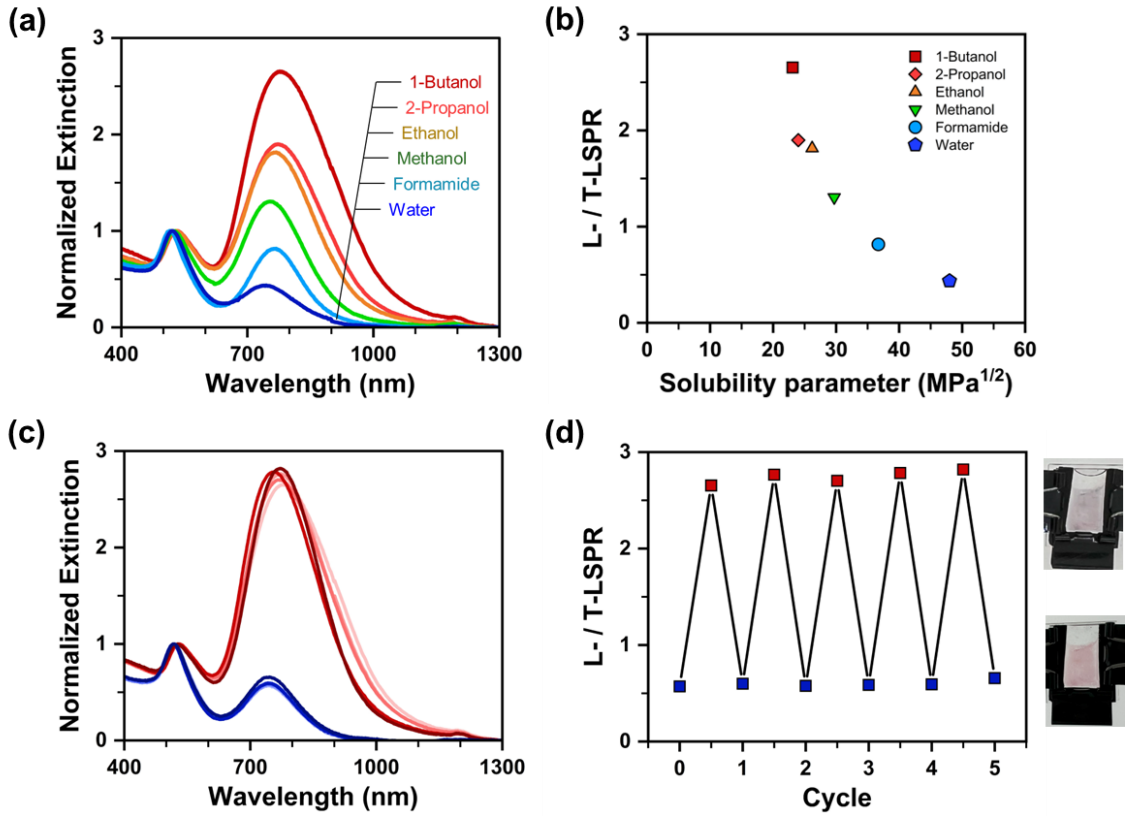

Figure 4-10. (a) Extinction spectra of AuNRs in a PSS brush in various solvents. (b) L-LSPR / T-LSPR values against solubility parameter of PSS. (c) Extinction spectra of AuNRs in a PSS brush under repeated solvent exchange between 10 mM Tris-HCl (pH 7.6) and 1-Butanol. (d) L-LSPR / T-LSPR intensities on repeated solvent exchanges between 10 mM Tris-HCl (pH 7.6) and 1-butanol. The insets show photographs of the PSS brush substrate (2.0 cm × 1.5 cm) with AuNRs corresponding to the different solvent.

4-3-7. Difference of plasmonic coupling effect in relation to solvent types

Previous research has reported on the morphology differences of PSS brushes depending on ion types and solvents.[136,160,162–164] Monovalent ions and some divalent ions, such as Mg^{2+} and Ca^{2+}, induce homogeneous shrinkage of PSS brushes. However, other multivalent ions, such as Y^{3+}, and poor solvent cause heterogeneous shrinkage resulting in a collapsed micellar structure or a disordered structure.[165–168] Based on these findings, the behavior of attached AuNRs depending on solvent types was investigated besides the AuNR orientation change mentioned above. To induce homogeneous and drastic shrinkage of PSS brushes, $MgCl_2$ was used as the stimulus. Upon the addition of $MgCl_2$ to PSS brushes with AuNRs, the L-LSPR peak intensity of AuNRs significantly increased without substantial change in the peak wavelength of the L-LSPR (**Figure 4-11a, b**). In contrast, the peak wavelength was higher when the AuNRs tilted due to poor solvent (**Figure 4-11c**). The difference in the L-LSPR peak wavelength and the shape of the extinction spectrum from the attached AuNRs is shown in **Figure 4-11d**. Despite the similar orientation degree, the L-LSPR peak wavelengths for the AuNRs under 5 mM $MgCl_2$, 1 mM YCl_3, and 1-butanol were different, measuring 772 nm, 782 nm, and 803 nm, respectively. The extinction spectrum of AuNRs in PSS brushes under 5 mM $MgCl_2$ exhibited a sharp L-LSPR peak, while a broader L-LSPR was observed with YCl_3. The addition of 1-butanol to the substrate resulted in a considerably wider L-LSPR peak compared to the presence of multivalent ions. The longer wavelength peak and broadening toward the longer wavelength of L-LSPR suggest end-to-end plasmonic coupling among AuNRs.[127,128,169]

Subsequently, the morphologies of PSS brushes and AuNRs were explored. The AFM image of a PSS brush with AuNRs in 5 mM $MgCl_2$ did not show a significant pattern,

and its roughness did not increase compared to that of a PSS brush with AuNRs in 10 mM Tris-HCl (**Figure 4-6e**, **Figure 4-12a (top)**). However, **Figure 4-12a (bottom)** showed both a patterned structure and an increase in roughness in 1 mM YCl_3. These results are consistent with other studies conducted without AuNRs, indicating that the attachment of AuNRs onto PSS brushes does not prevent the formation of heterogeneous morphology of PSS brushes. To investigate the assembly state of tilted AuNRs in PSS brushes, the AuNRs on PSS brush substrates were visualized using SEM after immersion in various solvents. The attached AuNRs after immersing in 5 mM $MgCl_2$ showed a partially aligned orientation (**Figure 4-12b (top)**), while those after immersing in 1 mM YCl_3 resulted in a random orientation of the tilted AuNRs with the proximity to the AuNR edges (**Figure 4-12b (middle)**). The AuNRs evaporated from 1-butanol displayed an aggregated structure of the AuNR array (**Figure 4-12b (bottom)**). Although these images do not directly visualize AuNRs in solution, these results suggest a difference in the assembly state of tilted AuNRs under different solvent types.

The plasmonic coupling effect is induced by the difference in the assembly state of tilted AuNRs, which in turn is caused by the morphological differences of PSS brushes. This mechanism suggests that changes in the plasmonic properties of AuNRs can be controlled not only by brush shrinkage/swelling, but also by partial morphology.

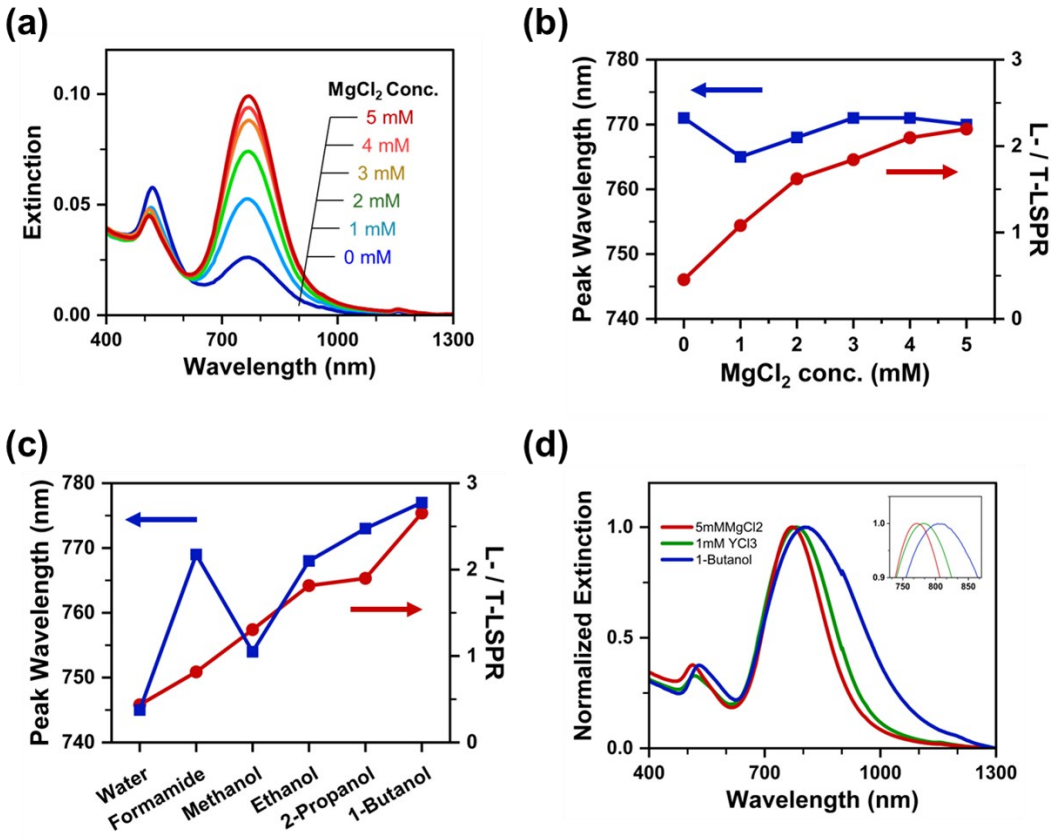

Figure 4-11. (a) Extinction spectra of AuNRs inserted in PSS brushes with different $MgCl_2$ concentration. (b, c) L-LSPR peak wavelength and orientation degree (L-/T-LSPR) of attached AuNRs plotted against (b) $MgCl_2$ concentration and (c) different solvents. (d) Extinction spectra of AuNRs in PSS brushes with different types of multivalent salt (Mg^{2+} or Y^{3+}) and poor solvent for PSS.

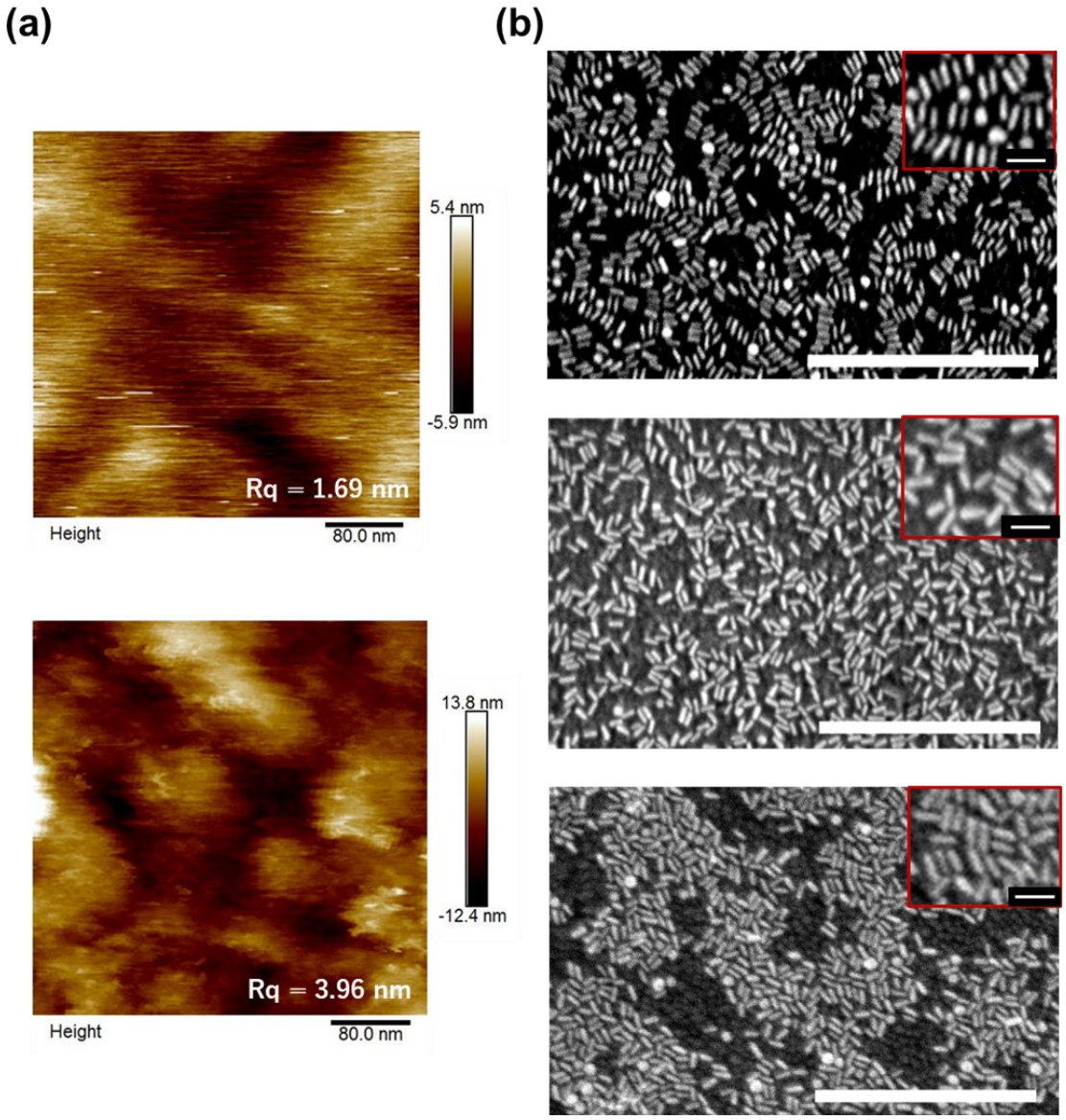

Figure 4-12. (a) AFM height images of PSS brushes with AuNRs in (top) 5 mM $MgCl_2$ and (bottom) 1 mM YCl_3. Scan size, 400 nm × 400 nm (scale bars, 80 nm). (b) SEM images of AuNRs in PSS brushes on ITO substrates after immersing (top) 5 mM $MgCl_2$, (middle) 1 mM YCl_3, and (bottom) 1-butanol (scale bars, 500 nm). Insets are enlarged view of AuNRs (scale bars, 50 nm).

4-4. Conclusion

The alignment and reversible orientation change of AuNRs using PSS brushes synthesized through the "grafting-from" method have been achieved. Successful fabrication of PSS brushes was confirmed through absorption spectrum and X-ray photoelectron spectroscopy (XPS) measurements. Frequency modulation atomic force microscopy (FM-AFM) measurements were conducted on PSS brushes to confirm the shrinkage of the brushes due to increasing NaCl concentration. Upon attaching cationic AuNRs to the PSS brushes, the AuNRs were aligned within the brushes at an interchain distance of about 8.0 nm. However, when the interchain distance was narrower, the AuNRs exhibited a tilted orientation on the PSS brushes. Furthermore, an investigation into the effect of the cationic ratio of AuNRs revealed an optimal ratio of 20% for achieving AuNR alignment. Reversible orientation control of AuNRs within PSS brushes was demonstrated through the induced shrinking and swelling triggered by changes in salt concentration and PSS solubility. Additionally, research indicates that the plasmonic properties of AuNRs can be affected not only by the thickness but also the morphology of PSS brushes. The discoveries from Chapter 4 have expanded the usefulness of the orientation control system. This system can also apply to hybrid materials that include versatile polymer brushes and anisotropic nanoparticles.

Chapter 5

General conclusion

In this thesis, I focused on the orientation control of gold nanorods in polymer brushes for their plasmonic control. In this chapter, I summarize this thesis and afford the significance and prospects.

In chapter 2, I presented interaction strength-triggered dynamic orientation changes in AuNRs in DNA polymer (dsDNA and ssDNA) brushes by pH changes. I fabricated pH-responsive AuNRs modified with 10% amine-terminated ligands, whose zeta-potential of the AuNRs gradually increased with decrease in the solution pH. The AuNR orientation on the DNA brushes was reversibly changed by the modulation of the electrostatic interactions between the AuNRs and polymers via changes in the solution pH. The AuNR orientation changed in a wider pH range (pH 4.0–7.6) on ssDNA brushes, while the L-LSPR peak changed drastically and in a narrow pH range (pH 4.0–5.0) on the dsDNA brushes. These results imply that the degree of AuNR orientation can be tuned depending on polymer rigidity and anionic content of polymer.

In chapter 3, I demonstrated that thickness change of ssDNA brushes induced orientation change of AuNRs in the brushes, and the orientation degree was generalized with brush thickness as a valuable. The AuNRs in the brushes vertically align in relation to the substrates when the thickness is longer than the AuNR length. In cases where the thickness is shorter than the AuNR length, the attached AuNRs tilt depending on thickness across a wide range of angles, and the tilt orientation reaches close to parallel when the thickness decreases to almost half of the AuNR length. The generalized insights obtained from this research can lead to the expansion of this platform to a variety of polymer brushes with different stimulus-induced shrinkage and swelling properties.

In chapter 4, poly(styrene sulfonate) (PSS) brushes were fabricated for AuNRs' alignment and their orientation change. With suitable PSS density on substrates for AuNR

insertion, AuNRs were attached to the PSS brushes along with PSS (perpendicular to the substrates). AuNRs modified with a 20% cationic ligand displayed the most vertical orientation compared to other cationic ratios. Shrinkage of PSS brushes induced by salt or poor solvent tilt the vertical AuNRs, and the brush swelling results in returning the AuNR orientation. Additionally, investigations suggest that the plasmonic properties of AuNRs can be influenced not only by the thickness but also by the morphology of PSS brushes.

In this thesis, I showed a method for the dynamic orientation control of AuNRs using polymer brushes on solid substrates. Unlike alternative approaches for controlling the orientation of AuNRs, the polymer brush-templated method allows for the dynamic manipulation of the plasmonic properties of AuNRs on solid substrates, mitigating concerns related to particle aggregation. The demonstration of these platforms introduces a new strategic approach within the research domains of both polymer brushes and plasmonic particles. In the future, I believe that diverse polymer will be utilized for the system, enabling more complexed dynamic movement of nanoparticles and fabricating other functional materials.

References

[1] S. E. McNeil, *J Leukoc Biol* **2005**, *78*, 585.

[2] E. A. Goodilin, P. S. Weiss, Y. Gogotsi, *ACS Nano* **2019**, *13*, 12206.

[3] Y. Chen, *Microelectron Eng* **2015**, *135*, 57.

[4] S. Hamajima, H. Mitomo, T. Tani, Y. Matsuo, K. Niikura, M. Naya, K. Ijiro, *Nanoscale Adv* **2019**, *1*, 1731.

[5] V. K. Valev, *Langmuir* **2012**, *28*, 15454.

[6] L. Wang, Y. Sun, Z. Li, A. Wu, G. Wei, *Materials* **2016**, *9*, 53.

[7] A. Biswas, I. S. Bayer, A. S. Biris, T. Wang, E. Dervishi, F. Faupel, *Adv Colloid Interface Sci* **2012**, *170*, 2.

[8] K. A. W. Horowitz, M. Woodhouse, H. Lee, G. P. Smestad, *AIP Conf Proc* **2015**, *1679*, 100001.

[9] R. Anghilante, D. Colomar, A. Brisse, M. Marrony, *Int J Hydrogen Energy* **2018**, *43*, 20309.

[10] K. A. Willets, R. P. Van Duyne, *Annu Rev Phys Chem* **2007**, *58*, 267.

[11] I. De Feijter, L. Albertazzi, A. R. A. Palmans, I. K. Voets, *Langmuir* **2015**, *31*, 57.

[12] R. Klajn, K. J. M. Bishop, B. A. Grzybowski, *Proc Natl Acad Sci U S A* **2007**, *104*, 10305.

[13] R. Iida, H. Mitomo, Y. Matsuo, K. Niikura, K. Ijiro, *Journal of Physical Chemistry C* **2016**, *120*, 15846.

[14] Y. Torii, N. Sugimura, H. Mitomo, K. Niikura, K. Ijiro, *Langmuir* **2017**, *33*, 5537.

[15] H. Wang, L. Chen, X. Shen, L. Zhu, J. He, H. Chen, *Angewandte Chemie - International Edition* **2012**, *51*, 8021.

[16] B. L. Gretchen A. DeVries, Markus Brunnbauer, YingHu, Alicia M. Jackson, F. S. Brian T. Neltner, Oktay Uzun, Benjamin H. Wunsch, *Science (1979)* **2007**, *315*, 358.

[17] T. Nishio, K. Niikura, Y. Matsuo, K. Ijiro, *Chemical Communications* **2010**, *46*, 8977.

[18] T. P. Bigioni, X. M. Lin, T. T. Nguyen, E. I. Corwin, T. A. Witten, H. M. Jaeger, *Nat Mater* **2006**, *5*, 265.

[19] J. Song, L. Pu, J. Zhou, B. Duan, H. Duan, *ACS Nano* **2013**, *7*, 9947.

[20] K. Niikura, N. Iyo, T. Higuchi, T. Nishio, H. Jinnai, N. Fujitani, K. Ijiro, *J Am Chem Soc* **2012**, *134*, 7632.

[21] J. He, Y. Liu, T. Babu, Z. Wei, Z. Nie, *J Am Chem Soc* **2012**, *134*, 11342.

[22] P. Priecel, H. A. Salami, R. H. Padilla, Z. Zhong, J. A. Lopez-Sanchez, *Chinese Journal of Catalysis* **2016**, *37*, 1619.

[23] C. J. Orendorff, T. K. Sau, C. J. Murphy, *Small* **2006**, *2*, 636.

[24] J. Cao, T. Sun, K. T. V. Grattan, *Sens Actuators B Chem* **2014**, *195*, 332.
[25] H. Chen, L. Shao, Q. Li, J. Wang, *Chem Soc Rev* **2013**, *42*, 2679.
[26] Y. Bai, L. Fu, L. Zhen, Y. Yin, W. Wang, Y. Liu, M. Wang, E. L. Chronister, *Nanoscale* **2015**, *7*, 14483.
[27] J. Cao, T. Sun, K. T. V. Grattan, *Sens Actuators B Chem* **2014**, *195*, 332.
[28] X. Huang, M. A. El-Sayed, *J Adv Res* **2010**, *1*, 13.
[29] A. Apte, P. Joshi, P. Bhaskar, D. Joag, S. Kulkarni, *Appl Surf Sci* **2015**, *355*, 978.
[30] B. Peng, G. Li, D. Li, S. Dodson, Q. Zhang, J. Zhang, Y. H. Lee, H. V. Demir, X. Yi Ling, Q. Xiong, *ACS Nano* **2013**, *7*, 5993.
[31] B. Peng, Z. Li, E. Mutlugun, P. L. Hernández Martínez, D. Li, Q. Zhang, Y. Gao, H. V. Demir, Q. Xiong, *Nanoscale* **2014**, *6*, 5592.
[32] M. Wang, C. Gao, L. He, Q. Lu, J. Zhang, C. Tang, S. Zorba, Y. Yin, *J Am Chem Soc* **2013**, *135*, 15302.
[33] M. H. Rizvi, R. Wang, J. Schubert, W. D. Crumpler, C. Rossner, A. L. Oldenburg, A. Fery, J. B. Tracy, *Advanced Materials* **2022**, *34*, 2203366.
[34] Q. Liu, Y. Yuan, I. I. Smalyukh, *Nano Lett* **2014**, *14*, 4071.
[35] N. J. Greybush, K. Charipar, J. A. Geldmeier, S. J. Bauman, P. Johns, J. Naciri, N. Charipar, K. Park, R. A. Vaia, J. Fontana, *ACS Nano* **2019**, *13*, 3875.
[36] C. Shen, M. Matsubara, M. Yabushita, S. Maki, A. Muramatsu, K. Kanie, *Nanoscale Adv* **2020**, *2*, 814.
[37] Y. Zhang, Q. Liu, H. Mundoor, Y. Yuan, I. I. Smalyukh, *ACS Nano* **2015**, *9*, 3097.
[38] M. R. Thomas, S. Klein, R. J. Greasty, S. Mann, A. W. Perriman, R. M. Richardson, *Advanced Materials* **2012**, *24*, 4424.
[39] H. Kang, S. S. Kim, S. Il Yoo, B. H. Sohn, *Adv Mater Interfaces* **2019**, *6*, 1901257.
[40] R. Ashkar, M. J. A. Hore, X. Ye, B. Natarajan, N. J. Greybush, T. Lam, C. R. Kagan, C. B. Murray, *ACS Appl Mater Interfaces* **2017**, *9*, 25513.
[41] H. Zhang, Y. Liu, M. F. S. Shahidan, C. Kinnear, F. Maasoumi, J. Cadusch, E. M. Akinoglu, T. D. James, A. Widmer-Cooper, A. Roberts, P. Mulvaney, *Adv Funct Mater* **2021**, *31*, 2006753.
[42] Y. J. Cha, D. S. Kim, D. K. Yoon, *Adv Funct Mater* **2017**, *27*, 1703790.
[43] H. Wang, H. Qian, W. Li, K. Wang, H. Li, X. Zheng, P. Gu, S. Chen, M. Yi, J. Xu, J. Zhu, *Small* **2023**, *19*, 2208288.
[44] B. Peng, Z. Li, E. Mutlugun, P. L. Hernández Martínez, D. Li, Q. Zhang, Y. Gao, H. V. Demir, Q. Xiong, *Nanoscale* **2014**, *6*, 5592.
[45] D. Nepal, M. S. Onses, K. Park, M. Jespersen, C. J. Thode, P. F. Nealey, R. A. Vaia, *ACS Nano* **2012**, *6*, 5693.

[46] W. Wei, F. Bai, H. Fan, *Angewandte Chemie - International Edition* **2019**, *58*, 11956.
[47] J. G. Turner, J. H. Og, C. J. Murphy, *Soft Matter* **2020**, *16*, 6582.
[48] G. Zhao, Y. Zhou, J. Wang, Z. Wu, H. Wang, H. Chen, *Advanced Materials* **2019**, *31*, 1900363.
[49] J. Pérez-Juste, B. Rodríguez-González, P. Mulvaney, L. M. Liz-Marzán, *Adv Funct Mater* **2005**, *15*, 1065.
[50] H. Pletsch, M. Tebbe, M. Dulle, B. Förster, A. Fery, S. Förster, A. Greiner, S. Agarwal, *Polymer (Guildf)* **2015**, *66*, 167.
[51] H. Gehan, L. Fillaud, M. M. Chehimi, J. Aubard, A. Hohenau, N. Felidj, C. Mangeney, *ACS Nano* **2010**, *4*, 6491.
[52] M. Nguyen, A. Kanaev, X. Sun, E. Lacaze, S. Lau-Truong, A. Lamouri, J. Aubard, N. Felidj, C. Mangeney, *Langmuir* **2015**, *31*, 12830.
[53] S. Christau, T. Moeller, J. Genzer, R. Koehler, R. Von Klitzing, *Macromolecules* **2017**, *50*, 7333.
[54] J. Zhao, J. Shan, G. Van Assche, H. Tenhu, B. Van Mele, *Macromolecules* **2009**, *42*, 5317.
[55] S. Christau, T. Möller, Z. Yenice, J. Genzer, R. Von Klitzing, *Langmuir* **2014**, *30*, 13033.
[56] Y. C. Kim, R. J. Composto, K. I. Winey, *ACS Nano* **2023**, *17*, 9224.
[57] W. L. Chen, R. Cordero, H. Tran, C. K. Ober, *Macromolecules* **2017**, *50*, 4089.
[58] Z. Lian, S. Qi, *Macromolecules* **2022**, *55*, 8162.
[59] R. K. W. Spencer, B. Y. Ha, *Macromolecules* **2021**, *54*, 1304.
[60] D. Boyaciyan, P. Krause, R. Von Klitzing, *Soft Matter* **2018**, *14*, 4029.
[61] D. Kesal, S. Christau, M. Trapp, P. Krause, R. Von Klitzing, *Physical Chemistry Chemical Physics* **2017**, *19*, 30636.
[62] A. R. Ferhan, D. H. Kim, *J Mater Chem* **2012**, *22*, 1274.
[63] R. Oren, Z. Liang, J. S. Barnard, S. C. Warren, U. Wiesner, W. T. S. Huck, *J Am Chem Soc* **2009**, *131*, 1670.
[64] S. Diamanti, S. Arifuzzaman, J. Genzer, R. A. Vaia, *ACS Nano* **2009**, *3*, 807.
[65] A. R. Ferhan, L. Guo, X. Zhou, P. Chen, S. Hong, D. H. Kim, *Anal Chem* **2013**, *85*, 4094.
[66] H. Gehan, L. Fillaud, M. M. Chehimi, J. Aubard, A. Hohenau, N. Felidj, C. Mangeney, *ACS Nano* **2010**, *4*, 6491.
[67] I. Tokarev, I. Tokareva, S. Minko, *ACS Appl Mater Interfaces* **2011**, *3*, 143.
[68] I. Tokareva, S. Minko, J. H. Fendler, E. Hutter, *J Am Chem Soc* **2004**, *126*, 15950.
[69] Y. Roiter, I. Minko, D. Nykypanchuk, I. Tokarev, S. Minko, *Nanoscale* **2012**, *4*, 284.

[70] G. Y. Zhou, A. W. Lee, J. Y. Chang, C. H. Huang, J. K. Chen, *J Mater Chem C Mater* **2014**, *2*, 8226.

[71] J. K. Chen, P. C. Pai, J. Y. Chang, S. K. Fan, *ACS Appl Mater Interfaces* **2012**, *4*, 1935.

[72] O. Azzaroni, A. A. Brown, N. Cheng, A. Wei, A. M. Jonas, W. T. S. Huck, *J Mater Chem* **2007**, *17*, 3433.

[73] S. Christau, T. Möller, F. Brose, J. Genzer, O. Soltwedel, R. von Klitzing, *Polymer (Guildf)* **2016**, *98*, 454.

[74] S. Nakamura, H. Mitomo, M. Aizawa, T. Tani, Y. Matsuo, K. Niikura, A. Pike, M. Naya, A. Shishido, K. Ijiro, *ACS Omega* **2017**, *2*, 2208.

[75] S. Nakamura, H. Mitomo, Y. Sekizawa, T. Higuchi, Y. Matsuo, H. Jinnai, K. Ijiro, *Langmuir* **2020**, *36*, 3590.

[76] G. Shen, N. Tercero, M. A. Gaspard, B. Varughese, K. Shepard, R. Levicky, *J Am Chem Soc* **2006**, *128*, 8427.

[77] D. Bracha, E. Karzbrun, G. Shemer, P. A. Pincus, R. H. Bar-Ziv, *Proc Natl Acad Sci U S A* **2013**, *110*, 4534.

[78] P. S. Gil, D. J. Lacks, P. Parisse, L. Casalis, M. D. Nkoua Ngavouka, *Soft Matter* **2018**, *14*, 9675.

[79] M. D. Nkoua Ngavouka, A. Bosco, L. Casalis, P. Parisse, *Macromolecules* **2014**, *47*, 8748.

[80] M. B. Ross, C. A. Mirkin, G. C. Schatz, *The Journal of Physical Chemistry C* **2016**, *120*, 816.

[81] A. Klinkova, R. M. Choueiri, E. Kumacheva, *Chem Soc Rev* **2014**, *43*, 3976.

[82] M. A. Boles, M. Engel, D. V. Talapin, *Chem Rev* **2016**, *116*, 11220.

[83] L. M. Liz-Marzán, *Langmuir* **2006**, *22*, 32.

[84] K. L. Kelly, E. Coronado, L. L. Zhao, G. C. Schatz, *Journal of Physical Chemistry B* **2003**, *107*, 668.

[85] L. Xu, W. Ma, L. Wang, C. Xu, H. Kuang, N. A. Kotov, *Chem. Soc. Rev.* **2013**, *42*, 3114.

[86] H. Zhang, J. Cadusch, C. Kinnear, T. James, A. Roberts, P. Mulvaney, *ACS Nano* **2018**, *12*, 7529.

[87] W. Wei, Y. Wang, J. Ji, S. Zuo, W. Li, F. Bai, H. Fan, *Nano Lett* **2018**, *18*, 4467.

[88] N. Jiang, X. Zhuo, J. Wang, *Chem Rev* **2018**, *118*, 3054.

[89] I. Tokarev, S. Minko, *Soft Matter* **2012**, *8*, 5980.

[90] Q. Jiang, Q. Liu, Y. Shi, Z. G. Wang, P. Zhan, J. Liu, C. Liu, H. Wang, X. Shi, L. Zhang, J. Sun, B. Ding, M. Liu, *Nano Lett* **2017**, *17*, 7125.

[91] P. Zhan, P. K. Dutta, P. Wang, G. Song, M. Dai, S. X. Zhao, Z. G. Wang, P. Yin, W. Zhang, B. Ding, Y. Ke, *ACS Nano* **2017**, *11*, 1172.

[92] L. Wang, G. J. Exarhos, A. D. Q. Li, *J Am Chem Soc* **2004**, *126*, 2656.

[93] S. T. Jones, Z. Walsh-korb, S. J. Barrow, S. L. Henderson, O. A. Scherman, *ACS Nano* **2016**, *10*, 3158.

[94] R. Iida, H. Mitomo, Y. Matsuo, K. Niikura, K. Ijiro, *Journal of Physical Chemistry C* **2016**, *120*, 15846.

[95] J. Simard, C. Briggs, A. K. Boal, V. M. Rotello, *Chemical Communications* **2000**, *14*, 1943.

[96] C. Fan, T. Bian, L. Shang, R. Shi, L. Z. Wu, C. H. Tung, T. Zhang, *Nanoscale* **2016**, *8*, 3923.

[97] Y. Torii, N. Sugimura, H. Mitomo, K. Niikura, K. Ijiro, *Langmuir* **2017**, *33*, 5537.

[98] R. Klajn, K. J. M. Bishop, B. A. Grzybowski, *Proceedings of the National Academy of Sciences* **2007**, *104*, 10305.

[99] P. K. Kundu, D. Samanta, R. Leizrowice, B. Margulis, H. Zhao, M. Börner, T. Udayabhaskararao, D. Manna, R. Klajn, *Nat Chem* **2015**, *7*, 646.

[100] H. Chen, L. Shao, Q. Li, J. Wang, *Chem Soc Rev* **2013**, *42*, 2679.

[101] Z. Sun, W. Ni, Z. Yang, X. Kou, L. Li, J. Wang, *Small* **2008**, *4*, 1287.

[102] H. S. Park, A. Agarwal, N. A. Kotov, O. D. Lavrentovich, *Langmuir* **2008**, *24*, 13833.

[103] R. Iida, H. Mitomo, K. Niikura, Y. Matsuo, K. Ijiro, *Small* **2018**, *14*, 1704230.

[104] Q. Liu, Y. Cui, D. Gardner, X. Li, S. He, I. I. Smalyukh, *Nano Lett* **2010**, *10*, 1347.

[105] M. Wang, C. Gao, L. He, Q. Lu, J. Zhang, C. Tang, S. Zorba, Y. Yin, *J Am Chem Soc* **2013**, *135*, 15302.

[106] N. J. Greybush, K. Charipar, A. Geldmeier, S. J. Bauman, P. Johns, J. Naciri, N. Charipar, K. Park, R. A. Vaia, J. Fontana, *ACS Nano* **2019**, *13*, 3875.

[107] M. Kang, J.-J. Kim, Y.-J. Oh, S.-G. Park, K.-H. Jeong, *Advanced Materials* **2014**, *26*, 4510.

[108] A. Yang, A. J. Hryn, M. R. Bourgeois, W.-K. Lee, J. Hu, G. C. Schatz, T. W. Odom, *Proceedings of the National Academy of Sciences* **2016**, *113*, 14201.

[109] M. L. Tseng, J. Yang, M. Semmlinger, C. Zhang, P. Nordlander, N. J. Halas, *Nano Lett* **2017**, *17*, 6034.

[110] S. Fujii, S. P. Armes, T. Araki, H. Ade, *J Am Chem Soc* **2005**, *127*, 16808.

[111] H. Mitomo, K. Horie, Y. Matsuo, K. Niikura, T. Tani, M. Naya, K. Ijiro, *Adv Opt Mater* **2016**, *4*, 259.

[112] S. Hamajima, H. Mitomo, T. Tani, Y. Matsuo, K. Niikura, M. Nayad, K. Ijiro, *Nanoscale Adv* **2019**, *1*, 1731.

[113] L. Fu, Y. Liu, W. Wang, M. Wang, Y. Bai, E. L. Chronister, L. Zhen, Y. Yin, *Nanoscale* **2015**, *7*, 14483.
[114] I. Tokareva, S. Minko, J. H. Fendler, E. Hutter, *J Am Chem Soc* **2004**, *126*, 15950.
[115] S. Z. Nergiz, S. Singamaneni, *ACS Appl Mater Interfaces* **2011**, *3*, 945.
[116] R. Oren, Z. Liang, J. S. Barnard, S. C. Warren, U. Wiesner, W. T. S. Huck, *J Am Chem Soc* **2009**, *131*, 1670.
[117] S. Nakamura, H. Mitomo, M. Aizawa, T. Tani, Y. Matsuo, K. Niikura, A. Pike, M. Naya, A. Shishido, K. Ijiro, *ACS Omega* **2017**, *2*, 2208.
[118] T. K. Sau, C. J. Murphy, *J Am Chem Soc* **2004**, *126*, 8648.
[119] Y. Sekizawa, H. Mitomo, M. Nihei, S. Nakamura, Y. Yonamine, A. Kuzuya, T. Wada, K. Ijiro, *Nanoscale Adv* **2020**, *2*, 3798.
[120] J. U. Kim, B. O'Shaughnessy, *Phys Rev Lett* **2002**, *89*, 238301.
[121] M. Mille, *J Colloid Interface Sci* **1981**, *81*, 169.
[122] K. P. Fears, S. E. Creager, R. A. Latour, *Langmuir* **2008**, *24*, 837.
[123] J. Brahms, W. F. H. M. Mommaerts, *J Mol Biol* **1964**, *10*, 73.
[124] J. B. Mills, E. Vacano, P. J. Hagerman, *J Mol Biol* **1999**, *285*, 245.
[125] Q. Chi, G. Wang, J. Jiang, *Physica A* **2013**, *392*, 1072.
[126] H. H. Chang, C. J. Murphy, *Chemistry of Materials* **2018**, *30*, 1427.
[127] Y. Xie, S. Guo, Y. Ji, C. Guo, X. Liu, Z. Chen, X. Wu, Q. Liu, *Langmuir* **2011**, *27*, 11394.
[128] P. K. Jain, S. Eustis, M. A. El-Sayed, *Journal of Physical Chemistry B* **2006**, *110*, 18243.
[129] R. Iida, H. Mitomo, K. Niikura, Y. Matsuo, K. Ijiro, *Small* **2018**, *14*, 1704230.
[130] B. Zhao, G. Yuan, X. Chu, J. Yang, J. Zhao, *Langmuir* **2018**, *34*, 6757.
[131] P. Gaddam, W. Ducker, *Langmuir* **2019**, *35*, 5719.
[132] L. Shao, X. Zhuo, J. Wang, *Advanced Materials* **2018**, *30*, 1704338.
[133] J. S. Mitchell, J. Glowacki, A. E. Grandchamp, R. S. Manning, J. H. Maddocks, *J Chem Theory Comput* **2017**, *13*, 1539.
[134] E. Roth, A. Glick Azaria, O. Girshevitz, A. Bitler, Y. Garini, *Nano Lett* **2018**, *18*, 6703.
[135] J. B. Mills, E. Vacano, P. J. Hagerman, *J Mol Biol* **1999**, *285*, 245.
[136] X. Xu, D. Mastropietro, M. Ruths, M. Tirrell, J. Yu, *Langmuir* **2019**, *35*, 15564.
[137] G. C. Ritsema Van Eck, L. Chiappisi, S. De Beer, *ACS Appl Polym Mater* **2022**, *4*, 3062.
[138] J. J. Keating, J. Imbrogno, G. Belfort, *ACS Appl Mater Interfaces* **2016**, *8*, 28383.

[139] R. Wang, Q. Wei, W. Sheng, B. Yu, F. Zhou, B. Li, *Angewandte Chemie - International Edition* **2023**, *62*, e202219312.
[140] T. Nishimura, F. Tamura, S. Kobayashi, Y. Tanimoto, F. Hayashi, Y. Sudo, Y. Iwasaki, K. Morigaki, *Langmuir* **2017**, *33*, 5752.
[141] G. W. De Groot, S. Demarche, M. G. Santonicola, L. Tiefenauer, G. J. Vancso, *Nanoscale* **2014**, *6*, 2228.
[142] A. Johnson, P. Bao, C. R. Hurley, M. Cartron, S. D. Evans, C. N. Hunter, G. J. Leggett, *Langmuir* **2017**, *33*, 3672.
[143] F. Weissenfeld, L. Wesenberg, M. Nakahata, M. Müller, M. Tanaka, *Soft Matter* **2023**, *19*, 2491.
[144] F. K. Metze, H. A. Klok, *ACS Polymers Au* **2023**, *3*, 228.
[145] S. Uenuma, K. Endo, N. L. Yamada, H. Yokoyama, K. Ito, *ACS Appl Mater Interfaces* **2021**, *13*, 60446.
[146] B. Yameen, A. Kaltbeitzel, G. Glasser, A. Langner, F. Müller, U. Gösele, W. Knoll, O. Azzaroni, *ACS Appl Mater Interfaces* **2010**, *2*, 279.
[147] G. Emilsson, K. Xiong, Y. Sakiyama, B. Malekian, V. Ahlberg Gagnér, R. L. Schoch, R. Y. H. Lim, A. B. Dahlin, *Nanoscale* **2018**, *10*, 4663.
[148] R. Y. H. Lim, *ACS Nano* **2009**, *3*, 2911.
[149] D. Li, L. Xu, J. Wang, J. E. Gautrot, *Adv Healthc Mater* **2021**, *10*, 2000953.
[150] K. Nagase, S. Ishii, K. Ikeda, S. Yamada, D. Ichikawa, A. M. Akimoto, Y. Hattori, H. Kanazawa, *Sci Rep* **2020**, *10*, 11896.
[151] K. Saha, S. S. Agasti, C. Kim, X. Li, V. M. Rotello, *Chem Rev* **2012**, *112*, 2739.
[152] Y. Shi, Q. Chen, Y. Liu, G. Wang, *Analyst* **2022**, *147*, 3578.
[153] Z. He, Q. Chen, S. Ding, G. Wang, T. Takarada, M. Maeda, *Analyst* **2023**, *148*, 1291.
[154] M. Zheng, Y. Shen, L. Zheng, X. She, C. Jin, *ACS Appl Mater Interfaces* **2023**, *15*, 45239.
[155] H. Gehan, L. Fillaud, M. M. Chehimi, J. Aubard, A. Hohenau, N. Felidj, C. Mangeney, *ACS Nano* **2010**, *4*, 6491.
[156] A. Idili, A. Vallée-Bélisle, F. Ricci, *J Am Chem Soc* **2014**, *136*, 5836.
[157] C. Burel, A. Teolis, A. Alsayed, C. B. Murray, B. Donnio, R. Dreyfus, *Small* **2020**, *16*, 1903897.
[158] J. Wang, H. A. Klok, *Angewandte Chemie - International Edition* **2019**, *58*, 9989.
[159] M. B. Perez, M. Cirelli, S. de Beer, *ACS Appl Polym Mater* **2020**, *2*, 3039.
[160] J. Yu, N. E. Jackson, X. Xu, B. K. Brettmann, M. Ruths, J. J. De Pablo, M. Tirrell, *Sci Adv* **2017**, *3*, eaao1497.

[161] W. H. Ferrell, D. I. Kushner, M. A. Hickner, *J Polym Sci B Polym Phys* **2017**, *55*, 1365.
[162] N. E. Jackson, B. K. Brettmann, V. Vishwanath, M. Tirrell, J. J. De Pablo, *ACS Macro Lett* **2017**, *6*, 155.
[163] J. Yu, J. Mao, G. Yuan, S. Satija, W. Chen, M. Tirrell, *Polymer (Guildf)* **2016**, *98*, 448.
[164] B. Brettmann, P. Pincus, M. Tirrell, *Macromolecules* **2017**, *50*, 1225.
[165] J. M. Y. Carrillo, A. V. Dobrynin, *Langmuir* **2009**, *25*, 13158.
[166] E. Zhulina, C. Singh, A. C. Balazs, *Journal of Chemical Physics* **1998**, *108*, 1175.
[167] G. L. He, H. Merlitz, J. U. Sommer, *Journal of Chemical Physics* **2014**, *140*, 104911.
[168] L. Liu, P. A. Pincus, C. Hyeon, *Macromolecules* **2017**, *50*, 1579.
[169] Z. He, G. Wang, X. Liang, T. Takarada, M. Maeda, *Analytical Sciences* **2021**, *37*, 415.

Acknowledgement

These studies presented in this thesis have been performed under the guide of Prof. Kuniharu IJIRO and Associate Prof. Hideyuki MITOMO. I would like to express my sincerest gratitude for their invaluable guidance and continuous encouragement throughout these studies.

I am deeply grateful to Prof. Takayuki KUROKAWA (Faculty of Science, Hokkaido University), Prof. Hiroshi HINOU (Faculty of Science, Hokkaido University), for valuable guidance and suggestion to summarize this thesis.

I gratefully appreciate to Assistant Prof. Yusuke YONAMINE (Research Institute for Electronic Science, Hokkaido University) and Specially Appointed Assistant Prof. Satoshi NAKAMURA (Research Institute for Electronic Science, Hokkaido University) for their kind and valuable guidance.

I owe a very important debt to Prof. Toshifumi SATOH, Associate Prof. Kenji TAJIMA, Associate Prof. Takuya ISONO, Assistant Prof. Li FENG, all the other members in Polymer chemistry lab. (Graduate School of Engineering, Hokkaido University) for sharing their precious knowledge of polymerization technique and their unconditional support.

I also appreciate to Prof. Masaru TANAKA and Assistant Prof. Shohei SHIOMOTO (Institute for Materials Chemistry and Engineering, Kyushu University) for their tolerant and kind support to tell me how to handle the AFM without destruction of cantilever.

This study was supported in part by Research Fellowship of the Japan Society for the Promotion of Science for Young Scientists.

I wish to thank Postdoc Takehiro YACHI, Ms. Chie TAKEUCHI, Ms. Aki OKUHARA, Dr. MBA Joshua CHIDIEBERE, Dr. Kun XIONG, Mr. Han LIN, Ms. Melda

TASPIKA, Ms. Jingyan YANG, Ms. Yali SHI, Mr. Ryo SUGIYAMA, Ms. Wenting WEI, Ms. Zhiyu HE, Mr. Yingqi MU, Mr. Tianxu GAO, Mr. Dongyu ZHANG, Mr. Haoran ZHANG, Mr. Abdul KAIYUM, Mr. Weijie CHEAH, Mr. Kaito SHISHIDO, Ms. Yuka HASEGAWA, Ms. Honoka NIWA, Ms. Honoka WATANABE, Mr. Tomoki IKEMIZU, Ms. Mio NAKAMURA, Ms. Hono OGIHARA, Ms. Erika KURIMOTO and other previous members for their support during my irreplaceable laboratory life in Molecular Device Laboratory.

Finally, I would like to express my special gratitude to my family and friends for their warm and heartfelt encouragement and support, which was essential to completing this challenging task.

Yu Sekizawa